3-16-2022

Effects of Pore-Forming Peptides (Melittin and Magainin 2) on the Phospholipid Bilayer Interior

Elmukhtar Ehmed Alhatmi
Portland State University

Effects of Pore-Forming Peptides (Melittin and Magainin 2) On the Phospholipid Bilayer Interior

by

Elmukhtar Ehmed Alhatmi

A dissertation submitted in partial fulfillment of the
requirements for the degree of

Doctor of Philosophy
in
Applied Physics

Dissertation Committee:
Drake Mitchell, Chair
Christopher Butenhoff
Andrew Rice
Jay Nadeau
Albert Benight

Portland State University
2022

ABSTRACT

Antimicrobial peptides (AMPs) are one of the most promising solutions to drug-resistant bacteria. Melittin and magainin 2 are two of the most representative and extensively studied AMPs. In this research, I investigated the interaction of these two AMPs with three models of cell membranes: 80% POPC 20% POPG, 40%POPC 40% POPE and 20% POPG, and 80%POPC 20%POPG plus 30% mole fraction of cholesterol. Time-resolved fluorescence emission and fluorescence anisotropy decays of the fluorescent probe 1,6-diphenyl-1,3,5-hexatriene (DPH) were analyzed to determine the effects of AMPs on the bilayer headgroup packing and changes in the interior of the phospholipid bilayer during the process of pore formation. Time-resolved fluorescence anisotropy of DPH was employed to investigate the dynamics and acyl chain ensemble order in the core of the membrane bilayers. DPH anisotropy decay was interpreted in terms of the Brownian Rotational Diffusion model (BRD). A wide range of molar ratio of peptides to lipids (P/L) 0.33% to 30% was studied and I found that at high P/L> 1/50 DPH fluorescence lifetime decreases with increasing melittin concentration but there was no effect of the magainin 2 on the fluorescence lifetime. The motion of DPH is slowed by adding more melittin as shown by the increasing the rotational correlation lifetime $\langle\emptyset\rangle$ of DPH. The anisotropy decay analysis leads to characterization of the order of the phospholipid acyl chains ensemble throughout the depth of the bilayer by calculating the orientational probability distribution function, $f(\theta)\sin(\theta)$ of DPH. I found the effect of peptide concentration on the interior of the membrane bilayers by calculating the orientational distribution function, $f(\theta)\sin(\theta)$, and the rotational correlation time of DPH.

Steady-state fluorescence measurements were also used to study the charge density effect on the peptide bound lipid to vesicles, and it was confirmed that melittin binds to the membrane bilayer from the blue shift of the maximal emission wavelength λ_{max} of the emission of the intrinsic tryptophan residue in melittin. from the blue shift of the maximal emission wavelength λ_{max} of the intrinsic tryptophan residue in melittin.

These results, which were based on three model bilayers, could have significant ramifications for our knowledge of peptides' mechanism of action on more sophisticated model cell membranes with higher physiological significance.

Acknowledgements

Thank you to my advisor Dr. Drake C. Mitchell for his guidance and help over the years throughout my time as a graduate student, and for being role models in all the various aspects of science, the scientific method, teaching, collaborating, and presenting scientific findings.

Thank you to all the teachers and professors I have been fortunate to have learned from and who have been kind enough to impart some of their knowledge.

Thanks, must also be given to my parents, family, friends for their continued support and motivation that makes everything in my life more meaningful and enjoyable. Special thanks to my wife, Wesal Ahmed, for doing all the many big things and countless little things to directly support me through my education. Thank you to my boys, Zeyad, Jad, Mohab, Eyad and Rawad for their patience, support, inspiration, and love.

Table of Contents

ABSTRACT i

Acknowledgements iii

List of Tables vi

List of Figures viii

List of Abbreviations xiv

List of Symbols xv

1. Introduction 1

1.1. Antimicrobial Peptides 8

1.1.1. Melittin 8

1.1.2. Magainin 2 11

1.2. Cell plasma Membranes 12

1.3. Phospholipids 14

1.3.1. 1-Palmitoyl-2-oleoyl-sn-gylcero-3-phosphocholine (POPC, or 16:0, 18:1 PC) 16

1.3.2. 1-Palmitoyl-2-oleoyl-sn-gylcero-3-phosphoglycerol (POPG, or 16:0, 18:1 PG) 17

1.3.3. 1-palmitoyl-2-oleoyl-sn-glycero-3-phosphoethanolamine (POPE, or 16:0, 18:1 PE) 18

1.3.4. Cholesterol 19

1.4. Liposomes 21

1.5. Jablonski Energy Diagram 22

1.5.1. Diphenyl-1,3,5-hexatriene (DPH) 25

1.5.2. Tryptophan (Trp) 26

2. Materials and Methods 29

2.1. Sample Preparation 29

2.1.1. Preparation of Liposomes 29

2.1.2. Preparation of peptides 30
2.2. Methods....31
2.3. Instrumentation 31
2.3.1. ISS PC1 Photon Counting Spectrofluorometer....31
2.3.2. ISS Chronos Spectrometer....32
2.3.3. Fluorescence measurements....37
2.3.4. Analysis of Steady-State Fluorescence Measurements....39
2.3.5. Analysis of Time-Resolved fluorescence intensity decay measurements....40
2.3.6. Analysis of Time-Resolved Anisotropy decay measurements....44
2.4. Brownian Rotational Diffusion Model (BRD) 48
3. Results and data analysis 52
3.1. Steady-State fluorescence measurements of lipid-bound melittin....52
3.2. Time-resolved fluorescence measurements of melittin-lipid bilayer interaction...55
3.2.1. Fluorescence lifetime of tryptophan of lipid-bound melittin....55
3.3. Fluorescence lifetime measurements of DPH as a function of added melittin....74
3.4. Fluorescence anisotropy measurements of DPH as a function of added melittin..78
3.5. DPH Orientational probability distribution function as a function of added melittin 83
3.6. Time-resolved fluorescence measurements of DPH as a function of added magainin 2....93
4. Discussion....103
5. Conclusions....114
6. Future studies....116
References....117

List of Tables

Table 3. 1 Maximal Trp emission wavelength as a function of Melittin/ Lipids molar ratios at room temperature (20°C) 55

Table 3. 2 The fluorescence lifetime ⟨τ⟩ of the tryptophan residue in melittin as a function of the temperatures in buffer PH7.25 58

Table 3. 3 Fluorescence lifetime $\boldsymbol{\tau}$ of the tryptophan residue in melittin as a function of the ratio Melittin added to the vesicles POPC/POPG 8:2 (M/L) in the buffer pH 7.25. .. 65

Table 3. 4 Fluorescence lifetime ⟨τ⟩ of the tryptophan residue in melittin as a function ratio Melittin added to the vesicles POPC/POPE/POPG 4/4/2 (M/L) in the buffer PH7.25 67

Table 3. 5 Fluorescence lifetime ⟨τ⟩ of the tryptophan residue in melittin as a function of the ratio Melittin added to the vesicles POPC/POPG 8/2+ 30% of Cholesterol (M/L) in the buffer PH7.25. 68

Table 3. 6 Effect of melittin on fluorescence lifetime ⟨τ⟩ of DPH embedded in POPC /POPG 8/2 at 30 ºC. 76

Table 3. 7 Effect of melittin on fluorescence lifetime ⟨τ⟩ of DPH embedded in POPC/POPE/POPG 4/4/2 at 30 ºC. 77

Table 3. 8 Effect of melittin on fluorescence lifetime ⟨τ⟩ of DPH embedded in POPC/POPG 8/2+ 30% of Cholesterol at 30 ºC 77

Table 3. 9 Effect of melittin on fluorescence anisotropy of DPH embedded in POPC/ POPG 8/2 at 30 ºC 80

Table 3. 10 Effect of melittin on fluorescence anisotropy of DPH embedded in POPC/POPE/POPG 4/4/2 at 30 ºC. 80

Table 3. 11 Effect of melittin on fluorescence anisotropy of DPH embedded in POPC/POPG 8/2+ 30% of Cholesterol at 30 ºC 81

Table 3. 12 The parameter f_{random} of DPH embedded in all of the three bilayer compositions. 90

Table 3. 13 Effect of magainin 2 on fluorescence lifetime ⟨τ⟩ of DPH embedded in POPC /POPG 8/2 at 30 ºC 94

Table 3. 14 Effect of magainin 2 on fluorescence lifetime ⟨τ⟩ of DPH embedded in POPC/POPE/POPG 4/4/2 at 30 ºC 95

Table 3. 15 Effect of magainin 2 on fluorescence lifetime ⟨τ⟩ of DPH embedded in POPC/POPG 8/2+ 30% of Cholesterol at 30 ºC 95

Table 3. 16 Effect of magainin 2 on fluorescence anisotropy of DPH embedded in POPC/ POPG 8/2 at 30 ºC 97

Table 3. 17 Effect of magainin 2 on fluorescence anisotropy of DPH embedded in POPC/POPE/POPG 4/4/2 at 30 ºC 98

Table 3. 18 Effect of magainin 2 on fluorescence anisotropy of DPH embedded in POPC/POPG 8/2+ 30% of Cholesterol at 30 ºC 98

List of Figures

Figure 1. 1 Antimicrobial peptides (total 2818) from the antimicrobial peptide database as of September 2017 [13]. 2

Figure 1. 2 The number of articles containing the terms antimicrobial peptide, cell-penetrating peptide, or membrane active peptide in the last 40 years [14]..... 3

Figure 1. 3. Main approaches used in biophysical characterization of peptide-membrane interaction. 5

Figure 1. 4 The schematic structures of the eukaryotic membrane and bacterial membrane [25]. 7

Figure 1. 5 Schematic models and processes of antimicrobial peptides interacting with membrane, A) Barrel Stave model, B) Toroidal model and C) Carpet model [19]. 7

Figure 1. 6 Structure of melittin. 10

Figure 1. 7 Pore formation mechanism by association of melittin on a lipid bilayer[42] [43]. 11

Figure 1. 8 The schematic helical structures of magainin 2 with hydrophobic side (green) and hydrophilic side (positive charged groups) (blue) [49]. 12

Figure 1. 9 Diagram showing the fluid mosaic model of the cell membrane structure [50]. 13

Figure 1. 10 Diagram showing the phospholipid molecules in cell membrane bilayers, red color is a hydrophilic “head groups”, and the black region is hydrophobic “acyl tails.”. This bilayer is the basis of the membranes of living cell. 14

Figure 1. 11 The schematic diagram illustrating the phospholipids molecules with two acyl saturated chain (straight structure 1) and unsaturated acyl chain (bent structure 2). Also, showing the polar head group. 14

Figure 1. 12 The schematic diagram of the POPC (16:0, 18:1) [60]. 17

Figure 1. 13 The schematic diagram of the POPG (16:0, 18:1) [61] 18

Figure 1. 14 The schematic diagram of the POPE (16:0, 18:1) [65] 18

Figure 1. 15 The schematic diagram of the cholesterol chemical structure [66] [77]. 20

Figure 1. 16 This an overview of liposome types. From left to right, multi-lamellar vesicles (MLV) that range in size from 300–5,000 nm. Large unilamellar vesicles (LUV) range in size from 100–300 nm, and small unilamellar vesicles (SUV) range in size from 20–100 nm. 21

Figure 1. 17 Jablonski diagram illustrates the transition between the electronic states of the molecule [78]. 24

Figure 1. 18 Electronic spectra of the molecules [78]. 25

Figure 1. 19 DPH absorption (a) and emission (b) spectra in ethanol**.** 26

Figure 1. 20 A. Tryptophan absorption and fluorescence spectra [84]. B. Tryptophan electronic absorption transitions in [85] 27

Figure 2. 1 Schematic of the ISS PC1 Photon Counting Spectrofluorometer [87]..... 31

Figure 2. 2 Schematic of Chronos, the Frequency-Domain Fluorometer from ISS [87]. 32

Figure 2. 3 The modulation ratio and phase delay of the lifetime intensity decay of Trp from Chronos instrument (Examples of Raw Lifetime Data)..... 34

Figure 2. 4 The modulation ratio and phase delay of the lifetime intensity decay of DPH from Chronos instrument (Examples of Raw Lifetime Data)..... 35

Figure 2. 5 The modulation ratio and phase delay of the anisotropy decay of DPH Chronos instrument (Examples of Raw Anisotropy Data). 36

Figure 2. 6 The black is excitation spectrum , and the red is the emission spectrum [97]. 39

Figure 2. 7 Excitation light is modulated at a certain frequency 41

Figure 2. 8 The anisotropy decay of a fluorophore which is not fully free to rotate. 46

Figure 2. 9 **A.** The polarized absorption light and polarized fluorescence emission light, **B.** The direction of the diploe moment between the absorption and the fluorescence emission. 46

Figure 3. 1 A. The effect of adding POPC on the fluorescence emission spectrum of tryptophan residue in melittin. **B.** The effect of adding POPC/POPG on the fluorescence emission spectrum of tryptophan in melittin. 54

Figure 3. 2 The maximum wavelength as a function of the addition of lipids to melittin. 54

Figure 3. 3 Fluorescence lifetime of the tryptophan residue in melittin vs temperature. 59

Figure 3. 4 The polarity parameter $\Delta \boldsymbol{f}$ of the solution vs temperature 60

Figure 3. 5 Fluorescence lifetime of the tryptophan residue in melittin vs polarity parameter $\Delta \boldsymbol{f}$. 61

Figure 3. 6 Fluorescence lifetime of the tryptophan residue in melittin vs dielectric constant. 62

Figure 3. 7 Natural log. of the fluorescence lifetime of the tryptophan residue in melittin vs 1/T (K^{-1}). 63

Figure 3. 8 Fluorescence lifetime of the tryptophan vs Melittin to lipids 66

Figure 3. 9 Fluorescence lifetime of the tryptophan vs Melittin to lipids 69

Figure 3. 10 Fluorescence lifetime of the tryptophan residue in melittin binding to vesicles vs temperature. 70

Figure 3. 11 Percentage of bound melittin to vesicles vs temperature. 71

Figure 3. 12 Comparison between the Lifetime of DPH in three compositions of lipids vs the molar ratio of melittin to lipids. 77

Figure 3. 13 Comparison between Rotational relaxation lifetime of the DPH of the three compositions of lipids vs Melittin molar ratio to lipids. 81

Figure 3. 14 The average fluorescence anisotropy $\boldsymbol{r}$ of the DPH of the three compositions vs melittin to lipids molar ratio. 82

Figure 3. 15 The angular orientational probability distribution function $f(\theta)sin\theta$ of DPH with respect to bilayer normal for Vs the temperature for PC vesicles. 85

Figure 3. 16 The angular orientational probability distribution function $f(\theta)sin\theta$ of DPH with respect to bilayer normal for the three compositions for different melittin to lipids concentrations melittin/L. 87

Figure 3. 17 The orientational probability distribution function $f(\theta)sin\theta$ of DPH with respect to bilayer normal for the three compositions for different melittin to lipids concentrations Mel/L. 88

Figure 3. 18 $F_{rand.}$ parameter vs melittin to lipids ratio Mel/L. 90

Figure 3. 19 The orientational probability distribution function $f(\theta)sin\theta$ of DPH with respect to bilayer normal for the PC//PG composition for different melittin to lipids concentrations Mel/L. 91

Figure 3. 20 The orientational probability distribution function $f(\theta)sin\theta$ of DPH with respect to bilayer normal for the PC/PE/PG composition for different melittin to lipids concentrations Mel/L. 92

Figure 3. 21 The angular orientational probability distribution function $f(\theta)sin\theta$ of DPH with respect to bilayer normal for PC/PG+30% Cho composition for different melittin to lipids concentrations Mel/L. 92

Figure 3. 22 Comparison between excited state lifetime of DPH with two peptides (melittin and magainin 2) as a function of peptides to lipids molar ratio. A) PC/PG, B) PC/PE C) PC/PG+ Chol. 96

Figure 3. 23 Comparison between Rotational relaxation lifetime $\langle\emptyset\rangle$ of the DPH of the three compositions of lipids vs Magainin molar ratio to lipids. 99

Figure 3. 24 Comparison between correlation rotational lifetime $\langle\emptyset\rangle$ of DPH with two peptides (melittin and magainin 2) as a function of peptides to lipids molar ratio. A) PC/PG, B) PC/PE C) PC/PG+ Chol. 99

Figure 3. 25 The average fluorescence anisotropy $\boldsymbol{r}$ of the DPH of the three compositions vs magainin 2 to lipids molar ratio. 100

Figure 3. 26 The average fluorescence anisotropy $\boldsymbol{r}$ of the DPH of the three compositions vs magainin 2 to lipids molar ratio. 100

Figure 3. 27 Shows the angular orientational probability distribution function $f(\theta)\sin\theta$ of DPH with respect to bilayer normal for both compositions for different magainin 2 to lipids concentrations Mag2/L. A) PC/PG, B) PC/PE C) PC/PG+ Chol. 101

List of Abbreviations

AMPs Antimicrobial peptides

L Lipids

PLs Phospholipids

POPC 1-Palmitoyl-2-oleoyl-*sn*-gylcero-3-phosphocholine

POPG 1-Palmitoyl-2-oleoyl-*sn*-gylcero-3-phosphoglycerol

POPE 1-palmitoyl-2-oleoyl-sn-glycero-3-phosphoethanolamine

CHO Cholesterol

LUVs Large Unilamellar Vesicles

Mel Melittin

Mag2 Magainin 2

DPH 1,6-diphenyl-1,3,5-hexatriene

POPOP 1,4-bis(5-phenyloxazole-2-yl) benzene

THF Tetrahydrofuran

Trp Tryptophan

PC1 Photon Counting Spectrofluorometer

BRD Brownian Rotational Diffusion

List of Symbols

$\langle \boldsymbol{\tau} \rangle$ Excited state lifetime

$\langle \emptyset \rangle$ Average rotational correlation (or relaxation) time

$\boldsymbol{r_0}$ Initial anisotropy

$\boldsymbol{f(\theta)\sin(\theta)}$ Angular Orientational Probability Distribution Function

$\boldsymbol{\alpha_1, \alpha_2}$ The weighted fluorescence intensity decay factors

$\boldsymbol{\lambda_m}$ Maximum emission wavelength

1. Introduction

Various antibiotics have commonly been utilized to treat human diseases since the first antibiotic, Penicillin, was discovered by Alexander Fleming in 1928 [1]. Normally, antibiotics are highly effective as remedies for bacterial infections [2]. However, drug-resistant bacteria appeared, and the antibacterial ability of antibiotics gradually decreased with the use of large amounts of antibiotics and due to long-term use [1]. Recently, the World Health Organization (WHO) noted that the world is increasingly dangerous due to antibiotic-resistant bacteria [3]. In April 2019, WHO reported that about 700,000 people are killed each year around the world due to drug-resistant bacteria [4]. Thus, effective action has to be taken or this number will rise in the coming years [4]. Peptides were first discovered in the year 1939 and are one of the most promising solutions to drug-resistant bacteria [1][4][5]. They have been receiving more attention from scientists all over the world in the last decades as a solution to the serious threat of drug-resistant bacteria on global health [4]. Peptides typically consist of anywhere from six to around one hundred amino acids residues with most of them cationic (positively charged) and amphiphilic (hydrophilic and hydrophobic), and generally contain stretches of α-helical structure[1][6][7]. Initially, peptides were first identified by their ability to strongly interact with the lipid bilayer and disrupt their integrity [8]. They are unique molecules whose mechanism of action (MOA) with bilayers has been extensively researched since their discovery. Peptide-lipid bilayer interactions are involved in several important biological processes. Antimicrobial peptides (AMPs), for instance, can recognize and kill a wide range of pathogens, and several of these peptides have been recognized as important

components of the natural immune system [9]. AMPs, also known as host defense peptides, have been discovered in a variety of species [10]. During the last decades, a huge number of AMPs have been discovered in animals, plants, and fungi, such as melittin, ainin, cecropins, defensins, and indolicidin [11][12][13].

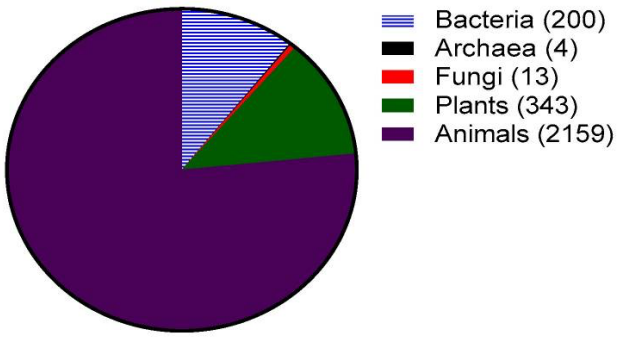

Figure 1. 1 Antimicrobial peptides (total 2818) from the antimicrobial peptide database as of September 2017 [13].

In the last decades, an increasing number of studies have been reported on lipid bilayer active peptides [14]. The number of articles containing the keywords "membrane active peptide", "antimicrobial peptide", or "cell-penetrating peptide" has increased at an exponential rate in the past ~40 years[14]. Lipid bilayer active peptides are attractive alternatives to currently utilized pharmaceuticals, and the number of peptides and antimicrobial peptides (AMPs) designed for drug and gene delivery is rising [14]. More than 600 articles just in the field of AMPs were published in 2017, see Fig. 1.2 [14].

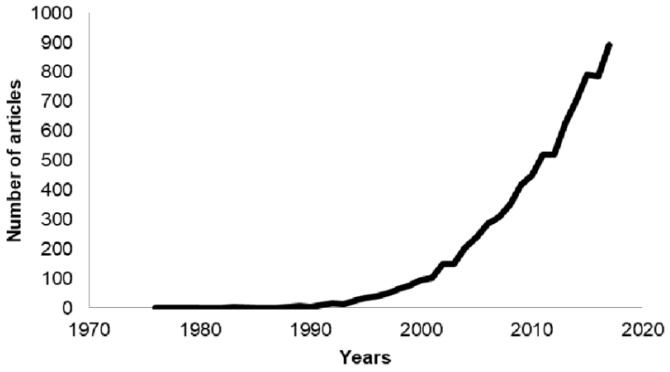

Figure 1. 2 The number of articles containing the terms antimicrobial peptide, cell-penetrating peptide, or membrane active peptide in the last 40 years [14].

These peptides interact with a phospholipid bilayer to disrupt it and cause bilayer lysis or passing through it to deliver the cargos to their target [14][15]. There are two main types of lipid active

peptides; bilayer-penetrating peptides (BPPs), which deliver cargos across the lipid bilayer, and antimicrobial peptides (AMPs), which kill cells [15] . It's not always obvious to tell the difference between AMPs and CPPs. Many AMPs have cell penetrating properties, and many CPPs can also function as AMPs [16]. Despite the fact that AMPs come in a wide variety of sequences, structures, and sources, they have several characteristics in common [13]. Generally, they have a positive net charge (from +2 to +13) and may have a distinct cationic domain [13]. The activity of AMPs depends on several molecular determinants, such as charge, length, hydrophobicity, and amphiphilicity[17] [10].

The basic mechanism of peptide-membrane interaction must involve at least two fundamental steps. First, cationic peptides bind to the outer surface of negatively charged bilayers due to the electrostatic interaction [18]. Second, peptides disrupt membrane bilayers when the concentration of peptides bound to the surface becomes sufficiently

large. To investigate the molecular details of the peptide–lipid bilayer interactions, researchers have used various experimental techniques or molecular dynamic (MD) simulation methods to study the steps of peptide actions with a phospholipid bilayer. Furthermore, studies of peptide-lipid interaction have led to several models of the complete process from membrane binding to pore formation, including the barrel-stave model, the carpet model, and the toroidal-pore model as shown in Fig. 1.5 [19]. In general, the mechanism of peptide-lipid bilayer actions can be categorized under pore-forming and non-pore-forming models [13]. The barrel-stave and toroidal models are the most widely accepted pore-forming models [20].

Both toroidal and barrel stave models are similar in the assumption of a spatially characterized pore [19]. However, whereas the barrel stave pore is assumed to be completely designed by peptides, the toroidal pore could also be stable additionally to peptide-peptide contacts by phospholipids head group interactions [19]. The carpet model, on the other hand, deviates from previous models by assuming that in the presence of high peptide concentrations, part of the lipids undergoes a phase transition from a bilayer to a micellar phase stabilized by peptides. Individual complexes can diffuse away from the membrane after the formation of these peptide-stabilized micelles, leaving holes in their backs, see Fig. 1.5 [19]. Various experimental techniques have also been used to characterize the membrane active peptides. Fig. 1.3 is a schematic representation of the main biophysical characterization approaches that have been used to examine the structural and dynamical features of peptide-lipid interaction [20].

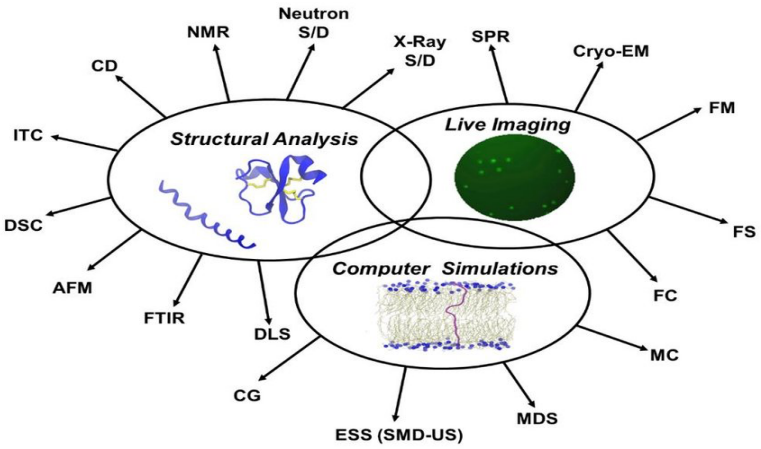

Figure 1. 3. Main approaches used in biophysical characterization of peptide-membrane interaction.

NMR: Nuclear netic Resonance spectroscopy; ITC: Isothermal Titration Calorimetry; CD: Circular Dichroism Spectroscopy; X-ray S/D scattering/diffraction; MDS: Molecular Dynamics Simulations; MC: Monte Carlo calculations; Cryo-EM: Cryoelectron Microscopy; FC: Flow Cytometry; DLS: Dynamic Light Scattering; DSC: Differential Scanning Calorimetry; AFM: Atomic Force Microscopy; FS: Fluorescence Spectroscopy; FM: Fluorescence Microscopy; SPR: Surface Plasmon Resonance. FTIR: Fourier Transform Infrared Spectroscopy; CG: Coarse Grained models; Neutron S/D: Neutron Scattering/Diffraction; ESS: Enhanced Sampling Simulations; SMD-US: Steered Molecular Dynamics Simulations-Umbrella Sampling [20].

Magainin 2 and melittin are often used as models for the peptide-lipid bilayer interaction. However, the mechanism and the conditions of peptides-lipid bilayer interactions, especially pore formation behavior, are still unclear [21]. The lipid compositions of the lipid bilayer play a significant role in the ability of peptides to induce pores and leakage of membrane bilayers. In this research, I investigated the interaction of two pore-forming peptides, magainin 2 and melittin, with bilayers composed of three different phospholipid mixtures: large unilamellar vesicles (LUVs), phosphatidylcholine (POPC), phosphatidylglycerol (POPG) and phosphatidylethanolamine (POPE). These mixtures were prepared with 80% POPC 20% POPG, 40%POPC 40% POPE and 20% POPG, and

80%POPC 20%POPG plus 30% mole fraction of cholesterol. All these compositions have the same charge surface density, due to the presence of 20% PG, but different headgroup composition (due to POPE) and different acyl chain packing, due to cholesterol (CHO). The goal of this research is to study the effect of headgroup and the interior bilayer composition on peptides-lipid bilayer interactions, see Fig. 1.5. Fluorescence spectroscopy is one of the most powerful techniques, and the one I used in this research to gain more details of the interactions between peptides and lipid bilayers. Fluorescent probes have been widely used to study phospholipid bilayers and have been used to examine the effects of peptides on the interior membrane. The linear probe 1,6-diphenyl-1,3,5-hexatriene (DPH) is one of the most popular fluorescent probes for bilayers and membranes since it partitions strongly into the hydrophobic core of bilayers [129][11]. Therefore, it is broadly used in this research to examine structural and dynamical properties of phospholipid bilayers via measuring both time-resolved fluorescence anisotropy decay and fluorescence intensity decay [23]. The effects of peptides on the acyl chains packing in the interior of the bilayer were studied by time-resolved fluorescence spectrscopy using the frequency domain (FD) technique. In this research, the fluorescence intensity average lifetime $\langle\tau\rangle$, and the dynamic anisotropy decay of the DPH probe molecule were calculated at 30°C as function of molar ratios of peptide/lipid. DPH anisotropy decay was interpreted in terms of an orientational distribution model that goes beyond the usual <P2> order parameter, derived from the 2nd Legendre polynomial, to include <P4>. DPH anisotropy decay was interpreted in terms of the Brownian Rotational Diffusion model (BRD). The results of anisotropy decay provide information about the orientational order and motion of DPH.

These physical parameters information of DPH provide an accurate picture of the ensemble of acyl chains throughout the depth of the phospholipid bilayer interior which is not well known from previous studies [24].

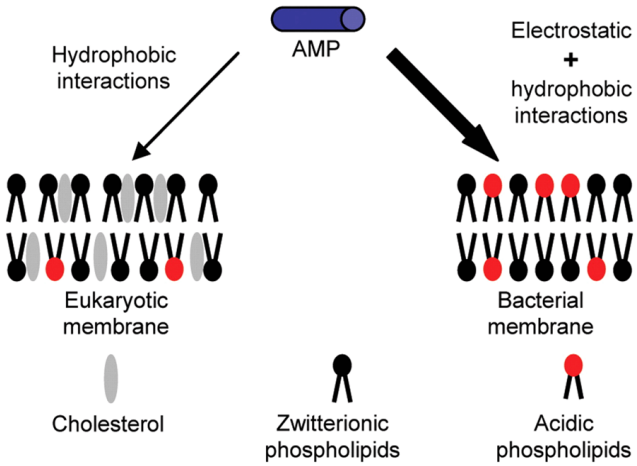

Figure 1. 4 The schematic structures of the eukaryotic membrane and bacterial membrane [25].

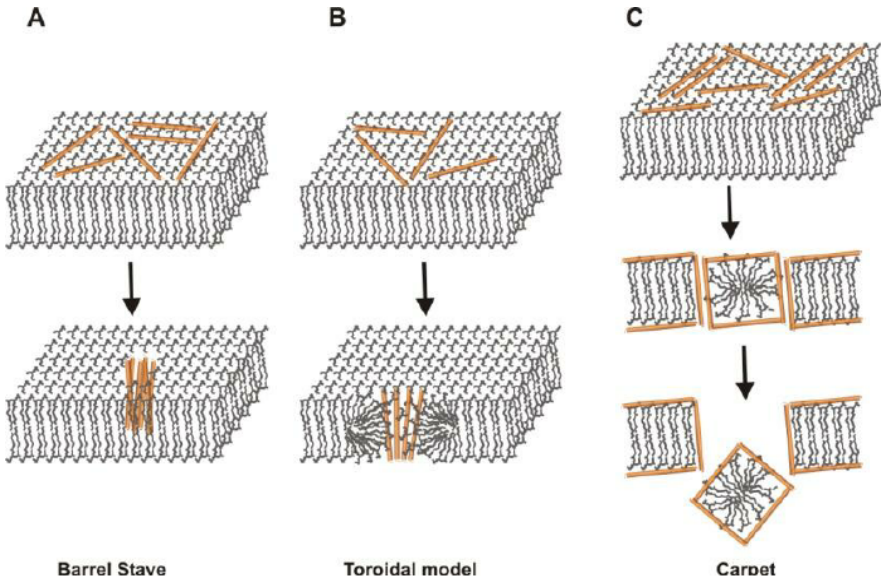

Figure 1. 5 Schematic models and processes of antimicrobial peptides interacting with membrane, A) Barrel Stave model, B) Toroidal model and C) Carpet model [19].

1.1. Antimicrobial Peptides

1.1.1. Melittin

Melittin (MEL) ($C_{131}H_{229}N_{39}O_{31}$, M.W = 2846.46 g/mole) is the principal toxic component of European honey bee venom, and was discovered around 1970 [26]. It represents approximately 50% of the dry weight of bee venom [26][27]. It is a linear cationic and amphipathic peptide composed of 26 amino acids (NH2-Gly-Ile-Gly-Ala-Val-Leu-Lys-Val-Leu-Thr-Thr-Gly-Leu-Pro-Ala-Leu-Ile-Ser-Trp-Ile-Lys-Arg-Lys-Arg-Gln-Gln-CONH2) in which the residues 1–20 are predominantly hydrophobic, whereas residues 21–26 are hydrophilic, see Fig. 1.6 [26]. This peptide has six positive charges and no negative charges; four of these six positive charges are in the latter region. The terminal residue Gly region (N-terminal) is predominantly hydrophobic whereas the terminal residue Gln region (C-terminal) is hydrophilic due to the presence of the positive charges. Thus, melittin forms an amphipathic helix with the polar groups protruding outwards into the solvent, while the non-polar groups come into contact with each other on the interior of the structure [28]. Because of its amphiphilic properties, this peptide has been used as a suitable model for studying peptide–membrane bilayer interaction. In addition, its amphiphilic properties makes melittin highly soluble in water [29] [4]. The interaction of melittin with phospholipids bilayer has been investigated extensively, both theoretically and experimentally [30]. The studies show that the interaction depends on many factors such as: aqueous solution, melittin concentration, phospholipids composition, and the membrane potential [31]. Melittin has a higher affinity for phospholipid bilayers that contain negative charges than for bilayers composed of only zwitterionic phospholipids

[30]. The partition constant of melittin into the phospholipids bilayer composed of POPC/POPG (80mol/20mol) is $K_p = 4.5 \times 10^4\ M^{-1}$, whereas into POPC it is $K_p = 2.1 \times 10^3\ M^{-1}$[32].This indicates that both hydrophobic and hydrophilic interactions are involved in the binding of melittin to the bilayer [33][34]. In general, melittin-membrane bilayer interaction can be divided into two stages: melittin binding to the bilayer driven by hydrophobic and electrostatic interactions, then accumulation on the surface of the bilayer, followed by insertion of melittin into the bilayer leading to the formation of transmembrane pores [4]. Melittin can orient either parallel or perpendicular to the bilayer, depending on composition of the bilayer and the environment conditions [35]. It was reported that it was necessary to insert at least three molecules of melittin into the bilayer [36]. The properties of the pores produced by melittin could be described with the toroidal or barrel-stave model [35]. By using oriented circular dichroism (OCD) and neutron scattering, it was found that the properties of melittin-induced pores are similar to the transmembrane pores predicted by the toroidal model and are similar to those of pores detected by using oriented circular dichroism (OCD) and neutron scattering [35][37]. Bogaart, Jeanette Guzman, et. al. (2017) reported that about 1 melittin per 90 lipid molecules was needed for leakage of the 623 Da calcein [38]. This value is consistent with the literature, however it is highly dependent on the specific experimental conditions, such as lipid composition, ionic strength of the buffer [39][40][41].

a

Peptide	Amino Acid Sequence *												
	1	2	3	4	5	6	7	8	9	10	11	12	13
Melittin	G	I	G	A	V	L	K	V	L	T	T	G	L
	14	15	16	17	18	19	20	21	22	23	24	25	26
	P	A	L	I	S	W	I	K	R	K	R	Q	Q

* Blue: hydrophobic; Orange: hydrophilic; Red: charged

b

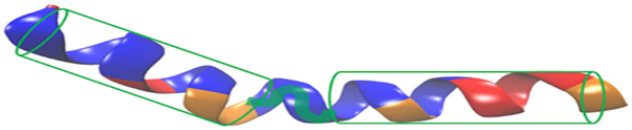

Figure 1. 6 Structure of melittin.

(a) The amino acid sequence of melittin. (b) the secondary structure of melittin showing the amphipathic α-helical configuration (when binding on a membrane) [4].

Below are some cartoons illustrating the prediction of melittin-lipid bilayer interaction.

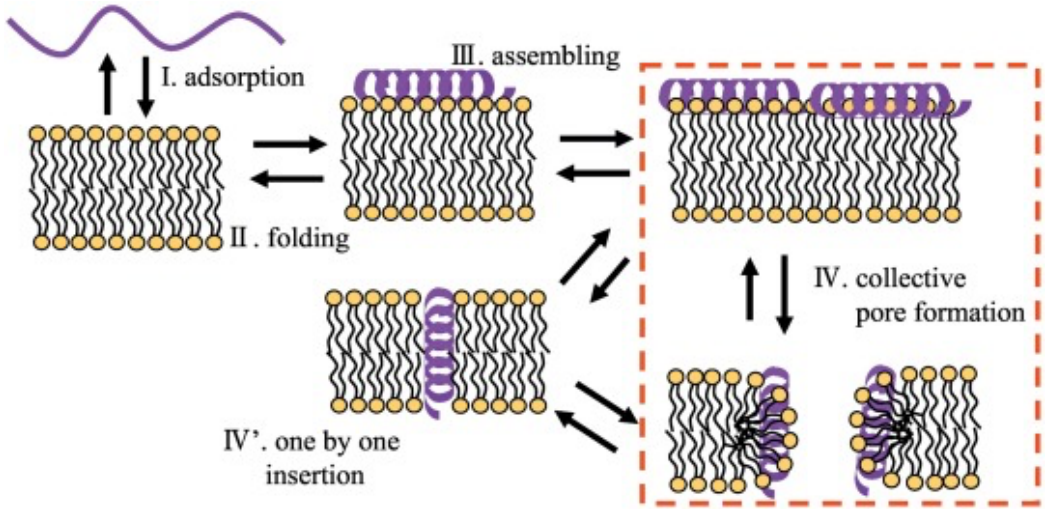

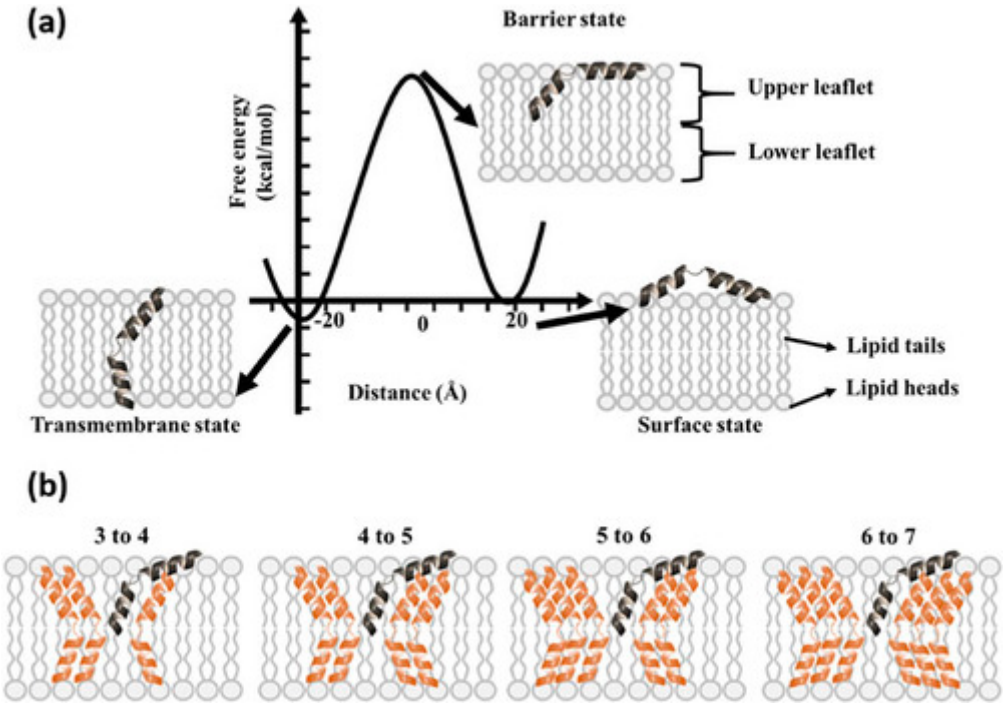

Figure 1. 7 Pore formation mechanism by association of melittin on a lipid bilayer[42] [43].

1.1.2. Magainin 2

Magainin 2 (Mag2) ($C_{114}H_{180}N_{30}O_{29}S$, M.W=2466.90 g/mole), from the skin granular gland of the African clawed frog, is a cationic and amphipathic peptide. It is composed of 23 amino acids (H-Gly-Ile-Gly-Lys-Phe-Leu-His-Ser-Ala-Lys-Lys-Phe-Gly-Lys-Ala-Phe-Val-Gly-Glu-Ile-Met-Asn-Ser-OH) and has a four positive net charge and no negative charges [44]. Magainin 2 is very sensitive to anionic phospholipids composition. As a result, magainin 2, like melittin, has a high affinity for negatively charged bilayers and this affinity decreases with the decrease of negatively charged phospholipids [30] [45]. As a result, the binding of magainin 2 to the mixture phosphatidylcholine bilayer of

PC/PG (50/50) is 20 times stronger than PC/PG (70/30) [45] due to the increase in negative charges. On the other hand, fluorophore-release studies revealed that magainin 2 exhibits transmembrane pores and lytic activities when added to phospholipid bilayers [46] [47]. Furthermore, structural studies reveal that as magainin 2 partitions into the membrane, it undergoes a spontaneous coil to helix transition [46]. Tamba and Masahito Yamazaki, (2019) found that at least the magainin 2 to lipids needed t for leakage is 1/30 [48].

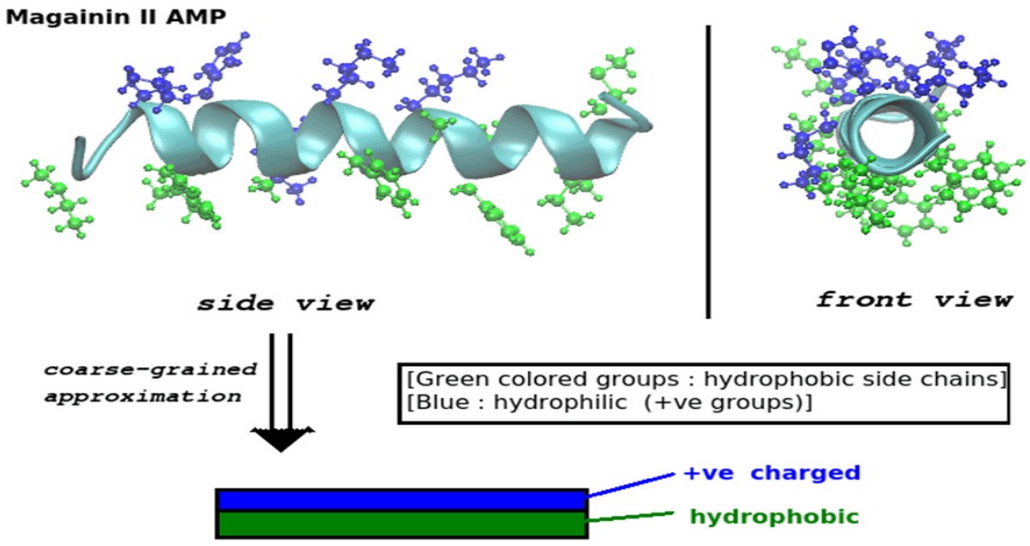

Figure 1. 8 The schematic helical structures of magainin 2 with hydrophobic side (green) and hydrophilic side (positive charged groups) (blue) [49].

1.2. Cell plasma Membranes

The cell plasma membrane (or cell membrane) is primarily composed of a lipid bilayer with embedded proteins. According to the fluid mosaic model (first proposed in 1972) the cell membrane is a disorganized mosaic of components of phospholipids, cholesterol, and proteins as shown in Fig.1.8 [50]. This model has evolved into a more organized model

that includes two distinct, coexisting fluid phases; liquid disorder and liquid-order. The latter phase is based on the strong attractive interaction between saturated phospholipid acyl chains and cholesterol, which is found in essentially all mammalian cell membranes. The majority of the lipids in membranes are phospholipids. All of the phospholipid molecules are amphipathic which means that they have a hydrophilic phosphate headgroup which is attracted to water and polar, hydrophobic acyl chains consisting of two fatty acid chains repelled by water or nonpolar ends as shown in Fig. 1.9. The overall nanostructure of the cell membrane is known, the average radius of the headgroup is~0.2-0.3 nm, and the length of the polar headgroup is~0.5-1 nm. The thickness of the bilayer (the distance between the hydrophobic headgroups of the membrane bilayer) is ~5 nm, and the average surface area per lipid molecule is~ 0.5 nm^2. The lipid bilayer has been established as the general basis for cell membrane structure. It is easily seen by electron microscopy. However, many techniques such as x-ray diffraction, scanning electron microscopy (SEM), nuclear magnetic microscopy (NMR), and fluorescence spectroscopy are needed to reveal the details of its organization and phase diagram.

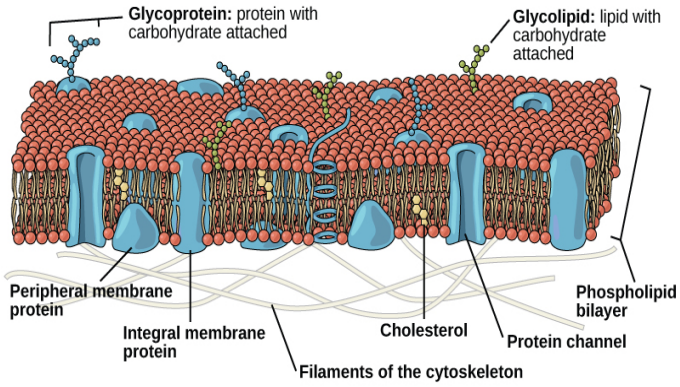

Figure 1. 9 Diagram showing the fluid mosaic model of the cell membrane structure [50].

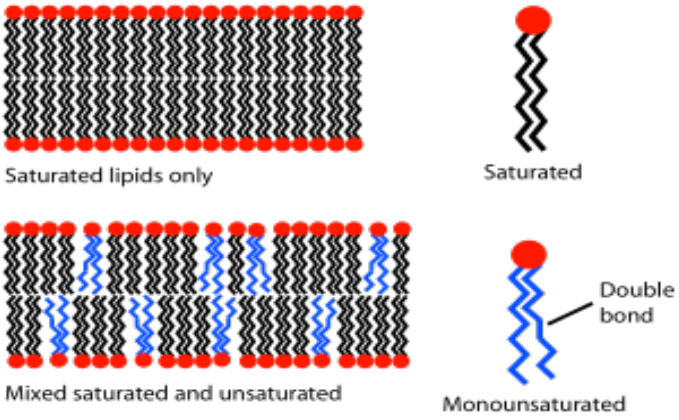

Figure 1. 10 Diagram showing the phospholipid molecules in cell membrane bilayers, red color is a hydrophilic "head groups", and the black region is hydrophobic "acyl tails.". This bilayer is the basis of the membranes of living cell.

The unsaturated lipids with a blue tail (double bond) disrupt the packing of the saturated tails one (black). The resulting membrane bilayer has more free space which allows more water and other small molecules move in and out of bilayer.

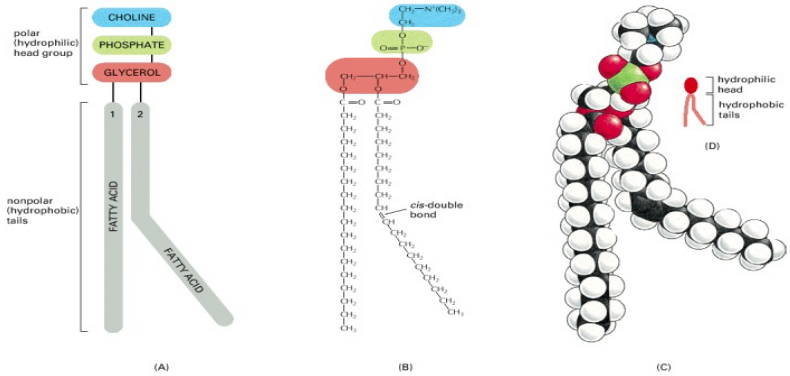

Figure 1. 11 The schematic diagram illustrating the phospholipids molecules with two acyl saturated chain (straight structure 1) and unsaturated acyl chain (bent structure 2). Also, showing the polar head group.

1.3. Phospholipids

Phospholipids (PLs) are the major component of biological cell membranes; Phospholipids account for nearly 50% of all lipids of the plasma membrane, with phosphatidylcholine (POPC) and phosphatidylethanolamine (POPE) being the two most common [52]. At the

simplest level they are built around a central glycerol group which links the polar headgroup, and usually two neutral fatty acid tails (nonpolar hydrocarbon chains). The net charge of the polar head group can be neutral (zwitterion) due a negative phosphate group and positive glycerol electrical charges as shown in Fig. 1.4. These PLs are an example of a zwitterion where functional groups have at least one negative and another positive charge. Therefore, the zwitterionic surface property of these PLs is one of the most important attributes which enable it to interact with external molecules such as peptides. The headgroup charges play a significant role in peptide-membrane interactions.

The fatty acid tails can contain between 10 and 36 carbon atoms, and these two fatty acid chains can be different in length. For instance, the acyl chains of the phospholipids used in this study consist of one saturated chain which has 16 carbon atoms and no double bonds, while the other chain has 18 carbon atoms and one cis double bond. The length and saturation differences in the fatty acid tails influence the ability of phospholipid molecules to compress against each other, thereby affecting the fluidity of the membrane. The relative phase of the lipids molecules is one of the most important properties of a lipid bilayer and the physical phase of the bilayer can be changed by many factors [53]. The main bilayer phases are liquid, gel, and crystalline (solid) phases which depend on temperature, water content, and the main phospholipids head group and acyl chain composition [54], [55].The phase behavior of lipid bilayers is largely dependent on the Van der Waals interactions between the acyl chains. The extent of this interaction is in turn governed by how well the acyl chains can pack together, how unsaturated they are, and how long they are. As a result, the mobility of lipids decreases in the gel (ordered phase) for long chains of lipids which

have more area, consequently increasing the Van der Waals interactions. However, short lipid chains will be more fluid (liquid or disordered) than those with long tails [1]. Furthermore, the saturated chains with only single bonds are straight and easy to pack tightly together, while the unsaturated chains bend and are harder to pack tightly [50].

Another important property of cell membrane bilayer is the surface charge density. The surface charge density of the membrane bilayers has been studied via many techniques. It is a key for many interactions of cell membranes with proteins and small molecules such as membrane-peptide interactions. The range of the surface charge density (σ) of cell membranes from many studies is $\sigma = 0.3 - 0.002\ C/m^2$. The change of dielectric constant from 80 in water to ~ 2 in the interior of the bilayer is very important to study the peptide- membrane bilayer interaction by using a spectroscopy technique. This information about the lipid bilayer is very significant to study the interaction between the bilayer and the peptides. Three types of phospholipids have been used in this research to study peptides -bilayers interactions, (POPC), (POPG), and (POPE). These PLs are chosen based on the majority of lipids present in the plasma membrane [52].More details about the chosen PLs and the cholesterol are described in the following sections.

1.3.1. 1-Palmitoyl-2-oleoyl-sn-gylcero-3-phosphocholine (POPC, or 16:0, 18:1 PC)

POPC ($C_{42}H_{82}NO_8P$, M. W = 760.091 g/mole) is the major lipid and one of the most common zwitterionic PLs components of animal cell membranes, and it is rarely present in the bacterial membrane [57][58]. It is more commonly found in the outer leaflet of most animal cell membrane bilayers, and it is very widely used for bilayer studies [59]. Fig. 1.11 shows the two hydrophobic acyl chains (1-palmitoyl-2-oleoyl) that provide the first two

letters ‘P’ and ‘O’, while the headgroup (phosphocholine) provides the last two ‘P’ and ‘C’ to the name POPC. Note that the upper saturated chain (palmitoyl chain) has only single bonds, while the lower unsaturated chain (oleoyl chain) has one double bond in the middle. POPC has been used in the preparation of the liposomes (vesicles) to study the properties of lipid bilayers such as the fluidity of the lipid bilayer. POPC is also used as the main model in biophysical experiments to study peptides-lipid bilayer interaction, and it has no change in phase above about 3 °C. The net charge of POPC is neutral but has separate negative and positive charges on the headgroup surface.

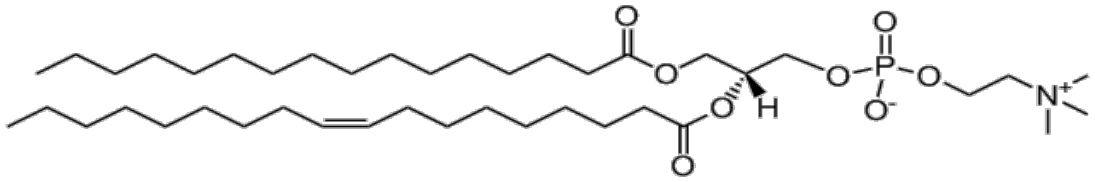

Figure 1. 12 The schematic diagram of the POPC (16:0, 18:1) *[60]*.

1.3.2. 1-Palmitoyl-2-oleoyl-sn-gylcero-3-phosphoglycerol (POPG, or 16:0, 18:1 PG)

POPG ($C_{40}H_{76}O_{10}PNa$, M.W = 770.989 g/mole) is very similar to POPC. It has the same two hydrophobic acyl chains as POPC, and a headgroup composed of phosphate and oxide which has the same cross-sectional area as PC, see Fig. 1.12. However, the net charge of POPG is a negative single charge. In this research POPC with POPG were mixed with molar ratios (80/20). Many previous studies used this ratio to study the effect of the charge surface density on the peptide-lipid interaction.

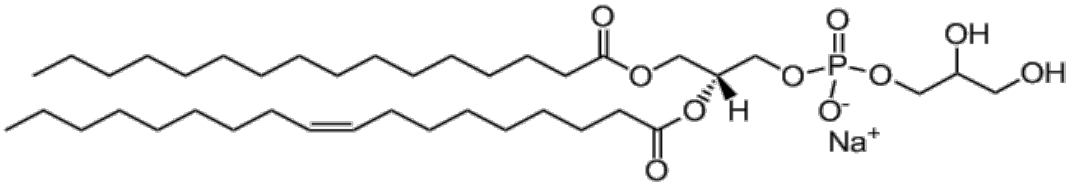

Figure 1. 13 The schematic diagram of the POPG (16:0, 18:1) [61]

1.3.3. 1-palmitoyl-2-oleoyl-sn-glycero-3-phosphoethanolamine (POPE, or 16:0, 18:1 PE)

POPE ($C_{39}H_{76}NO_8P$, M.W = 717.996 g/mole) has the same two hydrophobic acyl chains as POPC and POPG, but a different headgroup. In eukaryotic plasma membranes, PE and PC lipids are the most common zwitterionic lipids. The POPE phospholipid bilayer emphasizes the importance of the head group in acyl chain positioning against the peptides [52]. Since the PE molecule has a smaller cross-sectional area than the PC molecule, studies on PE and PC bilayers showed that the hydrocarbon chain order in PC is lower than in PE bilayers [62][63][64]. In this research I mixed the POPE with POPC and POPG at molar ratios (4/4/2), respectively. We used this ratio to study the effect of headgroups on the peptides-lipid interaction.

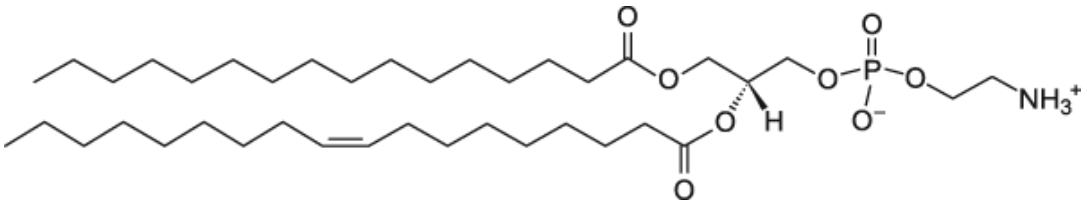

Figure 1. 14 The schematic diagram of the POPE (16:0, 18:1) *[65]*

1.3.4. Cholesterol

Cholesterol ($C_{27}H_{46}O$, M.W = 386.654g/mole) is a ubiquitous component of all animal tissues, where it is found in cell plasma membranes. It is a hydrocarbon compound containing 46 hydrogen 27 carbon atoms, and 1 oxygen atom [66]. Between the hydroxyl group and the hydrocarbon chain there are four hydrocarbon steroid rings, see Fig. 1.14 [66]. Due to its location in the lipid bilayer and interaction with other lipids, the cholesterol, along with the other lipid components, have an important role in bilayer fluidity [67][68]. It plays a crucial role in lipid bilayer organization, function, and dynamics [69][70]. The cholesterol has an amphiphilic property because most of its structure is hydrophobic (hydrocarbon composition), while the hydroxyl (OH) group is hydrophilic, see Fig. 1.14 [66]. Due to its amphipathic nature, the cholesterol is surface-active, enabling the polar hydroxyl group of cholesterol to interact with the polar head of the phospholipid, whereas the hydrophobic steroid ring is positioned parallel to and submerged in the phospholipid bilayer hydrocarbon chains [71] [72][73]. As a result, this causes the packaging of lipids in the bilayer to condense [74]. Furthermore, due to the rigidity of the cholesterol fused ring structure, it appears to segregate fatty acids with saturated acyl chains, resulting in the formation of less fluid phases and the more compact liquid-ordered phase [75][76]. In this research, a 30% mole fraction of cholesterol was mixed with POPC and POPG at molar ratios (80/20) to study the effect of the bilayer interior on the peptide-lipid interaction. The unique physical properties of cholesterol have a complex impact on lipid bilayer properties. Cholesterol has been found to reduce the permeability of a fluid phase bilayer to water [56]. Because cholesterol intercalates between lipid acyl chains, it fills up empty space and

reduces the flexibility of the lipid chains around it. Cholesterol plays a role in membrane phases and regulates membrane fluidity. Previous studies have revealed that cholesterol has a high condensing effect, meaning that the area per molecule of a phospholipid-cholesterol mixture is smaller than in optimal mixing, and this is caused by cholesterol attraction for saturated acyl chains. A decrease in the area per molecule is due to the fact that a membrane behaves like an incompressible fluid. In the cartoon below (Fig. 1.14) each grey head group corresponds to the choline and phosphate. And, it shows that how the cholesterol disrupts the interactions between phospholipids in the fluid phase.

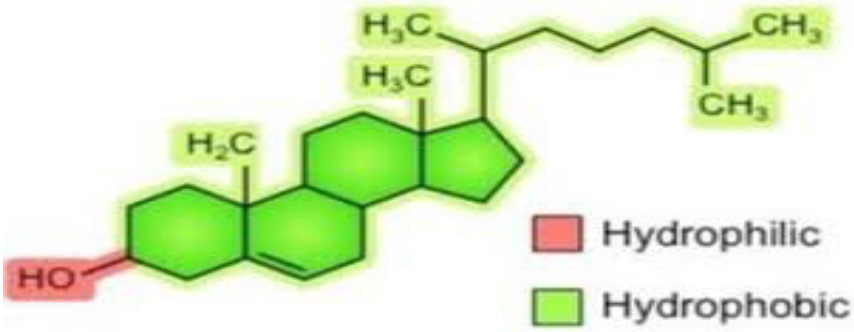

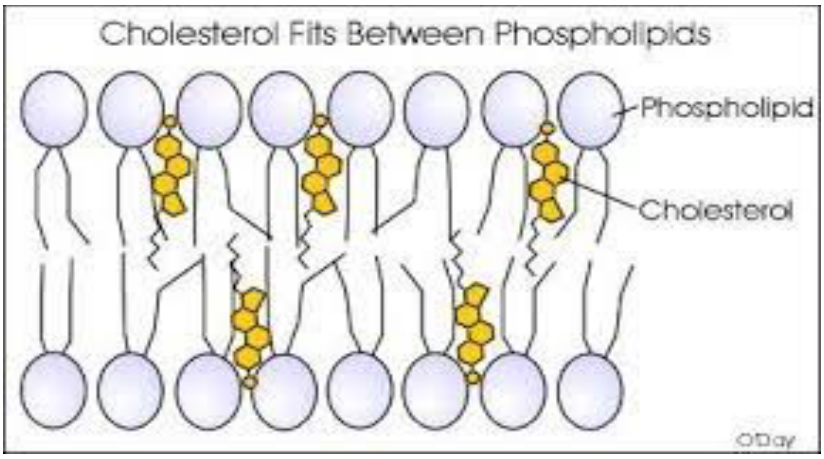

Figure 1. 15 The schematic diagram of the cholesterol chemical structure [66] [77].

1.4. Liposomes

A liposome is a tiny artificial vesicle of spherical shape consisting of one or more lipid bilayers. The name liposome is derived from two Greek words: 'Lipos' and 'Soma' meaning fat and body, respectively. Liposomes were described in the mid-60s by British hematologist Alec Douglas Bangham. Since then, liposomes have been useful in biophysics and biochemistry scientific research on bilayers and cell membranes. They have been used as tool to study drug delivery for cancers and other diseases, and for studying a wide range of membrane properties. In my research I used 100 nm diameter unilamellar liposomes as a model to study the AMP-bilayer interaction. Liposomes are sphere-shaped vesicles composed either of one layer of bilayer, known as unilamellar vesicles (ULVs) or multiple layers of bilayer, known as multilamellar vesicles (MLVs). Depending on the preparation methods, liposomes can vary in size from tens to thousands of nanometers. For instance, small unilamellar vesicles (SUVs) range in size from 20–100 nm, and large unilamellar vesicles (LUVs) range in size from 100–300 nm, while giant unilamellar vesicles (GUVs) are defined as greater than 300 nm, see Fig1.15.

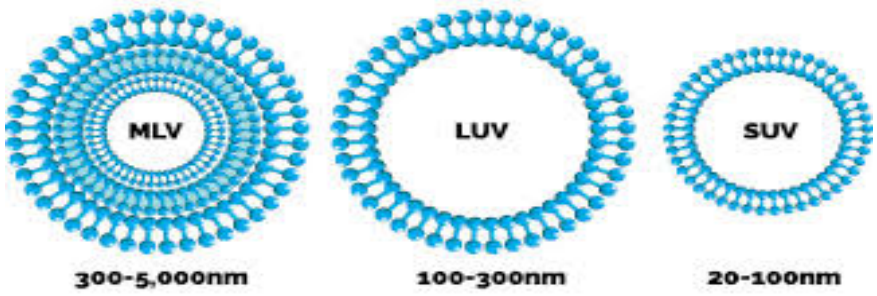

Figure 1. 16 This an overview of liposome types. From left to right, multi-lamellar vesicles (MLV) that range in size from 300–5,000 nm. Large unilamellar vesicles (LUV) range in size from 100–300 nm, and small unilamellar vesicles (SUV) range in size from 20–100 nm.

After we introduced the phospholipids and peptides, and the factors that affect the peptides-lipid bilayer interaction, now we should explain the properties of the fluorophores that are used in this research by using spectroscopy techniques, and the fluorescence measurements.

1.5. Jablonski Energy Diagram

A chromophore or fluorophore is a chemical group that absorbs light at a specific wavelength and then emits light. The wavelength of emitted light is longer, and therefore has a lower frequency (lower energy). Typically, the excited electrons relax due to vibrational and rotational energy transitions before reaching the ground state as shown in the Jablonski diagram in Fig. 1.16.

Fluorescence is the emission of a photon as an excited state decays back to its ground state. Fluorophores come in a variety of electronic states. The ground electronic state is represented by the symbol S0, and the excited electronic states are denoted as S1, S2, etc. There are multiple vibrational energy levels in each electronic state., demoted as 0, 1, 2, etc. as shown in Figure 1.17.

Using light instead of heat to induce fluorescence because the energy gap between the S0 and S1 excited states is often too big for thermal population of S1. A fluorophore is typically stimulated from the ground state S0 to a vibrational sub state of the S1 or S2. Non-radioactive decay causes the majority of the molecules to rapidly relax to the lowest vibrational level of S1. Internal conversion is the term for this procedure, which usually occurs within ~10^{-12} s. Internal conversion is normally complete prior to photon output because fluorescence lifetimes are typically ~10^{-9} s. As a result, fluorophores are usually emitted at S1's lowest vibrational level. The emission spectrum is the consequence of

fluorophores reverting to various vibrational levels of the S0 state. Because the electron decays to the lowest vibrational energy level of the excited state before emitting the photon and returning to the ground state, the emission wavelength is independent of the absorption wavelength. Interestingly, the emission spectrum is typically a mirror image of the absorption spectrum because all electronic transitions are vertical and occur without changing the location of the nuclei, according to the Franck-Condon principle. As a result, if a certain transition between the 0th and 1st vibrational levels has the highest absorption probability, the reciprocal transition has the highest emission probability. Intersystem crossing allows molecules in the S1 state to decay to the first triplet state T1. Because a transition from T1 to the singlet state S0 is banned, such a change takes longer, ranging from 0.1 milliseconds to minutes or even hours. Phosphorescence is the emission of light from T1 to S0, and it produces light with longer wavelengths than fluorescence. The phenomenon of absorption and emission of light is called fluorescence. The average time that it takes the excited electrons to return to the ground state is called the fluorescence emission lifetime. Fluorescence is an experimental method which enables studying of the detailed interactions of molecular mechanisms [71]. Fluorescence lifetime and anisotropy are the most important. There is nothing 'global' about f(t) or r(t) parameters of fluorescence phenomenon (more details about these parameters in the next chapter). Furthermore, the fluorescence parameters are very sensitive to the environment surrounding fluorophores such as the polarity, fluidity, and temperature. Normally, fluorophores are divided into extrinsic and intrinsic types. Intrinsic fluorophores are the natural components of a system such as tryptophan and phenylalanine residues in proteins.

Extrinsic fluorophores are molecules that are added to the composition, such as 1,6-diphenyl-1,3,5-hexatriene (DPH), which is injected into vesicles to study cell membrane properties such as cell membranes dynamics and cell peptides-lipid bilayer interactions.

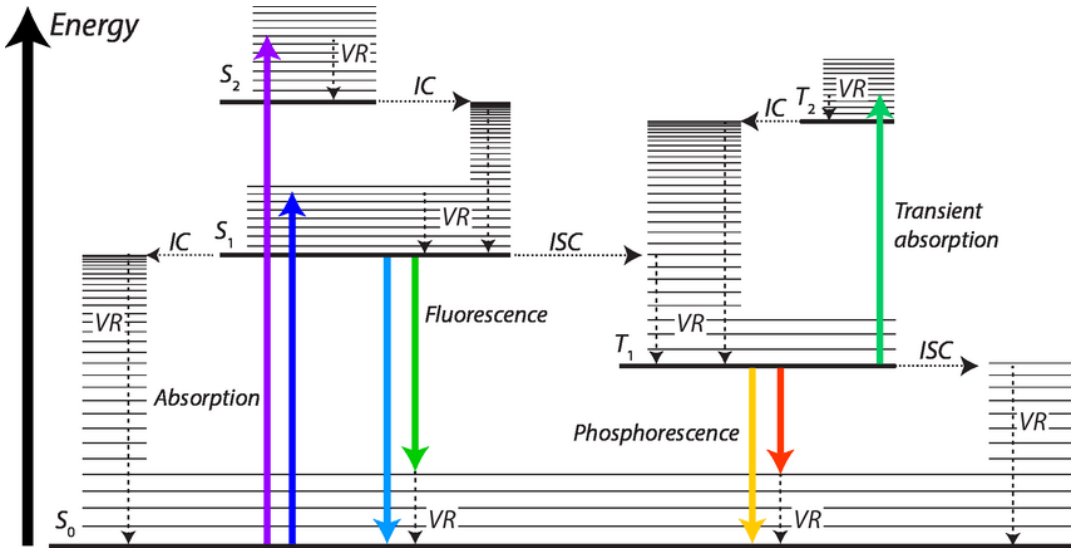

Figure 1. 17 Jablonski diagram illustrates the transition between the electronic states of the molecule [78].

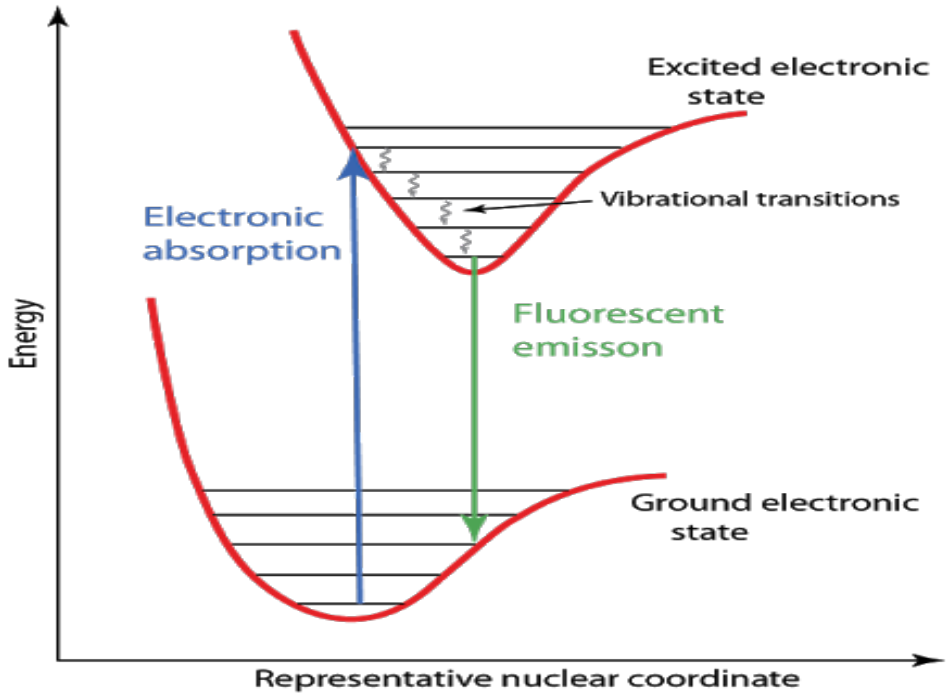

Figure 1. 18 Electronic spectra of the molecules [78].

1.5.1. Diphenyl-1,3,5-hexatriene (DPH)

DPH is one of the most popular fluorescent probes used to study membrane properties. The DPH probe has a high affinity for the lipid bilayer because of its hydrophobic interaction, and as a result it is always distributed into the membrane bilayer [79]. The spectrophotometric properties of DPH are extremely sensitive and extensively used to study membrane-peptide interactions [80][81]. From Fig. 1.19, the excitation and fluorescence spectra of DPH in methanol at room temperature peak at approximately 350 nm and 452 nm respectively and they are environment dependent. DPH fluorescence changes as the phase of membrane bilayer changes, but it is almost non-fluorescent in water. The fluorescence parameters, lifetime, and fluorescence anisotropy of DPH are sensitive to the surrounding environment, so DPH can be used to study the properties of

cell membranes such as polarity, fluidity, and lipids order. The fluorescence lifetime $\langle\tau\rangle$ of DPH in lipids membrane bilayer is ~8 ns at 23°C. The quantum yield Q_F of DPH ($Q_F = \frac{\#\ of\ photon\ emitted}{\#\ of\ photon\ absorbded}$) decreases as the concentration of water increases.

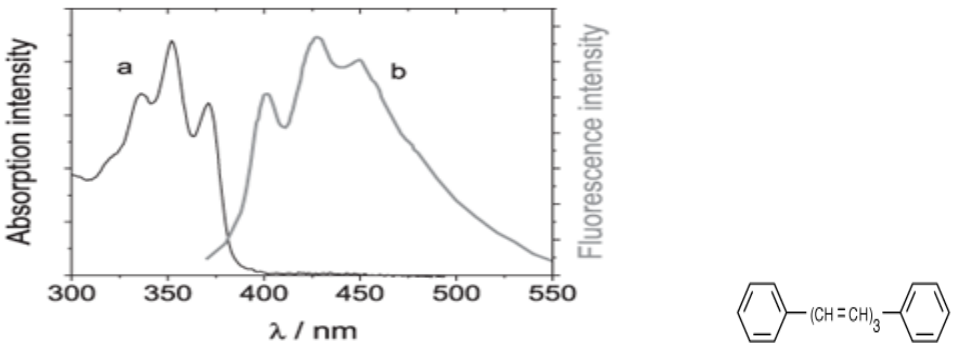

Figure 1. 19 DPH absorption (a) and emission (b) spectra in ethanol**.**

This effect of water on the DPH fluorescence is due to reducing the gap between the electronic excited state S_2 and vibration relaxation excited state S_1 (S_2-S_1 coupling) as shown in the Jablonski diagram in Figure 1.17 [81]. As a result, water does not shift the wavelength of the bands, which is reflected as a weak fluorescence emission or low quantum yield [16].

1.5.2. Tryptophan (Trp)

Melittin has a single tryptophan (Trp) residue, which is a sensitive probe for studying the interaction of melittin with the PLs bilayer [69]. Trp or W19 is one of the 26 amino acid sequence of melittin, as shown in Fig. 1.6. This is particularly useful since melittin contains no other aromatic amino acids, making fluorescence data analysis of Trp easier

due to the lack of heterogeneity and interference [69] [82]. As a result, Tryp fluorescence became an important method that had applied in this research to study the mechanism of melittin binding with membrane bilayers. The excitation and fluorescence spectra of tryptophan peaks are at ~280 nm and ~350 nm respectively, see Fig 1.20 [83]. Fluorescence lifetime of the tryptophan has long been known to be sensitive to the polarity of the environment surrounding it [82].

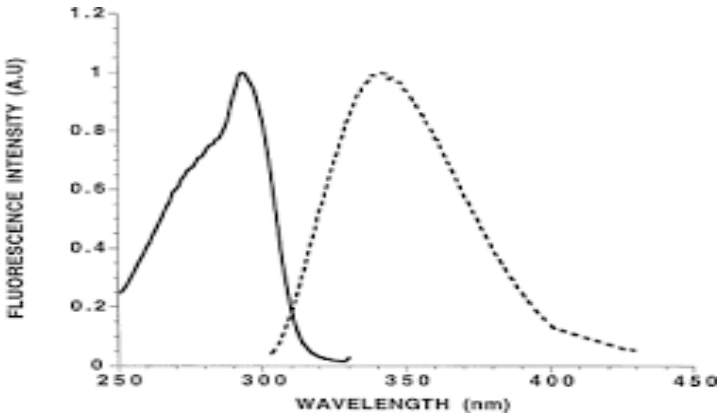

Figure 1. 20 A. Tryptophan absorption and fluorescence spectra [84]. B. Tryptophan electronic absorption transitions in [85]

The summary of this study is: Studying the effect of lipid compositions of the bilayer on the ability of peptides to disrupt it. Three different phospholipid mixtures were investigated in this research to study peptides-bilayer interaction. All these compositions have the same charge surface density, due to the presence of 20% PG, but have different headgroup compositions by adding POPE, and different acyl chain packing because of the cholesterol (CHO). These compositions were prepared with 80% POPC 20% POPG, 40% POPC 40% POPE and 20% POPG, and 80%POPC 20% POPG plus 30% mole fraction of cholesterol. Magainin 2 and melittin are used in the present study as peptides models for studying the

peptide-lipid bilayer interaction. However, the mechanism and the conditions of the interaction between these mixtures with the peptides have not been studied yet.

Based on these interconnected topics, the goals of the present study are:

(i) To investigate the impact of headgroup because of POPE in the peptides-bilayers interaction.

(ii) To elucidate the interior bilayer composition due to the cholesterol on the peptides-bilayers interaction.

(iii) To compare the impact of two peptides (magainin 2 and melittin) on the peptides-bilayers interaction.

In fact, it is widely acknowledged that no single experimental technique can provide a comprehensive structural picture of the interaction; rather, a combination of techniques is required [86].

2. Materials and Methods

2.1. Sample Preparation

2.1.1. Preparation of Liposomes

All phospholipids and cholesterol were acquired from Avanti Polar Lipids (Alabaster, AL), stored at -40°C and used without further purification. Molar ratios of POPC/POPG (8/2), POPC/POPE/POPG (4/4/2) and POPC/POPG (8/2) with molar fraction 0.3 of cholesterol in chloroform were added to glass vials. The vials were rotated under a stream of nitrogen gas to evaporate the chloroform, resulting in a thin lipid film on the inner surface of the vials. 1.0 mL of cyclohexane was added to dissolve the thin lipid film in the vial. The samples were vortexed for around three minutes and frozen for at least half an hour using an *n*-propyl alcohol and dry ice bath. The frozen samples were lyophilized for more than four hours to remove the cyclohexane completely, and to yield phospholipids in the form of a dispersed white powder. Final concentrations of all samples were fixed by adding buffer (HEPES 10 mM, KCl 60 mM, 30 NaCl 60 mM), pH 7.25) to the vials, which were then vortexed thoroughly and subjected to nine freeze/thaw cycles to produce large, multilamellar vesicles. Large unilamellar vesicles (LUVs) were formed by extruding the multilamellar vesicles 11 times through a pair of 0.1 μm membranes using an Avanti Mini Extruder at room temperature. DPH was acquired from Molecular Probes (Eugene, OR), dissolved in tetrahydrofuran (THF), to a concentration of 183 μM and stored under argon at -20°C in a light-proof container. Samples for all fluorescence measurements were prepared at a concentration of 150 μM phospholipid. This was a low concentration, so samples appeared almost clear, which ensured that inner filter effects (re-absorption of

emitted photons) were kept to a minimum. Samples were prepared in 1.5 ml quartz spectrophotometer cuvettes with magnetic stir bars. For samples containing DPH a0.5 μL of DPH stock solution was added to each cuvette to yield a final DPH to phospholipid molar ratio of 1:300.

2.1.2. Preparation of peptides

Melittin ≥85% (HPLC) and Magainin 2 ≥97% (HPLC) were purchased from Sigma-Aldrich and stored at -20°C. Stock solutions were prepared at 250 μM and 150 μM, respectively, by adding 1.4 mL of the buffer to 1.0 mg and 0.5 mg of melittin and magainin 2, then stored at -20°C. Melittin at a concentration of 5 μM in solution were put into 1.5 ml quartz spectrophotometer cuvettes with magnetic stir bars.

2.2. Methods

2.3. Instrumentation

2.3.1. ISS PC1 Photon Counting Spectrofluorometer

For steady-state fluorescence measurements a photon counting spectrofluorometer PC1 (ISS, Urbana, IL) was used in this research. A xenon direct-current (DC) arc lamp is used as the light source, see Fig. 2.5. These lamps, which emit wavelengths ranging from UV to near-infrared, are the brightest manufactured light sources with a wide wavelength range available. Because most of the light emitted by xenon arc lamps is in the UV-Visible region, they are ideal for steady-state measurements. An excitation monochromator is required to pick a narrow range of excitation wavelengths since the lamp emits a broad range of wavelengths. A quantum counter is used to adjust for variations in lamp intensity in steady state measurements.

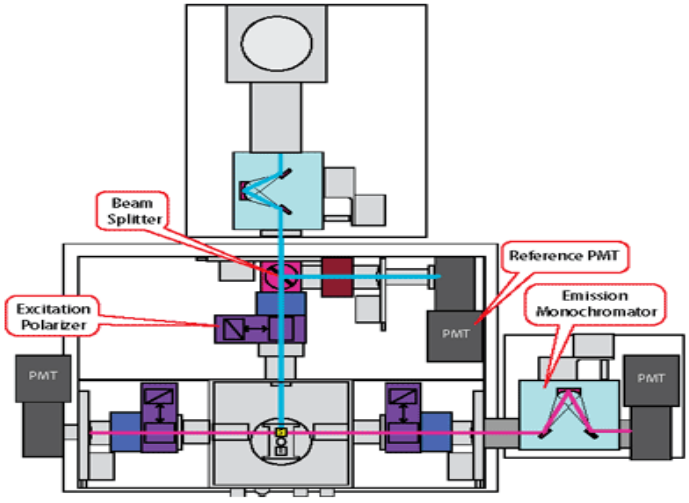

Figure 2. 1 Schematic of the ISS PC1 Photon Counting Spectrofluorometer [87].

PC1 was used in this research to measure the steady-state emission spectra of the tryptophan residue in melittin. Excitation light at 280 nm was shined on the sample, and sample temperature was kept constant at 20°C via a circulating water bath. Emission light from the sample is gathered at a 90° angle to the excitation optics axis. The incoming light is then scattered and scanned across the excitation photomultiplier tube (PMT) using a holographic grating element. Resulting spectra were plotted via Vinci software supported by ISS.

2.3.2. ISS Chronos Spectrometer

Fluorescence excited state and anisotropy decay measurements were performed with a Chronos fluorescence lifetime spectrometer (ISS, Urbana, IL). This Chronos fluorometer (frequency domain) contains the following components: laser source, reference and sample compartments, detectors, wavelength selection, computer, and software (Vinci), and polarizers as shown in Fig. 2.2.

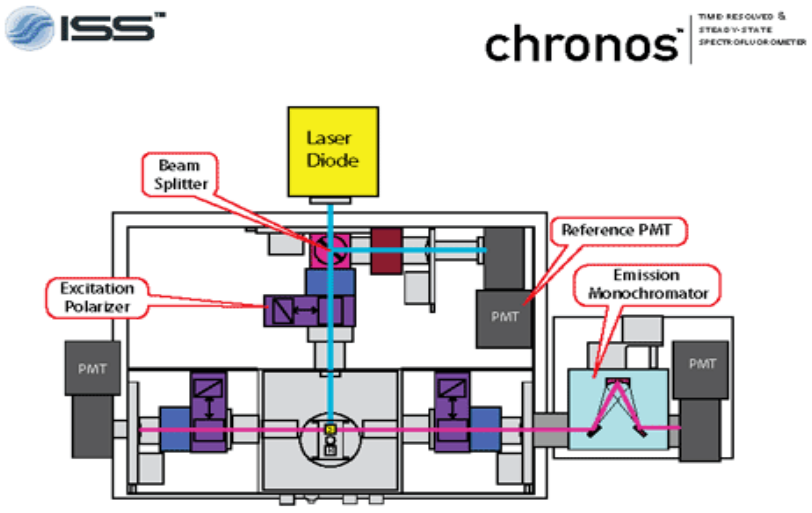

Figure 2. 2 Schematic of Chronos, the Frequency-Domain Fluorometer from ISS [87].

An external function generator modulates the polarized excitation source at high frequency, producing a sinusoidal wave with a typical frequency range of 5-350 MHz. A reference quantum counter and PMT must be employed to adjust for any variations in laser intensity and output wavelength because lasers can vary in intensity with age. A beam splitter is used to send photons from the laser diode to the reference arm. Fluorophore quantum counters, on the other hand, have been replaced due to the need for routine maintenance and the possibility of fluorophore quality variations. The photodiode's comparison spectral range is even wider, with low self-absorption compensation. At each measurement point, excitation photons incident shined on the reference cuvette and then the sample cuvette as sample compartment stage is automatically rotated. The emission photons are gathered and passed through the emission polarizer at an optical path that is aligned at 90° to the laser diode excitation light path. This polarizer is necessary for separating fluorescence lifetimes from rotational data. If we do not place a polarizer in the detection pathway, we are measuring $(I_{\parallel}(t) + I_{\perp}(t))$ which is not the total intensity. As a result, we must change the emission polarizer to the so-called "magic angle," for which $I_{\perp}(t)$ contributes twice as much intensity as the component polarized parallel to the polarized excitation, see equation (2.27) for details about how the magic angle (54.7^0) was calculated. Figs. 2.7-2.9 show some examples of raw data for both lifetime and anisotropy measurements.

Fig. 2.3 and 2.4 show the lifetime measurements raw data or Trp and DPH, respectively. The green symbols, right axis show the change in modulation ratio, while blue symbols on the left axis show the change in phase delay with increasing modulation frequency due to the excited state lifetime of the fluorophore. Excitation was at (290 nm for Trp, and at 37nm

for DPH). Similarly, in Fig. 2.5 the anisotropy decay measurement of the DPH shows the change in modulation ratio and phase delay due to the difference between the horizontally and vertically polarized excitation for vertically polarized emission [88].

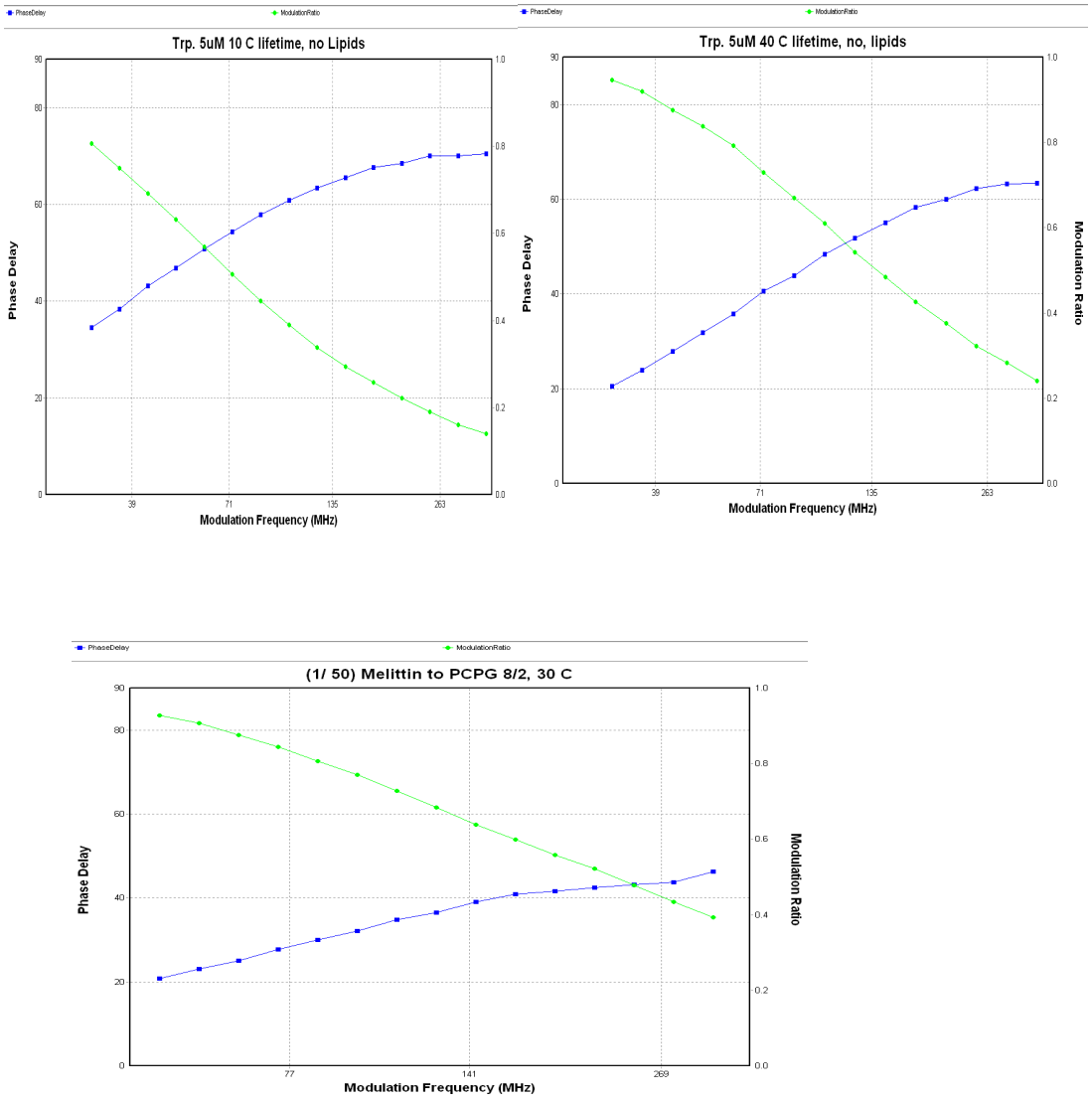

Figure 2. 3 The modulation ratio and phase delay of the lifetime intensity decay of Trp from Chronos instrument (Examples of Raw Lifetime Data).

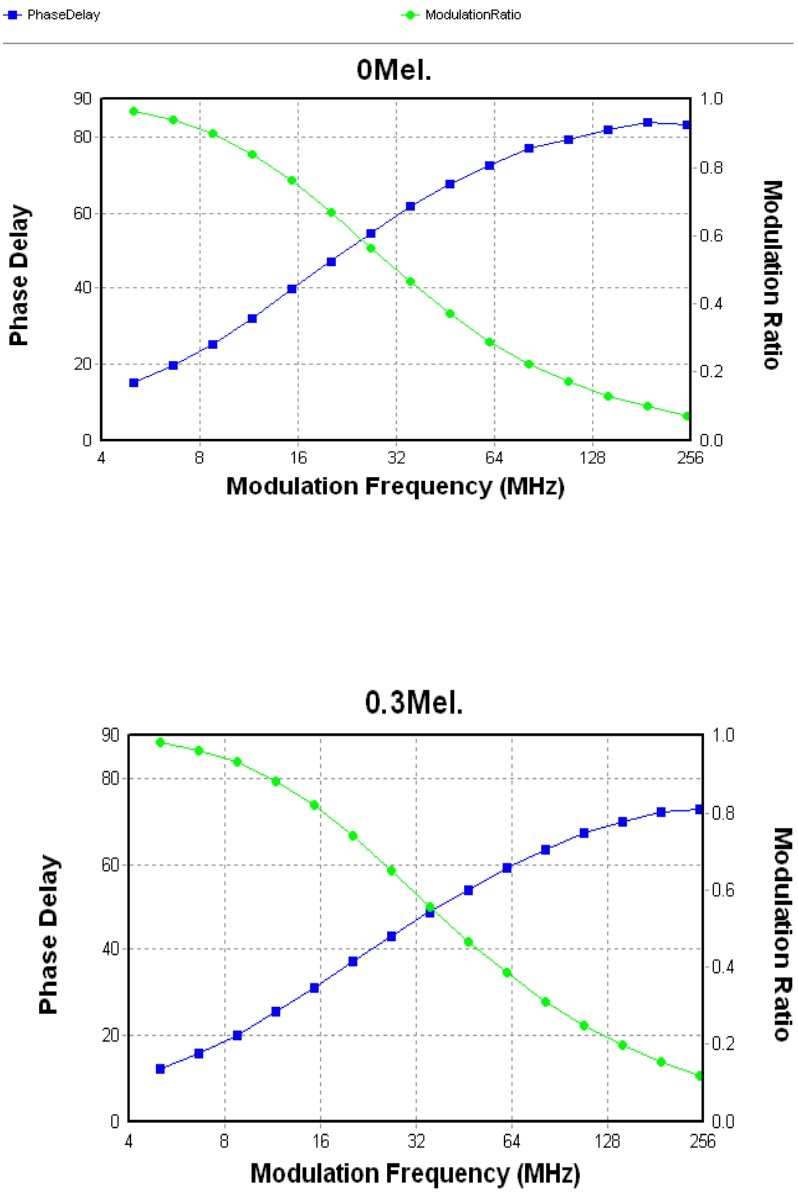

Figure 2. 4 The modulation ratio and phase delay of the lifetime intensity decay of DPH from Chronos instrument (Examples of Raw Lifetime Data).

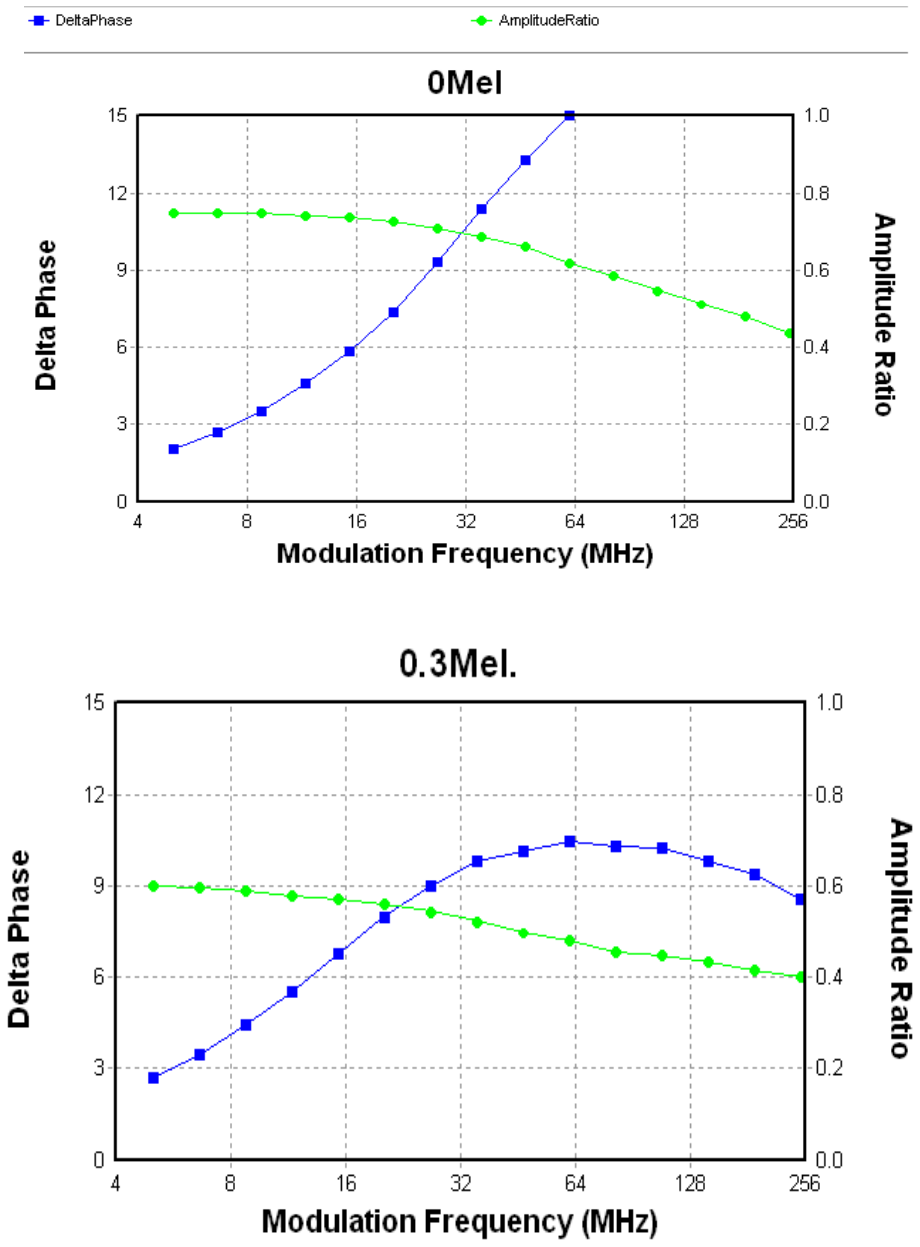

Figure 2. 5 The modulation ratio and phase delay of the anisotropy decay of DPH Chronos instrument (Examples of Raw Anisotropy Data).

2.3.3. Fluorescence measurements

Fluorescence spectroscopic analysis can provide structural and dynamical information of cellular membranes and lipid bilayers on the nanosecond timescale [89][90][91]. This information is contained in the steady-state florescence measurements or time-resolved fluorescence intensity decay and anisotropy decay of either extrinsic or intrinsic fluorophores such as DPH and tryptophan residue in melittin, respectively [92]. In principle, the parameters that characterize the time-resolved decays could be obtained by measurements in either the frequency-domain or in the time-domain [89] [92]. Frequency-domain measurements (FD) have been applied in this research for both fluorescence intensity and anisotropy decays [93][94]. Fluorescence lifetime and differential polarization measurements were performed with a frequency domain, or phase-mod, Chronos Lifetime Spectrometer (ISS, Urbana, IL). FD in which the intensity of the excitation source is modulated at a high frequency that related to the reciprocal of the lifetime. The theory of FD has been described extensively in the reference [95]. The laser source that was used to excite DPH has a wavelength $\lambda_{Exc.} = 374\ nm$ (supported by Chronos). Fifteen modulation frequencies were used (using a Chronos (ISS) frequency domain), logarithmically spaced from 5 to 250 MHZ. All the fluorescence intensity decay measurements of DPH were at 30°C maintained using a water-circulating thermostat, and a buffer with a PH=7.25. A cut-off filter was used in the emission light path to eliminate scattered light. Similarly, a wavelength $\lambda_{Exc.} = 290\ nm$ from an LED light source (supported by Chronos) was used in this experiment to excite the tryptophan residue in melittin, and appropriate filters in the emission light path were used to remove any scattered

excitation light. Fifteen modulation frequencies were used, similarly to DPH, but logarithmically spaced from 20 to 300 MHz for melittin in solution at temperature 10, 23, 30, 35 and 40°C, and from 50 to 350 MHz for other lifetime measurements with melittin added to lipids. For both fluorophores, the best fit to the fluorescence decay data was obtained using a two-exponential decay model as described in Eq. 2.11. Two fluorescence lifetimes for both Trp and DPH are consistent with the extensive literature for these two fluorophores. All lifetime measurements were made with the emission polarizer at the magic angle of 54.7° from the vertical polarized excitation beam, and with 1, 4-bis(5-phenyloxazole-2-yl) benzene (POPOP) ($\langle \boldsymbol{\tau} \rangle$=1.35 ns) in absolute ethanol as a lifetime reference [17].

2.3.4. Analysis of Steady-State Fluorescence Measurements

Steady state fluorescence spectra when fluorescent molecules are excited by a constant wavelength of light, and the emission photons are detected as a function of specific range of wavelengths [96]. The emission spectrum of the fluorophore provides information about the excited wavelengths that molecules will absorb in order to emit a single emission spectrum. The excitation and emission spectra for a fluorophore are mirror images of each other as shown in Fig. 2.6. The wavelength of the emission spectrum of a fluorophore is higher (lower energy) than the wavelength of the absorbance or excitation spectrum. The difference between the maximum fluorescence emission wavelength and the maximum absorption wavelength is called Stokes shift.

The changes of the peak wavelength or the intensity of the emission spectrum of a fluorophore are sensitive to the local environment such as pH, temperature, interaction with another molecule around it.

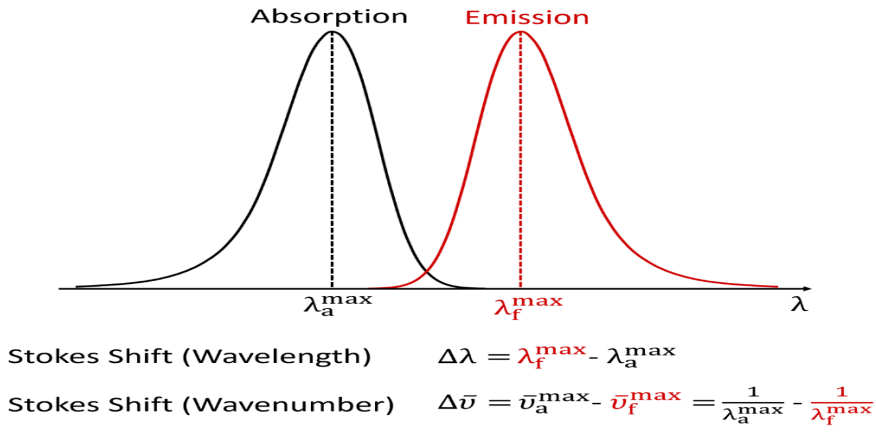

Figure 2. 6 The black is excitation spectrum , and the red is the emission spectrum [97].

2.3.5. Analysis of Time-Resolved fluorescence intensity decay measurements

In the frequency domain FD, the excitation light E(t) is intensity modulated at excessive frequency [95]. As a result, the emitted fluorescence F(t) is modulated on the identical excessive frequency, however the emitted fluorescence will display a phase-shift (∅) and demodulation because of non-instant fluorescence decay (lifetime) according to [18][95]:

$$E(t) = E_0[1 + M_E \sin(\omega t)] \quad (2.1)$$

$$F(t) = F_0[1 + M_F \sin(\omega t - \emptyset)] \quad (2.2)$$

Where, E_0 is the average excitation intensity, $F_0$is the average fluorescence intensity, and ω is the angular frequency of modulation, see Fig. 2.7 [98] [99]. The values of the phase-shift (∅) and demodulation M depend on the fluorescence lifetime (τ) of the fluorophore and can be described according to:

$$\tan(\emptyset) = \omega\tau_\emptyset \quad (2.3)$$

Therefore,

$$\tau_\emptyset = \frac{\tan(\emptyset)}{\omega} \quad (2.4)$$

Where, $\tau_\emptyset$ is the phase lifetime.

The modulations of the excitation (M_E) and the emission (M_F) are given by:

$$M_E = \left(\frac{b}{a}\right)_{EX.} \quad (2.5)$$

$$M_F = \left(\frac{B}{A}\right)_{EM.} \tag{2.6}$$

Where a, b are the amplitude and offset of the excitation wave, and A, B are the amplitude and offset of emission wave.

Therefore, the relative modulation, M, of the emission is then:

$$M = \frac{M_F}{M_E} = \frac{1}{\sqrt{1+(\omega\tau_M)^2}} \tag{2.7}$$

Therefore,

$$\tau_M = \frac{1}{\omega}\sqrt{\frac{1}{M^2} - 1} \tag{2.8}$$

Where, τ_M is the modulation lifetime

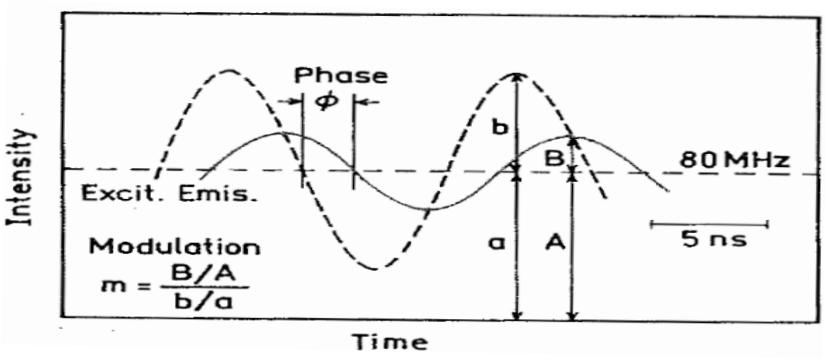

Figure 2. 7 Excitation light is modulated at a certain frequency

(dot line) is the excited light of the fluorophore, while (solid line) is the emitted light (fluorescence). We can determine the fluorescence lifetime of a fluorophore from the change in magnitude (M) and phase (Ø) *[100]*.

Time-resolved measurement is used to determine the fluorescence intensity decay law of the excited state of the fluorophore. The excited state decay law of a fluorophore to the ground state can be expressed as:

$$I(t) = I_0 e^{-\frac{t}{\tau}} \tag{2.9}$$

Where, I_0 is the intensity at t=0 (upon excitation), τ is the lifetime (the time for the intensity to drop by 1/e of it is initial value).

In terms of the rate constants k_r (radiative) and k_{nr} (non-radiative), the fluorescence lifetime can be written as below:

$$\tau = \frac{1}{k_r + k_{nr}} \tag{2.10}$$

Typically, samples display multi-exponential decay in time due to many factors such as resonance energy transfer and collisional quenching. For a double exponential the intensity excited state can be expressed as [98]:

$$I(t) = \alpha_1 e^{-\frac{t}{\tau_1}} + \alpha_2 e^{-\frac{t}{\tau_2}} \tag{2.11}$$

Where, α_1 and α_2 are the normalized pre-exponential factors (intensity weighted factors) such that $\sum_i \alpha_i = 1$, τ_1 and τ_2 are the fluorescence intensity decay time constants [101]. Therefore, the average fluorescence lifetime $\langle\tau\rangle$ can be determined from the equation below:

By taking the integral for the dominator and nominator of equation 10 we get:

$$\langle\tau\rangle = \frac{\int_0^\infty t\, I(t)\, dt}{\int_0^\infty I(t)\, dt} = \frac{\int_0^\infty t\left(\alpha_1 e^{-\frac{t}{\tau_1}} + \alpha_2 e^{-\frac{t}{\tau_2}}\right) dt}{\int_0^\infty \left(\alpha_1 e^{-\frac{t}{\tau_1}} + \alpha_2 e^{-\frac{t}{\tau_2}}\right) dt} \tag{2.12}$$

$$\langle\tau\rangle = \frac{\alpha_1\tau_1^2 + \alpha_2\tau_2^2}{\alpha_1\tau_1 + \alpha_2\tau_2} \tag{2.13}$$

The fluorescence decay data was analyzed by nonlinear least squares. [102]. For any decay law the modulation and phase shift values can be predicted by using cosine and sine transforms of the intensity decay I(t):

$$D_\omega = \frac{\int_0^\infty I(t)cos\omega t\, dt}{\int_0^\infty I(t)\, dt} \tag{2.14}$$

$$N_\omega = \frac{\int_0^\infty I(t)sin\omega t\, dt}{\int_0^\infty I(t)\, dt} \tag{2.15}$$

where ω is the angular modulation frequency ($\omega = 2\pi f$). In case of a sum of exponentials, the modulation and phase shift values can be determined from:

$$D_\omega = \frac{\sum_i \left[\frac{\alpha_i \tau_i}{(1+\omega^2\tau_i^2)}\right]}{\sum_i \alpha_i \tau_i} \tag{2.16}$$

$$N_\omega = \frac{\sum_i \left[\frac{\alpha_i \omega \tau_i^2}{(1+\omega^2\tau_i^2)}\right]}{\sum_i \alpha_i \tau_i} \tag{2.17}$$

Now, we can calculate the values of demodulation ($m_{c\omega}$) and phase shift ($\phi_{c\omega}$) by the following equations:

$$m_{c\omega} = (N_\omega^2 + D_\omega^2)^{1/2} \tag{2.18}$$

$$\phi_{c\omega} = \tan^{-1}(N_\omega / D_\omega) \tag{2.19}$$

In the least-squares analysis method, we vary the parameters α_i and τ_i to minimize the value of the goodness-of-fit parameter χ_R^2:

$$\chi_R^2 = \frac{1}{\upsilon}\sum_\omega \left[\frac{\phi_\omega - \phi_{c\omega}}{\delta_\phi}\right]^2 + \frac{1}{\upsilon}\sum_\omega \left[\frac{m_\omega - m_{c\omega}}{\delta_m}\right]^2 \tag{2.20}$$

Where υ equals the number of data points minus the number of parameters (the number of degrees of freedom). m_ω and ϕ_ω are measured data of the modulation and phase shift, δ_m and δ_ϕ are the standard deviation of the modulation and phase shift values and they are set equal to 0.004 and 0.2, respectively, by convention [103]. In this research, a

Fortran program was designed to minimize the value of χ_R^2 from the best fit values of $m_{c\omega}$and $\phi_{c\omega}$. χ_R^2 is expected to be near one for the appropriate initial parameters that were entered in the model, if χ_R^2 is significantly bigger than one, it is reasonable to reject the model.

2.3.6. Analysis of Time-Resolved Anisotropy decay measurements

Generally, fluorophores are oriented in time and space randomly even in the case of the fluorophore probe labeled in a molecular system such as DPH probe in bilayers membrane. Imagine that a stationary fluorophore was excited by a polarized light source followed by polarized fluorescence emission in the same plane see Fig. 2.8 A [104]. Anisotropy is a measure of the degree of polarization of the fluorescence emission and is a measure of how much a fluorophore in a molecular system such as a cell membrane bilayer has rotated. As a result, the anisotropy has been used to study the order and disorder (phase diagram) of the biological system [105] [21]. For instance, the anisotropy $r(t)$ of the fluorophores have a value of zero if the emission is unpolarized. The fluorophore DPH is a good model to study the phase diagram of the phospholipids in lipid bilayers due to both its dipole moment arranged parallel to an excited electric field of light and parallel rotation of the acyl chain of the lipids [103]. We can define the fluorescence anisotropy $r(t)$ as how much emission of fluorescence is polarized after polarized excitation see Fig. 2.8. B [104][106]. A measure of the fluorescence anisotropy $r(t)$ can be used to determine the rotational correlation time of a fluorophore in an environment, and it is defined as

$$r(t) = \frac{I_{\parallel}(t) - I_{\perp}(t)}{I(t)} = \frac{I_{\parallel}(t) - I_{\perp}(t)}{I_{\parallel}(t) + 2I_{\perp}(t)} \tag{2.21}$$

$I(t)$ is the total intensity $I(t) = I_{\parallel}(t) + 2I_{\perp}(t)$, and $I_{\perp}$ and $I_{\parallel}$ are the intensities of the observed perpendicular and parallel components, respectively.

In case of a fluorophore not fully free to rotate, see Fig. 2.9, then r_{∞} a non-zero limiting anisotropy will manifest in the a single exponential anisotropy decay as [90] [107].

$$r(t) = (r_0 - r_{\infty})e^{-t/\emptyset} + r_{\infty} \quad (2.22)$$

Where, $r(t)$ is the anisotropy, r_0 is the initial anisotropy, r_{∞} is the anisotropy at infinite time, and $\emptyset$ is the rotational correlation time. An empirical formula that describes anisotropy decay is a simple sum of exponentials:

$$r(t) = (r_0 - r_{\infty})\left[\sum_{i=1}^{N} \beta_i e^{-t/\emptyset_i}\right] + r_{\infty} \quad (2.23)$$

The model that we employed in this research to analyze our data (BRD model) was obtained via analysis in terms of just a simple sum of three exponentials for the anisotropy decay as:

$$r(t) = (r_0 - r_{\infty})\left[\beta_1 e^{-t/\emptyset_1} + \beta_2 e^{-t/\emptyset_2} + \beta_3 e^{-t/\emptyset_3}\right] + r_{\infty} \quad (2.24)$$

Where $\emptyset_1$ and $\emptyset_2$ are the rotational correlation times, and $\beta_1, \beta_2, \beta_3$ are weighing factors and:

$$\sum_{i=1}^{3} \beta_i = \beta_1 + \beta_2 + \beta_3 = 1 \quad (2.25)$$

The average rotational relaxation lifetime $\langle\emptyset\rangle$ can be obtained:

$$\langle\emptyset\rangle = \sum_{i=1}^{3}(\beta_i\, \emptyset_i) \quad (2.26)$$

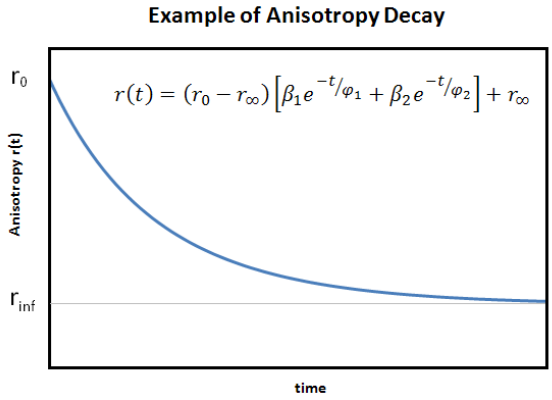

Figure 2. 8 The anisotropy decay of a fluorophore which is not fully free to rotate.

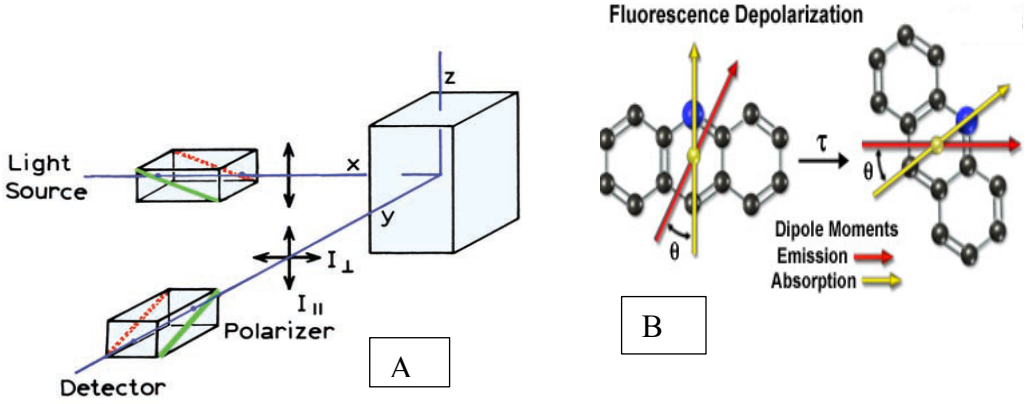

Figure 2. 9 **A.** The polarized absorption light and polarized fluorescence emission light, **B.** The direction of the diploe moment between the absorption and the fluorescence emission.

The initial anisotropy $r(0)=r_0$ can be defined according to:

$$r_0 = \frac{2}{5}\left(\frac{3\cos^2(\beta)-1}{2}\right) \tag{2.27}$$

Where β is the angle between the absorption and emission dipoles.

The maximum r_0 corresponds to the angle $\beta = 0$

Therefore, the theoretical max value for r_0 = 0.4. Since the angle β does not equal zero for the real molecule, the value r_0 is less than 0.4.

Order parameter S and the average of anisotropy $\langle r \rangle$ according to [108]:

$$S = \sqrt{\frac{r_\infty}{r_0}} \tag{2.28}$$

$$\langle r \rangle = \frac{\int_0^\infty r(t)\, I(t)\, dt}{\int_0^\infty I(t)\, dt} \tag{2.29}$$

By substituting the Eq. 2.9 and Eq. 2.22 in Eq. 2.29 and taking the integral:

$$\langle r \rangle = r_\infty + \frac{r_0 - r_\infty}{1 + \frac{\langle \tau \rangle}{\langle \emptyset \rangle}} \tag{2.30}$$

The first term of the Eq. 2.28 (r_∞) represents the structural contribution, and the second term $\frac{r_0 - r_\infty}{1 + \frac{\langle \tau \rangle}{\langle \emptyset \rangle}}$ represents the kinetic contribution.

From the equation (2.27) we can find the angle (magic angle) when $r_0 = 0$. In order $r_0 = 0$ the quantity $(3\cos^2(\beta) - 1)$ must be zero. Therefore, the magic angle can be obtained such as:

$(3\cos^2(\beta) - 1)$=0, then $\beta = \cos^{-1}\left(1/\sqrt{3}\right)$=$54.7^0$

The magic angle is very important parameter to set up the ISS for fluorescence intensity decay measurements.

2.4. Brownian Rotational Diffusion Model (BRD)

The empirical sum-of-exponentials model of anisotropy decay shown in Eq.2.23 can provide information about the rotational correlation times $\langle\emptyset\rangle$ of DPH, but it does not provide any information about the range of the DPH equilibrium angular orientations restricted by phospholipid acyl chains around it [109]. Therefore, the anisotropy decay data was analyzed using the Brownian Rotational Diffusion model (BRD model). The BRD model is based on an approximation of the solution of the Smoluchowski equation and establishes a theoretical framework for investigating the orientational distribution of a free-tumbling fluorescence probe with cylindrical symmetry [110] [111]. The analysis applies to the probe having effectively cylindrical symmetry. The symmetry is taken along Z axis. Therefore, the orientational distribution function of the probe depends only on θ. The predicted orientational distribution function can be written as a series expansion of the Legendre polynomials [110][111] [112]:

$$f(\theta) = \sum_n \frac{1}{2}(2n+1)\langle P_n\rangle P_n(\cos\theta) \tag{2.31}$$

Where $P_n(\cos\theta)$ Legendre polynomial for even ***n***, and $\langle P_n\rangle$ is the nth rank orientational order parameters that can be determined according to:

$$\langle P_n\rangle = \int_0^{\pi} \sin(\theta)\, f(\theta) P_n(\cos\theta)\ d\theta \tag{2.32}$$

For macroscopically isotropic systems, only the two order parameters $\langle P_2\rangle$ and another for $\langle P_4\rangle$, can be used to construct a symmetrical orientational distribution function $f(\theta)$ of the fluorophore molecule [103]:

$$f(\theta) = N^{-1}\exp\left[L_2 P_2(\cos\theta) + L_4 P_4(\cos\theta)\right] \tag{2.33}$$

Where L_2 and L_4 are weighting factors determined by simultaneously solving two versions of equation 2.32 , one for $\langle P_2 \rangle$ and another for $\langle P_4 \rangle$, and N is the normalization constant determined by [103]:

$$N = \int_0^{\pi} \sin(\theta) \exp\left[L_2 P_2(\cos\theta) + L_4 P_4(\cos\theta)\right] \, d\theta \tag{2.34}$$

For measurements on vesicle suspensions (macroscopically isotropic system), we can only extract the first two order parameters, $\langle P_2 \rangle$ and $\langle P_4 \rangle$ from the experimental data due to the symmetry of the dipole transition [24]. The BRD model depends on the diffusion coefficient D_{perp} about the symmetry axis of the molecule , the order parameters $\langle P_2 \rangle$ and $\langle P_4 \rangle$, and the anisotropy decay r_0 (at t=0) according to [24]:

$$r(t) = r_0 \left(\sum_{i=1}^{3} g_i e^{-t/\phi_i} + g_4 \right) \tag{2.35}$$

Where

$$g_1 = \frac{1}{5} + \frac{2}{7}\langle P_2 \rangle + \frac{18}{35}\langle P_4 \rangle - \langle P_2 \rangle^2$$

$$g_2 = \frac{2}{5} + \frac{4}{7}\langle P_2 \rangle - \frac{24}{35}\langle P_4 \rangle$$

$$g_3 = \frac{1}{5} - \frac{4}{7}\langle P_2 \rangle + \frac{6}{35}\langle P_4 \rangle$$

$$g_4 = \langle P_2 \rangle^2$$

And

$$\phi_1 = g_1 \Big/ \left[6D_T \left(\frac{1}{5} + \frac{1}{7}\langle P_2 \rangle - \frac{12}{35}\langle P_4 \rangle \right) \right]$$

$$\emptyset_2 = {g_2}\Big/\left[12D_T\left(\frac{1}{5}+\frac{1}{14}\langle P_2\rangle+\frac{8}{35}\langle P_4\rangle\right)\right]$$

$$\emptyset_3 = {g_3}\Big/\left[12D_T\left(\frac{1}{5}-\frac{1}{7}\langle P_2\rangle-\frac{2}{35}\langle P_4\rangle\right)\right]$$

The recovered values of $\langle P_2\rangle$ and $\langle P_4\rangle$, as well as the Legendre polynomials that go with them, can be used to build an orientational distribution function based on Eq. 2.31. The shortened series that results, however, can have negative values of $f(\theta)$. As a result, the recovered values of $\langle P_2\rangle$ and $\langle P_4\rangle$ in terms of an orientational distribution function require the use of a specific functional form for $f(\theta)$, which must satisfy the general constraints

$$f(\theta) \geq 0 \tag{2.36}$$

$$\int_0^\pi f(\theta)\ d\theta = 1 \tag{2.37}$$

Our findings for $f(\theta)$ support the theory that DPH orientation in lipid membranes is caused by a local effective orienting potential. Probes are trapped between lipid acyl chains in free volume cavities inside the bilayer structure, resulting in a confinement effect. Thus, our findings support the hypothesis that cylindrical probes in lipid membranes can be treated similarly to molecules in liquid crystals, using mean-field theoretical descriptions like Maier- Saupe potentials, which are also closely related to the BRD model's major assumptions. The order parameters $\langle P_2\rangle$ and $\langle P_4\rangle$ are related to $f(\theta)$ through the use of two connected integral equations of the sort illustrated in Eq. 2.32, which means that $f(\theta)$ can only have two parameters that can be two adjustable [113].

The Brownian Rotational Diffusion model (BRD) was used to determine the three pre-exponential factors in equation 2.24 and substituted in the equation 2.25 to calculate the rotational correlation time of DPH that describes the dynamics of DPH in the bilayer. Second, the anisotropy decay analysis leads to information regarding the order of the PLs acyl chains ensemble throughout the depth of the bilayer by using the angular orientational probability distribution function of the DPH probe, $f(\theta)\sin(\theta)$, as described in equation 2.31. Also, $f(\theta)\sin(\theta)$ was used to examine the changes induced by the concentration of peptides (melittin and magainin 2) in detail and how peptide- induced changes in ensemble acyl chains of order depends upon peptides concentration and the lipid bilayer composition.

3. Results and data analysis

3.1. Steady-State fluorescence measurements of lipid-bound melittin

The steady-state fluorescence emission spectra of the intrinsic tryptophan (Trp) residue in melittin were investigated to follow the binding of melittin to large unilamellar vesicles (LUVs). **The objective of this study was to characterize** the effect of the negatively charged (PC/PG) and zwitterionic (PC) on the binding of melittin to lipid vesicles and examine how the polarity of the environment can affect this binding. To study that, melittin at a concentration of 5 μM in buffer was excited at 280 nm, and the emission spectra of Trp was recorded from 320 nm to 400 nm. Our results show that in the absence of lipids, the maximum fluorescence emission wavelength is about λ_{max}~$352\ nm$, in agreement with values found in the literature [114][115][116].

The binding of melittin to POPC and POPC/POPG was monitored at different molar ratios of melittin to lipids, see table 1. A blue shift in the maximal emission wavelength (λ_{max}) of the emission spectra of the Trp was observed, which indicates melittin binds to the lipid bilayer, as shown in Fig. 3.1A. This shift was due to the different local polarities (dielectric constant) of the buffer and the bilayer interference between the hydrophilic headgroups and the hydrophobic bilayer interior [117][118]. The λ_{max} shift from the results was calculated and it ranged from 352 to 326 nm for POPG-containing lipid vesicles, and from 352 to 330 nm for POPC vesicles. By comparison, this blue shift is larger in negatively charged vesicles composed of POPC/POPG than in purely zwitterionic POPC due to more negative charges on the surface (PG), Fig. 3.1B. The photophysical characteristics of Trp are

extremely sensitive to its local surroundings [117] [119] [120]. Although many studies pointed out that the sensitivity of Trp fluorescence emission and fluorescence excited state decay due to the polarity of the local environment, specific details about the effect of the environment on the fluorescence parameters are still not clear. **One of the goals in this research is** to explain in detail the effect of the dielectric constant on the changes of the global parameters for both steady-state fluorescence intensity and time-resolved fluorescence decay of Trp (details of time-resolved results will be discussed in the next section). Dielectric constant information can provide details about lipid-bound melittin due to the changes of the fluorescence parameters of the Trp. Gramse et al., (2013) have shown that the dielectric of a lipid bilayer in the interfacial polar region can be estimated according to [121]:

$$\frac{\boldsymbol{h}}{\boldsymbol{\epsilon_{r,\ Vesicle}}} = \frac{\boldsymbol{h_{polar}}}{\boldsymbol{\epsilon_{r,\ polar}}} + \frac{\boldsymbol{h_{core}}}{\boldsymbol{\epsilon_{r,core}}} \tag{3.1}$$

$\boldsymbol{h}$ is the total thickness of the hydrophobic and polar regions together (including both leaflets), which is about 5 nm for all of lipids used in this research. $\epsilon_{r,\ polar}$ and $\epsilon_{r,core}$ are the dielectric constants of the headgroup (polar) and hydrocarbon (hydrophobic) regions, respectively.

Gramse and coworkers measured 3.2 for the entire, hydrated bilayer. Using this value, and assuming that the value for hexane approximates the dielectric in the hydrophobic core [121].

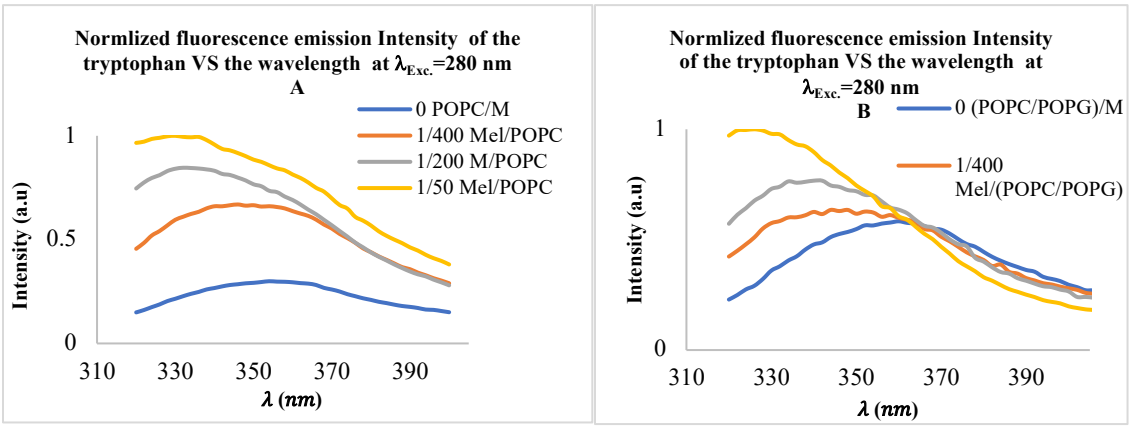

Figure 3. 1 A. The effect of adding POPC on the fluorescence emission spectrum of tryptophan residue in melittin. **B.** The effect of adding POPC/POPG on the fluorescence emission spectrum of tryptophan in melittin.

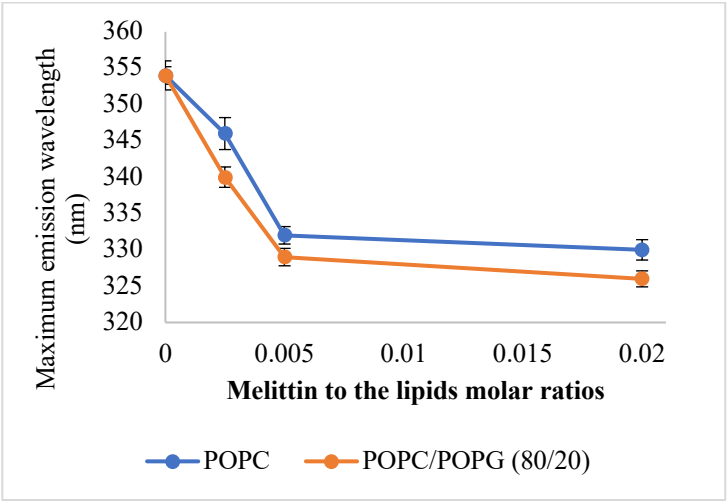

Figure 3. 2 The maximum wavelength as a function of the addition of lipids to melittin.

The comparatively more dramatic blue shift in the max peaks of these spectra indicates stronger binding of melittin to POPC/POPG (80:20) (in orange). POPC (in blue) shows slightly slower binding than POPC/POPG.

It is clear that the dielectric at room temperature changes from ~70 in buffer close to the bilayer surface to 30 in the polar headgroup region and then to ~2 in the bilayer core. Clearly in the dynamic environment of the lipid bilayer these changes in dielectric constant

cannot be abrupt, occurring suddenly at specific depths. It is more reasonable that they occur with steep gradients, particularly at the transition from the bulk to the headgroup region. The decrease in λ_{max} reflects the local effective dielectric constant, and it decreases for a more hydrophobic environment surrounding the intrinsic Trp residue [82][114].

Table 3. 1 Maximal Trp emission wavelength as a function of Melittin/ Lipids molar ratios at room temperature (20°C)

Mel/L (Molar ratio)	**Fluorescence emission maximum λ_{max}(nm)**		**Stokes Shift(nm) $\Delta\lambda = \lambda_{max} - \lambda_{Exc.}$**	
	Mel/POPC	**Mel/ (POPC/POPG)**	**Mel/POPC**	**Mel/ (POPC/POPG)**
Mel. in solution	352±1.82	352±1.82	72	72
1/400	346±1.61	340±1.23	66	60
1/200	332±1.10	329±1.08	52	49
1/50	330±1.14	326±1.04	50	46

The differences between Mel/l=1/400 and 1/200, was 14 nm (346 nm – 332 nm) for POPC and 11 nm (340 nm – 329 nm) for POC/PPG. The decrease in those differences with increasing melittin concentration implies that the blue shift essentially reaches a plateau for both vesicle compositions as shown in Fig. 3.2. This plateau indicates that all of the Trp is in the lower dielectric environment of the lipid groups, which corresponds to the near complete binding of melittin to the vesicles.

3.2. Time-resolved fluorescence measurements of melittin-lipid bilayer interaction

3.2.1. Fluorescence lifetime of tryptophan of lipid-bound melittin

Binding of melittin to bilayer could be affected by many factors such as pH, acyl chain packing in the bilayer interior, and packing stress in the headgroup region. For instance,

the presence of cholesterol in the phospholipid bilayer interior might inhibit melittin-induced bilayer lysis due to enhanced van der Waals attraction between the acyl chains. The presence of negatively charged headgroups will increase the binding and facilitate lysis, but this could be somewhat negated by the presence of hexagonal phase preferring headgroups like PE. [118][122][123].

In this study, I monitored the binding of melittin to POPC/POPG (8/2), POPC/POPE/POPG (4/4/2), and POPC/POPG (8/2) + 30% CHO vesicles (LUVs). All these vesicles have the same negative charge density due to the same molar content of POPG but different headgroup composition due to POPE, and different acyl chain packing properties due to cholesterol.

The goal in this experiment was to investigate the possible role of differences in headgroup region and the bilayer interior on the melittin-bilayer interaction, as reported by the fluorescence lifetime of the Trp in melittin. An additional goal was to determine the critical melittin/lipid molar ratios needed to reach complete binding of melittin. Time-resolved fluorescence lifetime measurements of the intrinsic Trp residue in melittin have been utilized in this research to investigate the binding of melittin to vesicles as a function of the melittin/lipid ratio. The sensitivity of Trp average lifetime,$\langle\boldsymbol{\tau}\rangle$**,** to the polarity of the medium is an important property for following the binding of melittin to vesicles. The results of the steady-state measurements in section 3.1 have shown that the polarity difference between the solution and the bilayer induces a blue shift in the Trp residue maximum emission upon binding. To gain more information regarding the detailed

environment of lipid-bound melittin, intrinsic Trp average fluorescence lifetime $\langle \boldsymbol{\tau} \rangle$ was measured to follow the binding of melittin to the three lipid vesicle compositions. Trp $\langle \tau \rangle$

was measured as function of melittin/lipid molar ratio over the temperature range from10 to 40°C.

It is well-known that the fluorescence decay of tryptophan is independent of pH from 4 to 8 and strongly dependent on pH above pH8. In this research all the samples for fluorescence measurements were maintained at pH 7.25. Knowledge of the possible excited-state fluorescence decay paths of the Trp can be used to follow the steps of melittin-lipid interaction [124][125]. **One of the objectives in this part of the experiment** was to examine the decay of the Trp dipole excited state to the ground state in order to determine if its dependence on temperature is altered when bound to lipids. Dufourcq and Faucon, 1977 quantified this blue shift and found that the shift reduced from 354 to 338 nm upon binding to POPC lipid vesicles, while Raghuraman and Chattopadhyay, 2004 found the shift decreased from 352 to 336 nm upon binding to DOPC vesicles [118][126]. As soon as the maximum emission reached the plateau at specific melittin/lipid molar ratio, melittin is completely bound to lipid vesicles. This information from previous studies of the steady-state measurements of Trp will be connected to the excited state decay measurements. I sought to determine if the excited state lifetime reaches a plateau-like value at a specific melittin/lipid molar ratio, which means melittin completely binding to vesicles bilayers.

The sensitivity of Trp $\langle \boldsymbol{\tau} \rangle$ in solution (lipid-free) was investigated as a function of temperature and the results are summarized in table 1. Melittin in buffer at a concentration

of 5 μM was excited at 290 nm, and the data were optimally fitted using the sum of two exponential decays. The intensity weighted average $\langle \boldsymbol{\tau} \rangle$ was calculated using Eq. 2.13, and the goodness-of-fit parameter, χ_R^2, of all analyses was relatively low, with values from 0.9 to 3.

Table 3. 2 The fluorescence lifetime ⟨τ⟩ of the tryptophan residue in melittin as a function of the temperatures in buffer PH7.25

T (°C)	$\boldsymbol{\alpha_1}$	$\boldsymbol{\tau_1}$ (ns)	$\boldsymbol{\alpha_2}$	$\boldsymbol{\tau_2}$ (ns)	$\langle \boldsymbol{\tau} \rangle$ (ns)
10	0.10±0.013	1.60±0.04	0.87±0.02	4.15±0.03	**4.01±0.02**
23	0.09±0.02	0.63±0.06	0.91±0.02	3.07±0.05	**3.01±0.02**
30	0.09±0.03	0.39±0.01	0.92±0.01	2.60±0.016	**2.57±0.01**
35	0.11±0.02	0.24±0.01	0.92±0.01	2.35±0.03	**2.32±0.02**
40	0.15±0.06	0.23±0.01	0.91±0.01	2.14±0.02	**2.07±0.03**

As expected, the Trp lifetime is reduced by an increase in temperature, see Fig. 3.3. In general, the relationship between the fluorescence lifetime and temperature of the Trp is linear at PH~7 [124][125][127]. The results summarized in table 3.2 show that the relationship between Trp $\langle \boldsymbol{\tau} \rangle$ as a function of temperature is linear with negative slope with a correlation coefficient of ~ 0.99.

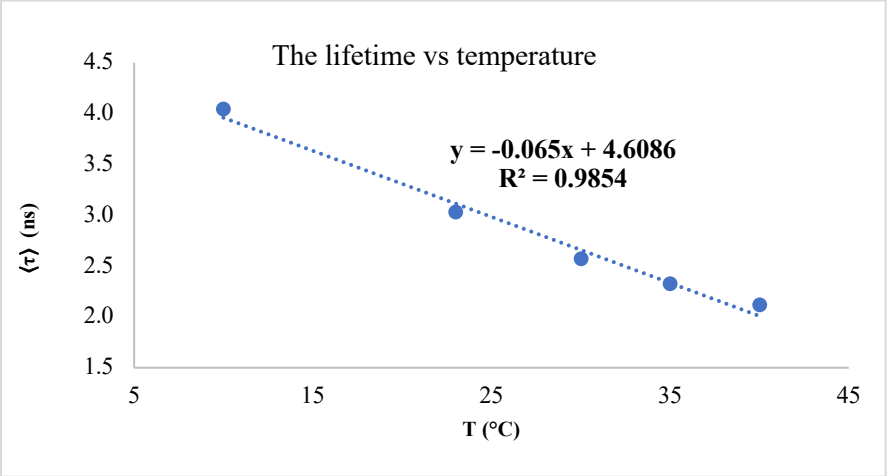

Figure 3. 3 Fluorescence lifetime of the tryptophan residue in melittin vs temperature.

The results show that the Trp lifetime is increased by about 100% when the temperature decreased from 40 to 10°C, see table 3.2. Trp lifetimes shown in table 2 at 23°C, and at the other temperatures are in good agreement with literature values [127][128][129][125].

The linear decrease of Trp lifetime over the temperature range 10-40°C (Table 2) can be explained according to the Lippert-Mataga equation [130] [131]:

$$\langle \Delta E \rangle = \frac{2(\vec{\mu}_e - \vec{\mu}_g)^2}{ha^3}\left(\frac{\epsilon - 1}{2\epsilon + 1} - \frac{n^2 - 1}{2n^2 + 1}\right) \tag{3.2}$$

Where $\langle \Delta E \rangle = \langle \Delta E_A \rangle - \langle \Delta E_B \rangle$, $\langle \Delta E_A \rangle$ and $\langle \Delta E_B \rangle$ are the shifts of the 0-0 absorption and fluorescence transition energies, respectively, [131], h is Planck's constant, ϵ and n are the dielectric constant and refractive index of the medium, respectively, $\vec{\mu}_e$ **and** $\vec{\mu}_g$ are the excited and ground state permanent dipole moments, respectively, and **a** is the radius of the solvent cavity (assumed to be a sphere)[131] [132].

The part between the parentheses in Eq. 3.2 is the Polarity parameter, Δ_f , [132]:

$$\Delta_f = \left(\frac{\epsilon-1}{2\epsilon+1} - \frac{n^2-1}{2n^2+1}\right) \tag{3.3}$$

Malmberg and Maryott, 1956, and Zhou et al, (2019) reported that the dielectric constant in water (pH~7) decreases continuously from 83.83, 79.5, 76.55, 74.83, 73.15 over the range 10, 23, 30, 35 and 40°C, respectively [133] [134]. Using their data I calculated the Polarity parameter, Δ_f, and the index of refraction was considered to be ~1.33, which shows very little variation in water over the range 10 to 40°C [133] [135]. The values of Δ_f as function of temperature were plotted, and I found that Δ_f decreases linearly as the temperature increases, see Fig. 3.4.

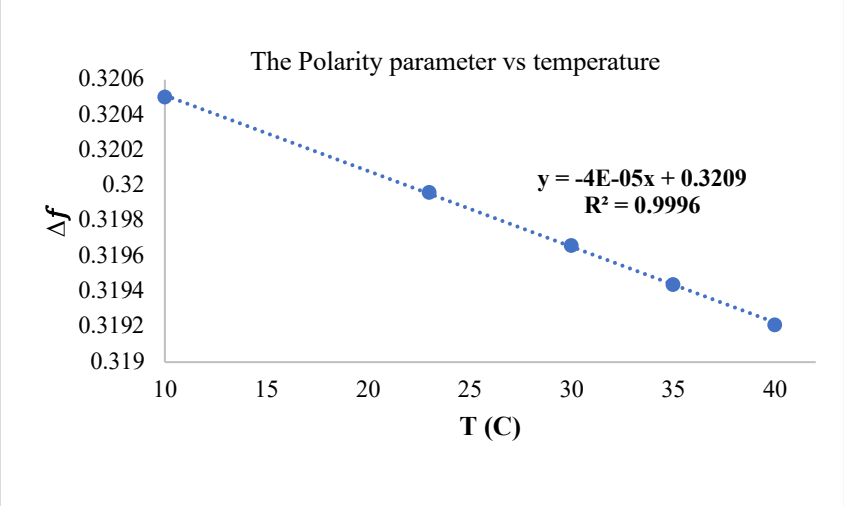

Figure 3. 4 The polarity parameter Δf of the solution vs temperature

From Eq.3.2, It is clear that $\langle \Delta E \rangle$ is proportional to Δ_f which means $\langle \Delta E \rangle$ also decreases as the polarity parameter decreases (or the temperature increases), and this result corresponds to the blue shift in the maximal emission wavelength of Trp when it binds to phospholipid bilayers.

This interpretation of the binding-induced blue shift by using the Lippert-Mataga equation and its connection to the excited state decay have not been previously reported.

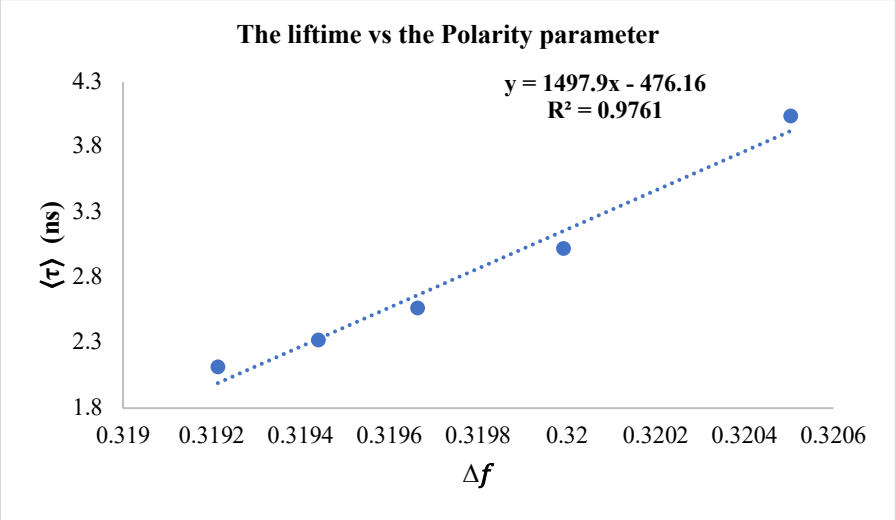

Figure 3. 5 Fluorescence lifetime of the tryptophan residue in melittin vs polarity parameter Δf.

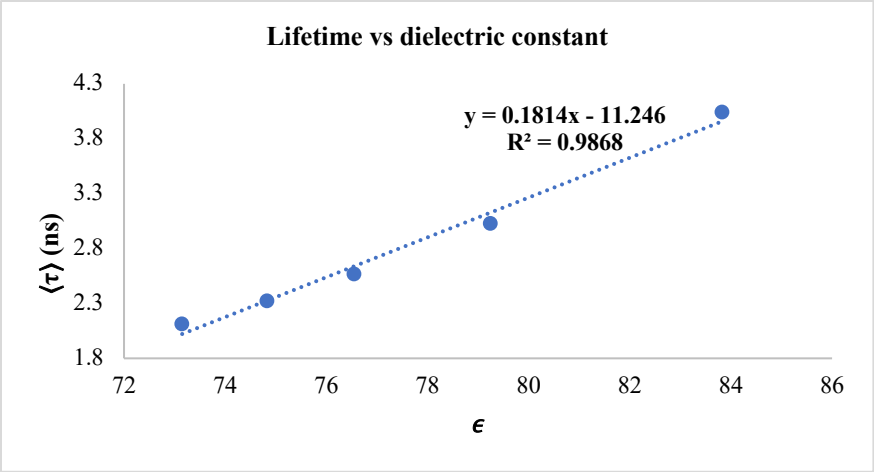

Figure 3. 6 Fluorescence lifetime of the tryptophan residue in melittin vs dielectric constant.

Lippert-Mataga and the polarity parameter equations, Eq. 3.2 and Eq. 3.3, provide an explanation of the behavior of the Trp excited state lifetime in solution. Finally, using the data in table 3.2, the amount of energy (energy barrier) for the excited state decay can be calculated from the Arrhenius equation. The decay rate $K_{rad.,}$ or $1/\langle\tau\rangle$, can be analyzed according to the Arrhenius equation, then the fluorescence lifetime is related to temperature, *T,* according to [127]:

$$1/\langle\boldsymbol{\tau}\rangle = K_0 e^{-\frac{E_a}{RT}} \tag{3.4}$$

Where R is the universal gas constant (R = 8.31 J/(mol · K), K_0 the pre-factor, and E_a the activation energy.

The straight-line fit of our data in table 2 between ln[1/⟨τ⟩ (s)] against 1/T (K^{-1}) as shown in Fig. 3.7 leads directly to an activation energy of 16 kJ/mole and pre-exponential factor temperature frequency $K_0 = 2 \times 10^{11} s^{-1}$. The activation energy and the pre-factor are in agreement with previous reports [127].

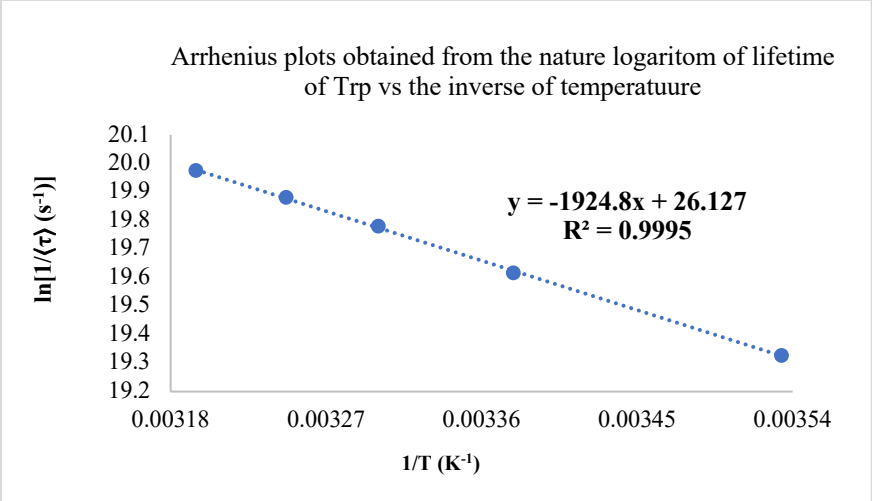

Figure 3. 7 Natural log. of the fluorescence lifetime of the tryptophan residue in melittin vs 1/T (K^{-1}).

Although the change of polarity parameter Δ_f with the dielectric constant was very small, the measurements in this experiment of Trp $\langle \boldsymbol{\tau} \rangle$ as function of temperature are consistent with the temperature-induced change in dielectric constant.

This demonstrates that intrinsic Trp can be used to understand more details about melittin bound to a lipid bilayer due to the sensitivity of its fluorescence lifetime to the dielectric constant [136] [137].

Time-resolved fluorescence lifetimes of the single Trp residue in melittin can be used to monitor melittin binding to lipids. The questions are: 1) How does the dielectric constant difference between the solution and the bilayer affect the Trp lifetime for melittin bound to lipids? 2) Does the temperature variation during the binding of melittin affect Trp $\langle\tau\rangle$ like it does in solution? 3) What is the percentage of bound melittin from the change of Trp $\langle\tau\rangle$?. To answer these questions, cuvettes 150 μM of each phospholipid composition were prepared to measure the lifetime of the tryptophan with concentration of melittin to lipids (Mel/L) and with four different temperatures 10, 23, 30, and 40°C, results are summarized in tables (2-4). At the lowest concentration of melittin (Mel/L=1/400) the lifetime of the intrinsic Trp decreases dramatically compared to the value for melittin in solution at all temperatures and all bilayer compositions. In Fig. 3.8 increasing the concentration of melittin to (Mel/L 1/200) caused a further decrease in $\boldsymbol{\langle\tau\rangle}$ of Trp for both POPC/POPG and PE-containing POPC/POPG. However, in the cholesterol containing bilayer there was no change of Trp lifetime when melittin was increased beyond 1/400. The plateau in the decrease in Trp lifetime occurs at 1/400 in cholesterol, while it occurs at MEL/L~1/100 in the POPE-containing bilayer. In POPC/POPG the plateau of Trp lifetime does not appear until Mel/L ~>1/50. From these results of excited state decay, it is clear that the cholesterol in the bilayer interior has an effect on reducing the binding due to the consistency of Trp lifetime at low concentration of melittin to lipid Mel/L above ~1/400, see Fig 3.11. One the other hand, PE also affected the binding above Mel/L~1/200. The reason for this drop of Trp lifetime is the gradient of the dielectric constant from the bulk solution to the headgroup region of the bilayer. The value of Trp fluorescence lifetime

is consistent as Mel/L is increased beyond1/400 for cholesterol-containing bilayers. This consistency implies that as additional melittin is added to the hydrophilic bilayer surface the melittin binding site, in terms of dielectric constant is unchanged.

Table 3. 3 Fluorescence lifetime $\langle\tau\rangle$ of the tryptophan residue in melittin as a function of the ratio Melittin added to the vesicles POPC/POPG 8:2 (M/L) in the buffer pH 7.25.

T (°C)	M/L	α_1	τ_1 (ns)	α_2	τ_2 (ns)	$\langle\tau\rangle$ (ns)
10	0	0.10±0.01	1.60±0.04	0.87±0.02	4.15±0.03	**4.01±0.02**
	1/400	0.14±0.01	0.34±0.0278	0.73±0.14	2.73±0.02	**2.68±0.01**
	1/200	0.14±0.05	0.02±0.03	0.86±0.02	1.98±0.04	**1.97±0.01**
	1/100	0.25±0.01	0.11±0.10	0.83±0.08	1.87±0.02	**1.8465±0.01**
	1/50	0.24±0.01	0.62±0.05	0.60±0.01	1.93±0.03	**1.78±0.02**
23	0	0.09±0.03	0.63±0.06	0.90±0.02	3.07±0.05	**3.01±0.01**
	1/400	0.13±0.01	0.46±0.04	0.69±0.01	2.35±0.03	**2.29±0.01**
	1/200	0.21±0.02	0.29±0.05	0.76±0.01	1.85±0.01	**1.79±0.01**
	1/100	0.20±0.016	0.08±0.11	0.80±0.01	1.79±0.02	**1.77±0.00**
	1/50	0.30±0.02	0.69±0.29	0.69±0.00	1.69±0.06	**1.56±0.04**
30	0	0.09±0.03	0.39±0.01	0.92±0.01	2.60±0.0159	**2.57±0.01**
	1/400	0.10±0.000	0.87±0.01	0.89±0.01	1.16±0.01	**1.13±0.03**
	1/200	0.42±0.021	1.06±0.05	0.58±0.02	1.23±0.02	**1.15±0.04**
	1/100	0.25±0.06	0.18±0.07	0.78±0.02	1.72±0.03	**1.68±0.02**
	1/50	0.32±0.07	0.13±0.05	0.76±0.08	1.54±0.01	**1.50±0.01**
40	0	0.15±0.06	0.23±0.01	0.91±0.01	2.14±0.02	**2.07±0.03**
	1/400	0.21±0.09	0.37±0.64	0.79±0.08	0.80±0.01	**0.800±0.00**
	1/200	0.44±0.10	0.85±0.06	0.55±0.10	1.12±0.04	**1.02±0.00**
	1/100	0.34±0.03	0.88±0.22	0.65±0.01	1.48±0.03	**1.35±0.04**
	1/50	0.21±0.14	0.97±0.29	0.80±0.12	1.50±0.09	**1.42±0.02**

Temperature also influences the process of Melittin binding to lipid, as shown in Fig. 3.9 and 3.10. At 10°C the Trp lifetime is almost constant for Mel/L ratios greater than 1/400 in all three lipid compositions. Above 10°C the Trp lifetime behavior depends on the lipid composition and Mel/L molar ratios. On the other hand, the temperature has no effect on the Trp lifetime for all of concentration Mel/L~>1/400 in the presence of cholesterol. From the Fig. 3.11, it is clear that at Mel/L~1/400 the melittin completely binds to cholesterol-containing lipid vesicles, and the temperature has no effect on this binding over the range of Mel/L studied.

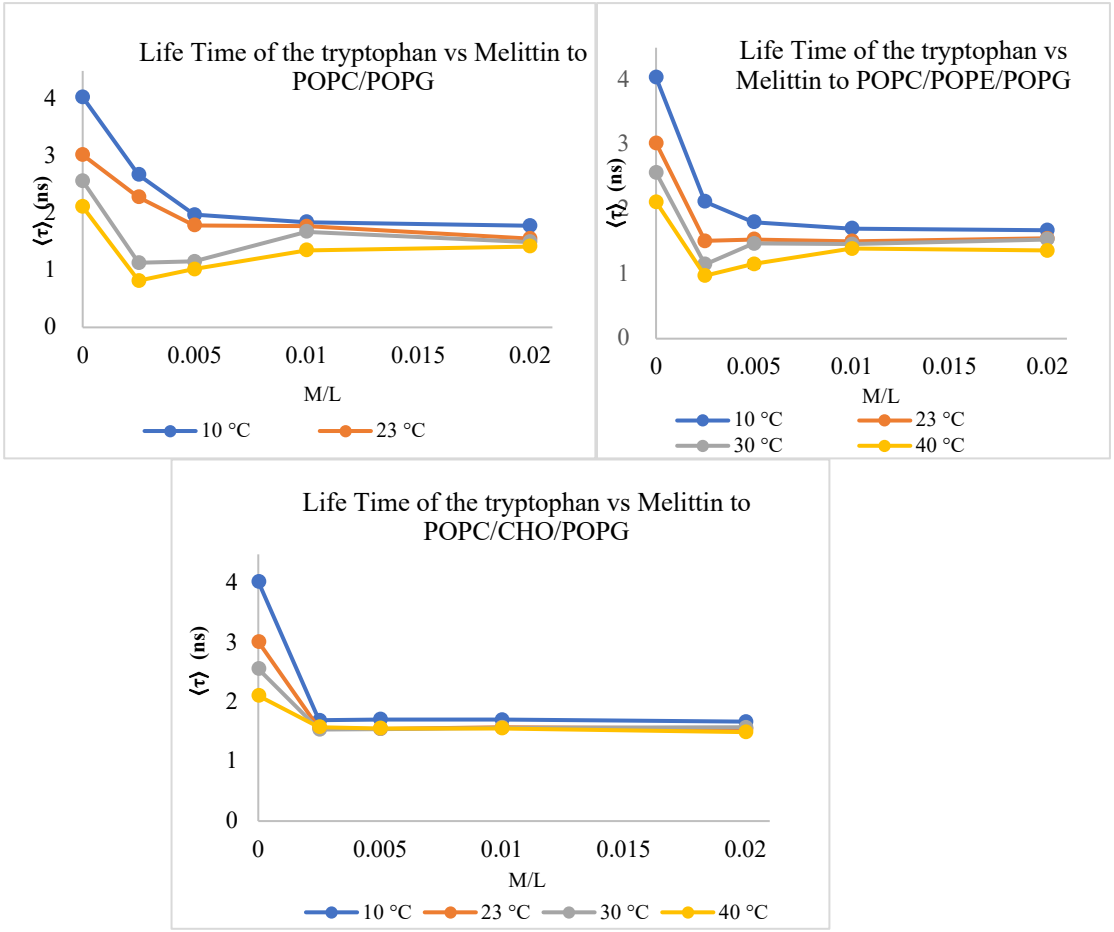

Figure 3. 8 Fluorescence lifetime of the tryptophan vs Melittin to lipids

Table 3. 4 Fluorescence lifetime ⟨τ⟩ of the tryptophan residue in melittin as a function ratio Melittin added to the vesicles POPC/POPE/POPG 4/4/2 (M/L) in the buffer PH7.25

T (°C)	M/L	α_1	τ_1 (ns)	α_2	τ_2 (ns)	$\langle\tau\rangle$ (ns)
10	0	0.10±0.01	1.60±0.04	0.87±0.02	4.15±0.0340	**4.01±0.01**
	1/400	0.18±0.02	0.22±0.03	0.86±0.02	2.15±0.0375	**2.10±0.03**
	1/200	0.15±0.02	0.17±0.01	0.87±0.01	1.83±0.0150	**1.79±0.00**
	1/100	0.14±0.04	0.70±0.07	0.88±0.00	1.77±0.0171	**1.70±0.03**
	1/50	0.17±0.01	0.66±0.01	0.84±0.01	1.75±0.0017	**1.68±0.01**
23	0	0.09±0.03	0.63±0.06	0.91±0.02	3.07±0.0467	**3.01±0.02**
	1/400	0.21±0.01	0.80±0.02	0.79±0.01	1.60±0.0156	**1.51±0.01**
	1/200	0.15±0.05	0.45±0.01	0.85±0.00	1.59±0.0033	**1.53±0.02**
	1/100	0.18±0.04	0.53±0.13	0.85±0.01	1.57±0.0476	**1.51±0.05**
	1/50	0.19±0.01	0.56±0.05	0.81±0.00	1.63±0.0048	**1.55±0.02**
30	0	0.09±0.03	0.40±0.01	0.92±0.01	2.60±0.016	**2.57±0.01**
	1/400	0.20±0.00	0.79±0.0086	0.80±0.00	1.20±0.01	**1.15±0.00**
	1/200	0.24±0.07	0.20±0.00	0.78±0.06	1.52±0.02	**1.47±0.01**
	1/100	0.17±0.01	0.71±0.09	0.83±0.01	1.53±0.00	**1.46±0.00**
	1/50	0.20±0.00	0.51±0.09	0.80±0.00	1.61±0.01	**1.54±0.00**
40	0	0.15±0.06	0.23±0.01	0.91±0.07	2.14±0.024	**2.07±0.03**
	1/400	0.20±0.00	0.80±0.00	0.80±0.001	1.01±0.01	**0.98±0.02**
	1/200	0.22±0.07	0.16±0.027	0.80±0.00	1.19±0.05	**1.17±0.05**
	1/100	0.25±0.05	0.383±0.09	0.76±0.05	1.45±0.02	**1.39±0.04**
	1/50	0.17±0.05	0.33±0.16	0.83±0.05	1.40±0.00	**1.36±0.02**

Table 3. 5 Fluorescence lifetime ⟨τ⟩ of the tryptophan residue in melittin as a function of the ratio Melittin added to the vesicles POPC/POPG 8/2+ 30% of Cholesterol (M/L) in the buffer PH7.25.

T (°C)	M/L	α_1	τ_1 (ns)	α_2	τ_2 (ns)	$\langle\tau\rangle$ (ns)
10	0	0.10±0.01	1.60±0.04	0.87±0.02	4.15±0.0340	**4.01±0.01**
	1/400	0.22±0.01	0.11±0.03	0.79±0.00	1.73±0.01	**1.70±0.01**
	1/200	0.19±0.01	0.08±0.01	0.81±0.01	1.73±0.01	**1.72±0.01**
	1/100	0.17±0.00	0.07±0.01	0.83±0.00	1.72±0.00	**1.71±0.00**
	1/50	0.18±0.01	0.06±0.01	0.82±0.01	1.69±0.00	**1.68±0.00**
23	0	0.09±0.03	0.63±0.06	0.90±0.02	3.07±0.05	**3.01±0.01**
	1/400	0.25±0.03	0.29±0.06	0.76±0.03	1.64±0.03	**1.60±0.01**
	1/200	0.22±0.02	0.28±0.05	0.78±0.02	1.62±0.02	**1.54±0.01**
	1/100	0.20±0.0112	0.12±0.06	0.80±0.01	1.61±0.023	**1.58±0.02**
	1/50	0.22±0.03	0.11±0.01	0.78±0.03	1.59±0.02	**1.56±0.02**
30	0	0.09±0.03	0.39±0.01	0.92±0.01	2.60±0.02	**2.57±0.01**
	1/400	0.30±0.01	0.24±0.03	0.71±0.0132	1.62±0.02	**1.54±0.01**
	1/200	0.26±0.01	0.24±0.02	0.74±0.00	1.63±0.02	**1.56±0.01**
	1/100	0.21±0.01	0.27±0.15	0.79±0.01	1.63±0.04	**1.57±0.02**
	1/50	0.21±0.01	0.05±0.04	0.80±0.003	1.59±0.03	**1.58±0.02**
40	0	0.15±0.06	0.23±0.01	0.91±0.01	2.14±0.02	**2.07±0.03**
	1/400	0.36±0.01	0.34±0.03	0.64±0.01	1.72±0.02	**1.58±0.01**
	1/200	0.31±0.02	0.37±0.01	0.69±0.0156	1.68±0.02	**1.56±0.01**
	1/100	0.24±0.0	0.25±0.11	0.76±0.00	1.62±0.02	**1.56±0.01**
	1/50	0.27±0.02	0.16±0.05	0.74±0.02	1.55±0.02	**1.50±0.01**

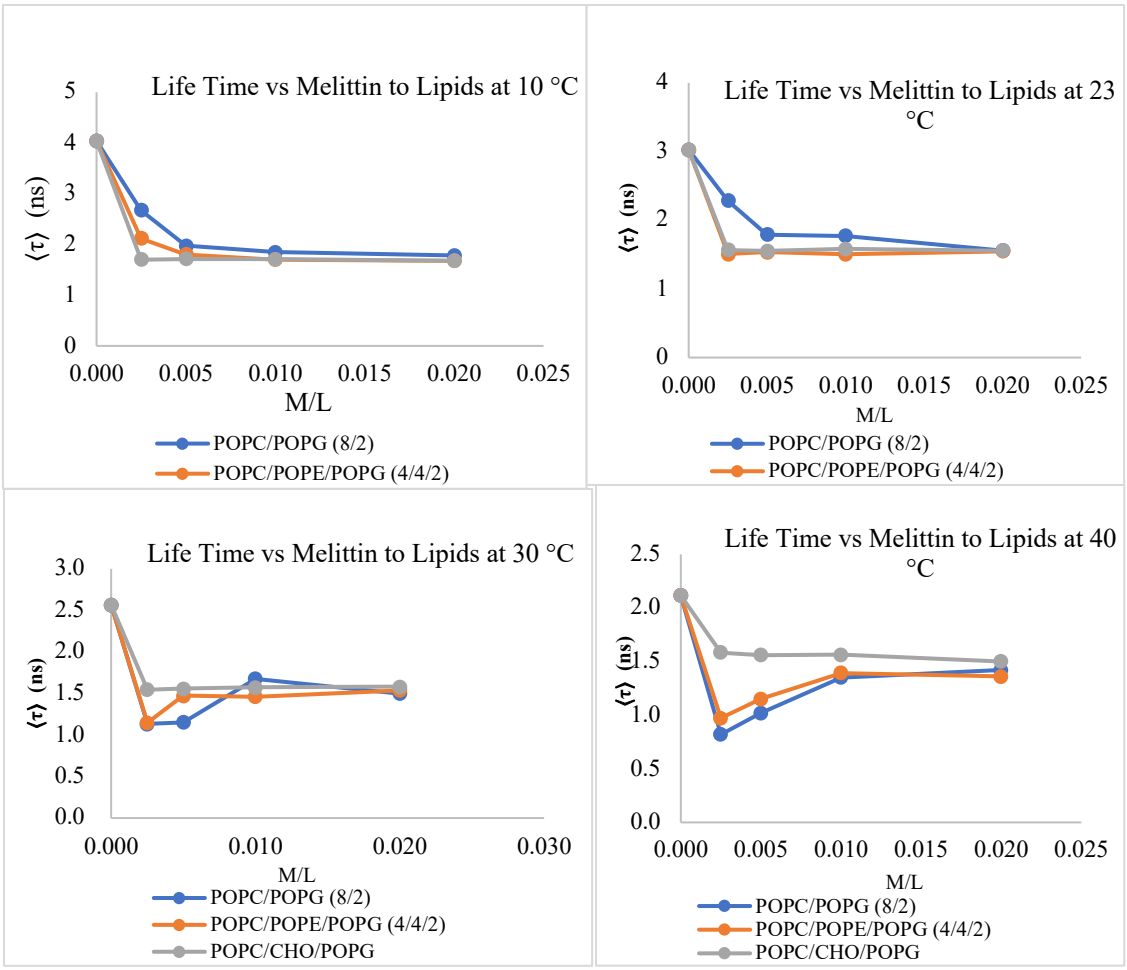

Figure 3. 9 Fluorescence lifetime of the tryptophan vs Melittin to lipids

The percentage of bound melittin can be obtained from the blue shift of the normalized emission spectra of the steady-state measurements [118]. By comparison to that, I assumed that the plateau in the concentration dependent decrease in $\langle \boldsymbol{\tau} \rangle$ of Trp indicated that all of the melittin was bound when the plateau value was reached. Then Eq. 3.5 can also be used to calculate the percentage of bound melittin (see Fig. 3.11) for any temperature and any Mel/L ratio according to:

$$\% \text{ bound melittin (T)} = \frac{\langle \tau \rangle_r(T) - \langle \tau \rangle_I(T)}{\langle \tau \rangle_F(T) - \langle \tau \rangle_I(T)} \times 100 \quad (3.5)$$

Where $\langle \tau \rangle_F(T)$ lifetime in the solution, $\langle \tau \rangle_I(T)$ lifetime when plateau was reached, and $\langle \tau \rangle_r(T)$ lifetime at specific ratio Mel/L at a specific temperature.

The results in Fig. 3.11 show that melittin completely binds to all three bilayer compositions at concentrations of Mel/L (1/50) and higher at all temperatures examined. At lower levels of Mel/L below 1/50, temperature has a distinct effect in each bilayer composition.

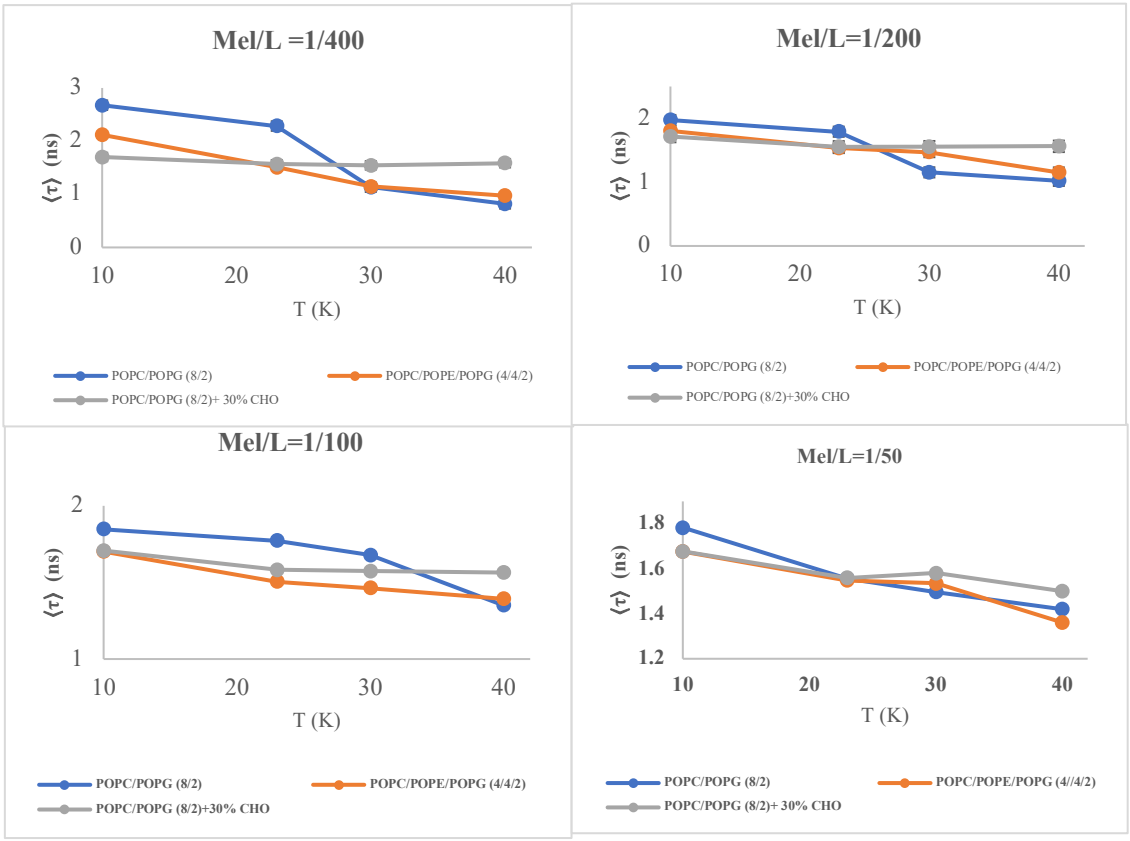

Figure 3. 10 Fluorescence lifetime of the tryptophan residue in melittin binding to vesicles vs temperature.

From my results, the percentage of melittin bound to cholesterol-containing vesicles decreases from about 99% at 10°C and 23°C to about 86% at 40°C at Mel/L 1/400, see Fig. 3.11. On the other hand, the percentage of bound melittin is affected by bilayer composition. For instance, at 10°C our results show that percentage increases from ~61% in the case of PC/PG to 81% and 99% in the case of PE and cholesterol-containing vesicles.

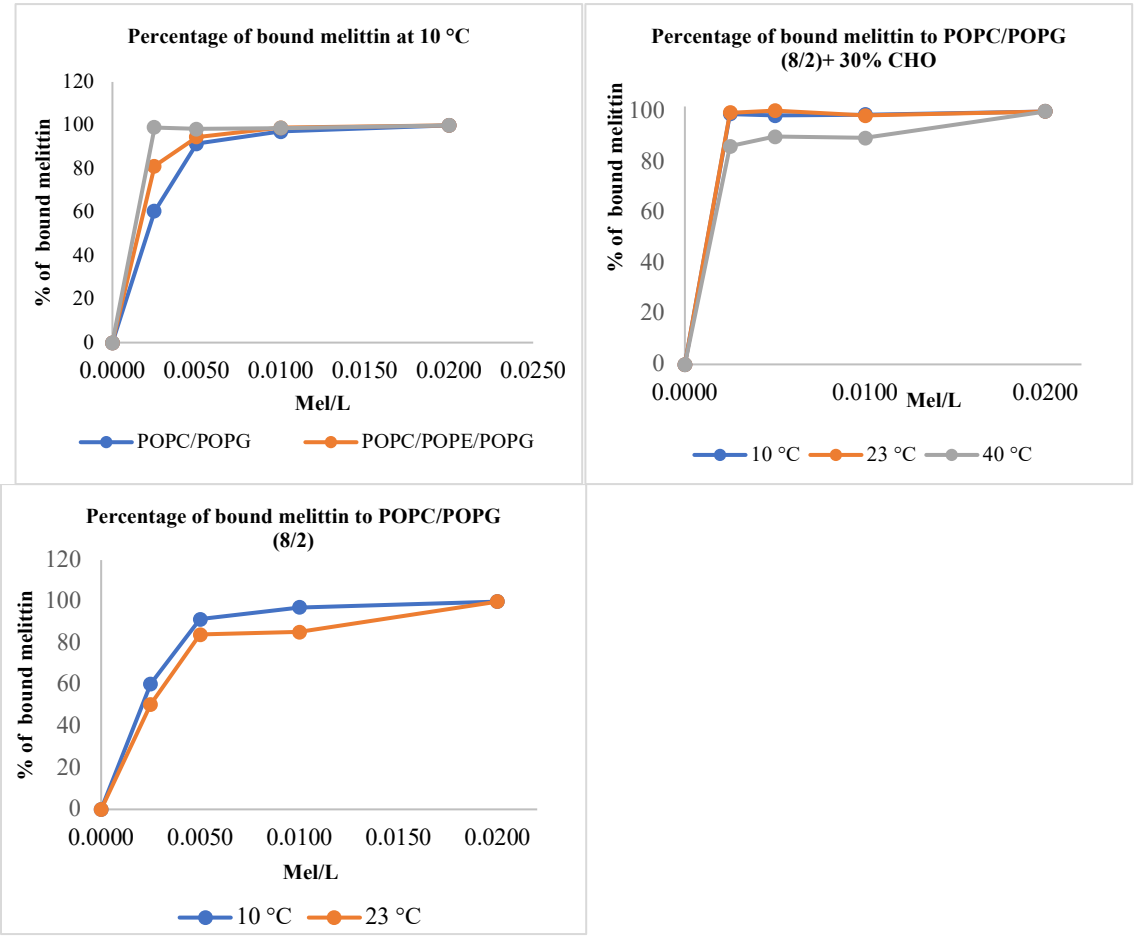

Figure 3. 11 Percentage of bound melittin to vesicles vs temperature.

Chen, et al. (1998) reported that the binding parameter for melittin interaction with lipid vesicles of different compositions can determine from the blue shift of the according [138]:

$$(\varepsilon - 1) = (\varepsilon_b - 1)\frac{m}{(\frac{k_d}{n}+m)} \quad (3.6)$$

$\varepsilon = \frac{\lambda_{max_0}}{\lambda_{max}}$, λ_{max_0} (in absence of lipid)

λ_{max} (Blue shift in presence of lipids)

m is the lipid concentration.

According to Eq. 3.5 and by comparison to Eq. 3.6, the binding parameter of tryptophan residue in melittin can be obtained from time-resolved lifetime measurands according to:

$$\frac{k_d}{n} = m\frac{(\gamma_0 - 1)}{(\gamma_1 - 1)}$$

γ_0 was defined as $\frac{\langle\boldsymbol{\tau}\rangle_r(T)}{\langle\boldsymbol{\tau}\rangle_I(T)}$ and $\gamma_1 = \frac{\langle\boldsymbol{\tau}\rangle_F(T)}{\langle\boldsymbol{\tau}\rangle_I(T)}$

$\frac{k_d}{n}$ were determined from the results of Try lifetime and lipid vesicles concentration which is **150 µM** in this research. The data between the binding parameter and Mel/L molar ratio were plotted as shown in Fig. 3,12.

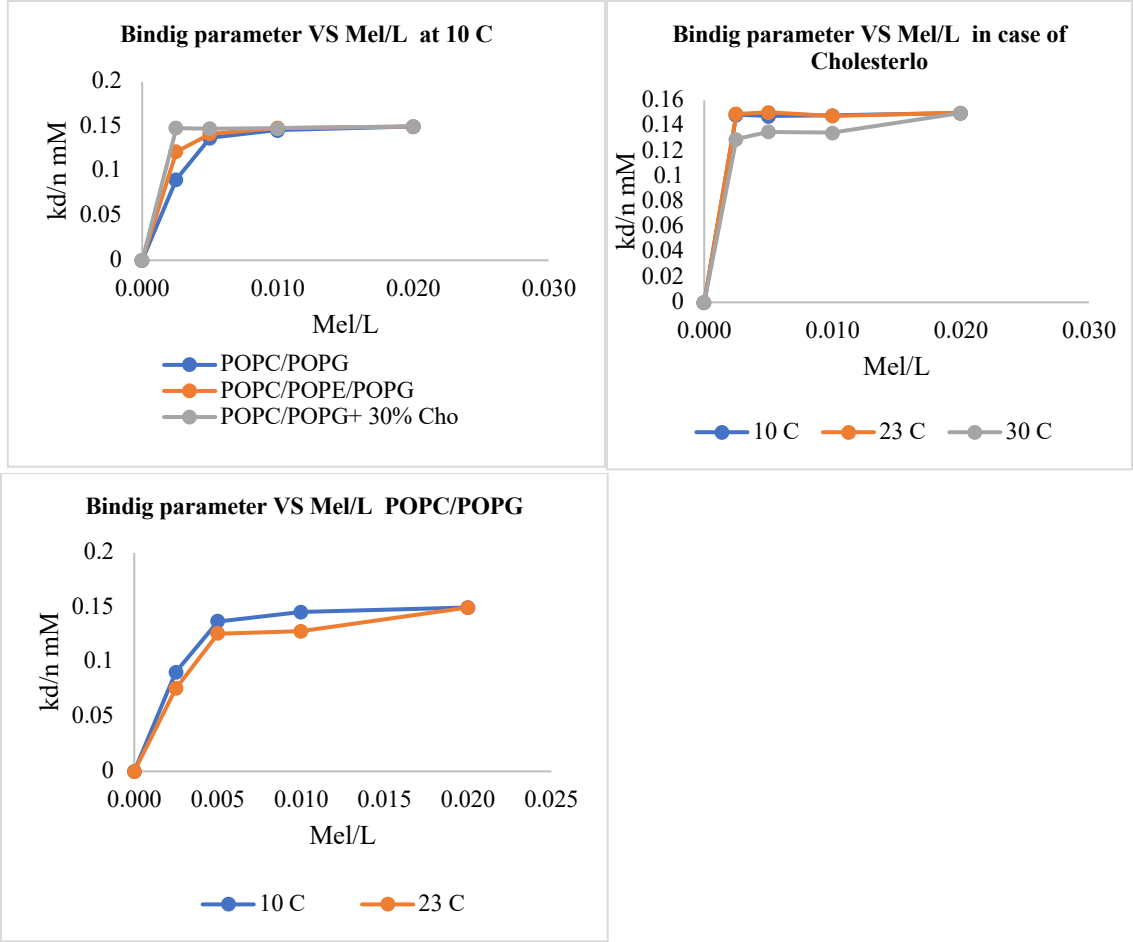

Figure 3.12 Binding parameter of melittin to Melittin/L molar ratio

The results from the graphs 3.12 show that the binding parameter $\frac{k_d}{n}$ (mM) of melittin to lipids depends on bilayer composition and temperature. The biggest value of the binding parameter from the results in this research were about 0.15 mM ($\frac{k_d}{n} = 1.5 \times 10^{-4}$ M). This results are close to that reported in Ref. [138]. If I can consider the binding parameter is the inverse of the partition constant which is in unit M^{-1}. Therefore, the partition constant from my results is $6.7 \times 10^3\ M^{-1}$ which is three times that reported in the literature [32].

3.3. Fluorescence lifetime measurements of DPH as a function of added melittin

Steady-state and time-resolved flourescence measurments of Trp were used to study melittin bound to phospholipid bilayers in the last sections. Despite extensive studies, aspects of peptide-lipid bilayer interaction are still unclear [139]. The fluorescent molecule 1,6-diphenyl-1,3,5-hexatriene (DPH) embedded in the phospholipid bilayer can be utilized to study the variations of the bilayer interior structure that may be influenced by peptides. **The objectives of this part of the research are:** 1) How is peptide-lipid inteaction is affected by properties of the bilayer interior and headgroup of vesicles? And what are the changes in the bilayer interior throughout the process of peptide interaction with lipid vesicles? Fluorescence lifetimes $\langle\tau\rangle$ of DPH were measured at 30°C as a function of the molar ratio of peptides to phospholipids for all three-phospholipid vesicle compositions; POPC/POPG, PE-containing, and cholesterol-containing. In most published studies two or three exponentials are required to describe the DPH fluorescence lifetime [101]. The best fits for the fluorescence decays in my results were obtained using a sum of two exponential decays, and the intensity-weighted average fluorescence lifetime, $\boldsymbol{\langle\tau\rangle}$**,** was calculated using Eq. 2.13.

The results in tables (3.6-3.8) show that DPH has two fluorescence lifetimes, that each depend on the composition of the bilayer and on the Mel/L molar ratio. DPH lifetime is known to be sensitive to physical properties of the bilayer such as dielectric constant [140]. The varying degrees of water penetration into the bilayer can be detected by the fluorescence intensity decay of DPH. It is known that DPH fluorescence

lifetime$\langle\tau\rangle$ decreases as the amount of water increases because the DPH excited state is quenched by water; it is nonfluorescent in water, but is highly fluorescent in the lipid bilayer environment [141]. The results in tables 3.6-3.8 show that the fluorescence lifetime $\langle\tau\rangle$ of DPH is the longest in cholesterol-containing lipid vesicles with no melittin, see Fig. 3.12. This demonstrates that enhanced attractive van der Waals forces between acyl chains conferred by cholesterol results in tighter headgroup packing and reduced penetration of water into the lipid bilayer [141][142]. The hydrophobic core of the bilayer for both POPC/POPG and PE-containing POPC/POPG vesicles are identical, however, the fluorescence lifetime$\langle\tau\rangle$ of DPH embedded in PE-containing POPC/POPG is longer than that embedded in POPC/POPG. This suggests that the PE-containing bilayer has tighter packing with respect to water penetration compared to the headgroup in absence of POPE. As a result, POPE-containing POPC/POPG decreases the amount of water penetration in comparison to POPC/POPG. This baseline information about the fluorescence lifetime $\langle\tau\rangle$ of DPH embedded into these three phospholipid bilayer compositions have not been previously reported in the literature. From this information one can examine the effect of peptide concentration on the lifetime $\langle\tau\rangle$ of DPH.

In POPC/POPG lipid vesicles at low concentrations of Mel/L, from 1/300 to 1/200, the results show that there is no observable change in the fluorescence lifetime $\langle\tau\rangle$ of DPH This invariance of $\langle\tau\rangle$ means the melittin over these low ratios did not disrupt the bilayer with respect to water penetration. In the POPE-containing vesicles, on the other hand, at the same concentrations (1/300 and 1/200) the fluorescence lifetime $\langle\tau\rangle$ of DPH. As result, PE-containing lipid vesicles allow water molecules to penetrate the bilayer at

Mel/L~1/300. Surprisingly, the fluorescence lifetime $\langle\tau\rangle$ of DPH increases over the range in between Mel/L=1/300 to 1/50. I reasoned that over this concentration range when melittin binds to the bilayer it acts to minimize packing defects that may arise among the mis-matched PC and PE headgroups. The result would be that the headgroups pack tighter and decrease water penetration into the bilayer. As a result, the fluorescence lifetime $\langle\tau\rangle$ for DPH increases due to less water between the two leaflets. At molar ratios above Mel/L~1/50, the decrease of fluorescence lifetime $\langle\tau\rangle$ for DPH observed for all bilayer compositions suggest disruption of optimal headgroup packing by melittin bound to the membrane.

Table 3. 6 Effect of melittin on fluorescence lifetime ⟨τ⟩ of DPH embedded in POPC /POPG 8/2 at 30 ºC.

M/L	α_1	τ_1 (ns)	α_2	τ_2 (ns)	$\langle\tau\rangle$ (ns)
0	0.15±0.03	4.89±0.31	0.85±0.03	8.38±0.05	8.07±0.03
1/300	0.33±0.03	7.96±0.16	0.67±0.03	8.02±0.17	8.11±0.14
1/200	0.13±0.03	5.03±0.12	0.87±0.04	8.48±0.16	8.26±0.12
1/100	0.04±0.00	2.56±0.11	0.96±0.00	8.16±0.05	8.10±0.04
1/50	0.09±0.00	3.69±0.07	0.91±0.02	8.38±0.06	8.15±0.07
1/25	0.12±0.03	3.77±0.22	0.88±0.03	8.31±0.14	8.05±0.07
1/10	0.16±0.03	2.97±0.35	0.83±0.03	7.82±0.19	7.48±0.10
1/5	0.21±0.02	2.90±0.21	0.77±0.02	7.58±0.04	7.14±0.08
3/10	0.25±0.01	2.23±0.05	0.73±0.01	7.37±0.12	6.89±0.09

Table 3. 7 Effect of melittin on fluorescence lifetime ⟨τ⟩ of DPH embedded in POPC/POPE/POPG 4/4/2 at 30 ºC.

M/L	α_1	τ_1 (ns)	α_2	τ_2 (ns)	⟨τ⟩ (ns)
0	0.41±0.01	10.28±0.13	0.58±0.01	7.62±0.10	8.93±0.020
1/300	0.10±0.03	4.96±0.18	0.90±0.04	9.05±0.17	8.87±0.113
1/200	0.14±0.06	5.59±0.24	0.86±0.03	8.89±0.10	8.60±0.06
1/100	0.16±0.01	5.44±0.24	0.84±0.03	8.96±0.14	8.59±0.03
1/50	0.09±0.02	4.19±0.55	0.91±0.02	8.68±0.11	8.48±0.06
1/25	0.12±0.03	4.00±0.29	0.88±0.01	8.75±0.12	8.48±0.05
1/10	0.21±0.02	4.32±0.20	0.78±0.02	8.63±0.08	8.11±0.04
1/5	0.25±0.02	3.48±0.11	0.73±0.00	7.33±0.03	6.78±0.03
3/10	0.33±0.01	2.19±0.13	0.64±0.01	6.61±0.08	5.96±0.08

Table 3. 8 Effect of melittin on fluorescence lifetime ⟨τ⟩ of DPH embedded in POPC/POPG 8/2+ 30% of Cholesterol at 30 ºC

M/L	α_1	τ_1 (ns)	α_2	τ_2 (ns)	⟨τ⟩ (ns)
0	0.19±0.03	8.45±0.56	0.804±0.14	10.28±0.32	9.98±0.14
1/300	0.09±0.08	9.98±0.83	0.908±0.07	9.70±0.37	9.80±0.18
1/200	0.21±0.04	15.08±0.69	0.789±0.04	8.78±0.17	10.71±0.04
1/100	0.24±0.03	12.28±0.70	0.759±0.03	9.53±0.38	10.64±0.27
1/50	0.34±0.04	6.79±0.51	0.651±0.09	11.70±0.46	10.53±0.09
1/25	0.21±0.04	5.10±0.53	0.780±0.04	11.00±0.25	10.34±0.09
1/10	0.25±0.01	3.55±0.04	0.734±0.01	8.76±0.05	8.13±0.02
1/5	0.19±0.00	2.27±0.05	0.791±0.01	8.60±0.04	8.23±0.04
3/10	0.31±0.02	2.35±0.16	0.662±0.02	8.29±0.10	7.60±0.10

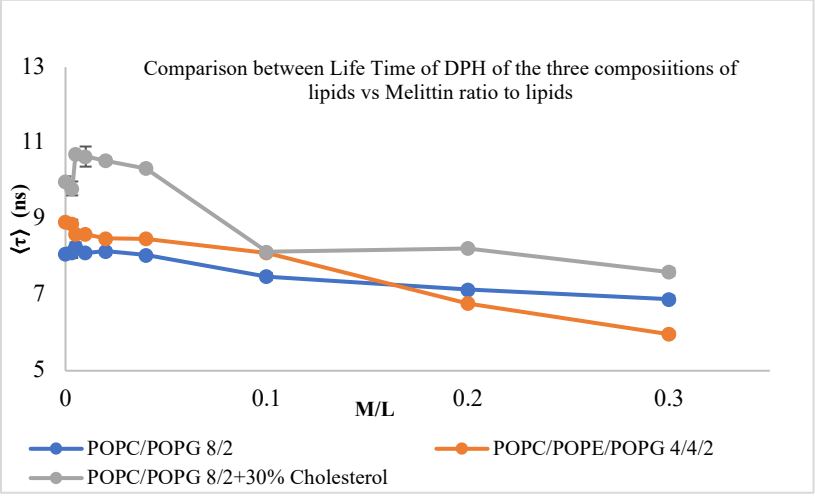

Figure 3. 12 Comparison between the Lifetime of DPH in three compositions of lipids vs the molar ratio of melittin to lipids.

3.4. Fluorescence anisotropy measurements of DPH as a function of added melittin

The fluorescence anisotropy decay, *r*(t), of the DPH probe molecule embeded in the phospholipid bilayer was studied at 30°C. The Brownian Rotational Diffusion model (BRD) was used to analyze the anisotropy decay data of DPH for each phospholipid composition with respect to the amount of melittin added (Mel/L), and the results are summarized in tables (3.9-3.11). The goal of this study was to provide more details of the structure and dynamics of the bilayer interior from the anisotropy parameters reported in the tables, and to show how these parameters are correlated to the fluorescence intensity decay discussed in section 3.2.1. The analysis of DPH anisotropy decay show that initial anisotropy values of r_0 for DPH are independent of bilayer compositions and Mel/L concentration. The averages of the initial anisotropy r_0 were determined from the BRD analysis of the anisotropy decays and found to be 0.377, 0.370, 0.366 (with errors of about 0.01 in all three cases) for POPC/POPG, PE-containing, and cholesterol-containing lipid vesicles, respectively. The results for r_0 agree with the data reported by Lentz, (1993) and Best et al., (1987) who had shown that the initial anisotropy r_0 for DPH depends on the bilayer interior embedded in it (They used DPPC and DLPC, and DMPC) [143][144]. However, Mitchell and Litman (1998) show that the r_0 is almost the same for different acyl chains composition of the PC bilayer. They reported that r_0 was between 0.334 and 0.361 [145][103].

The analysis of the fluorescence anisotropy $r(t)$ was used to determine the rotational correlation time $\langle\emptyset\rangle$ of the DPH for all three lipid compositions as a function of Mel/L.

Also, the average of anisotropy $\langle r \rangle$ of the fluorophore was evaluated using Eq. 2.28. The parameter $\langle r \rangle$ is calculated from the anisotropy decay and provides more details about the average orientational order of the DPH, which can be used to infer information regarding the order of the phospholipid acyl chains. The rotational correlation time $\langle \emptyset \rangle$ remains almost constant until Mel/L reaches above~1/50 as shown in Fig. 3.15. This ratio Mel/L=1/50 agrees with the results of the fluorescence lifetime reported in tables (3.6-3.8) which indicates water penetration to the bilayer.

The average of anisotropy $\langle r \rangle$ of DPH embedded in phospholipid bilayers was determined for all compositions with respect to Mel/L and summarized in tables (3.9-3.11). Average fluorescence anisotropy decay of the bilayer embedded DPH fluorophore is related to the rotational mobility of the fluorophore in the bilayer local environment, and is sensitive to phospholipid acyl chain packing [98]. Fig. 3.16 shows increases in average fluorescence anisotropy of DPH with increasing concentrations of Mel/L. As apparent from the Fig. 3.16, the average of fluorescence anisotropy is highest in cholesterol-containing lipid vesicles. This reflects the relatively more condensed packing of the fatty acyl chains in the presence of cholesterol. DPH average anisotropy in the PC/PG and PE-containing lipid vesicles is much lower than that in cholesterol-containing lipid vesicles. This indicates both PC/PG and PE-containing lipid vesicles have similar, relatively loose packing between the fatty acyl chains. There was no change in average anisotropy observed in cholesterol-containing lipid vesicles with Mel/L above 1/25. In the case of PC/PG and PE-containing lipid vesicles, the average anisotropy seems to plateau above Mel/L=1/5 and at Mel/L=3/10, the average fluorescence anisotropy $\langle r \rangle$ of DPH is almost the same for all

three phospholipid bilayers. This plateau is in general agreement with the changes in rotational correlation time ⟨∅⟩ shown in Fig. 3.15.

Table 3. 9 Effect of melittin on fluorescence anisotropy of DPH embedded in POPC/ POPG 8/2 at 30 ºC

M/L	r_0	⟨∅⟩ (ns)	P_2	P_4	$D_\perp$	S	⟨r⟩
0	0.367±0.007	2.325±0.051	0.177±0.0044	0.352±0.016	0.153±0.007	0.177±0.004	0.091
1/300	0. 364±0.014	1.812±0.134	0.220±0.0067	0.493±0.021	0.395±0.078	0.220±0.007	0.096
1/200	0.384±0.017	2.116±0.122	0.213±0.0139	0.393±0.037	0.197±0.050	0.213±0.014	0.092
1/100	0.379±0.010	2.064±0.062	0.228±0.0059	0.377±0.021	0.180±0.025	0.228±0.006	0.093
1/50	0.382±0.002	2.114±0.059	0.236±0.0082	0.387±0.006	0.180±0.008	0.236±0.008	0.096
1/25	0.370±0.010	2.346±0.059	0.246±0.0077	0.403±0.009	0.171±0.006	0.246±0.008	0.101
1/10	0.369±0.001	3.651±0.109	0.325±0.0104	0.500±0.029	0.158±0.030	0.325±0.010	0.147
1/5	0.353±0.005	7.562±0.351	0.306±0.0622	0.508±0.036	0.083±0.008	0.306±0.062	0.198
3/10	0.357±0.005	10.723±0.719	0.170±0.0215	0.479±0.006	0.066±0.004	0.170±0.022	0.221

Table 3. 10 Effect of melittin on fluorescence anisotropy of DPH embedded in POPC/POPE/POPG 4/4/2 at 30 ºC.

M/L	r_0	⟨∅⟩ (ns)	P_2	P_4	$D_\perp$	S	⟨r⟩
0	0.388±0.003	1.949±0.036	0.324±0.003	0.421±0.008	0.193±0.009	0.324±0.003	0.103
1/300	0.370±0.016	1.964±0.084	0.307±0.004	0.383±0.034	0.170±0.030	0.307±0.004	0.096
1/200	0.386±0.005	1.829±0.021	0.286±0.005	0.400±0.009	0.202±0.006	0.286±0.005	0.094
1/100	0.377±0.002	1.774±0.019	0.280±0.010	0.379±0.005	0.192±0.009	0.280±0.010	0.089
1/50	0.381±0.012	1.844±0.045	0.285±0.013	0.412±0.017	0.212±0.016	0.285±0.013	0.093
1/25	0.353±0.015	2.115±0.056	0.305±0.008	0.357±0.031	0.143±0.020	0.305±0.008	0.097
1/10	0.367±0.015	3.147±0.137	0.300±0.033	0.488±0.034	0.181±0.030	0.300±0.032	0.127
1/5	0.353±0.004	7.230±0.221	0.274±0.016	0.500±0.010	0.089±0.005	0.274±0.016	0.195
3/10	0.354±0.001	9.751±0.343	0.060±0.011	0.424±0.005	0.061±0.001	0.060±0.011	0.220

Table 3. 11 Effect of melittin on fluorescence anisotropy of DPH embedded in POPC/POPG 8/2+ 30% of Cholesterol at 30 ºC

M/L	r_0	⟨Ø⟩ (ns)	P_2	P_4	$D_\perp$	S	⟨r⟩
0	0.376±0.016	1.410±0.183	0.622±0.004	0.525±0.024	0.165±0.043	0.622±0.004	0.174
1/300	0.373±0.004	1.427±0.034	0.639±0.013	0.530±0.021	0.149±0.017	0.639±0.013	0.180
1/200	0.369±0.004	1.436±0.028	0.643±0.002	0.514±0.002	0.134±0.003	0.643±0.002	0.178
1/100	0.381±0.010	1.346±0.064	0.655±0.011	0.559±0.023	0.171±0.042	0.654±0.011	0.188
1/50	0.363±0.006	1.506±0.018	0.695±0.003	0.552±0.008	0.112±0.002	0.695±0.003	0.198
1/25	0.360±0.001	1.672±0.057	0.759±0.004	0.610±0.006	0.083±0.002	0.759±0.004	0.228
1/10	0.363±0.008	6.523±0.292	0.601±0.007	0.648±0.029	0.08±0.019	0.602±0.006	0.234
1/5	0.361±0.003	10.551±0.912	0.452±0.027	0.603±0.010	0.074±0.004	0.453±0.027	0.236
3/10	0.348±0.007	12.541±0.722	0.321±0.163	0.550±0.064	0.061±0.002	0.350±0.163	0.232

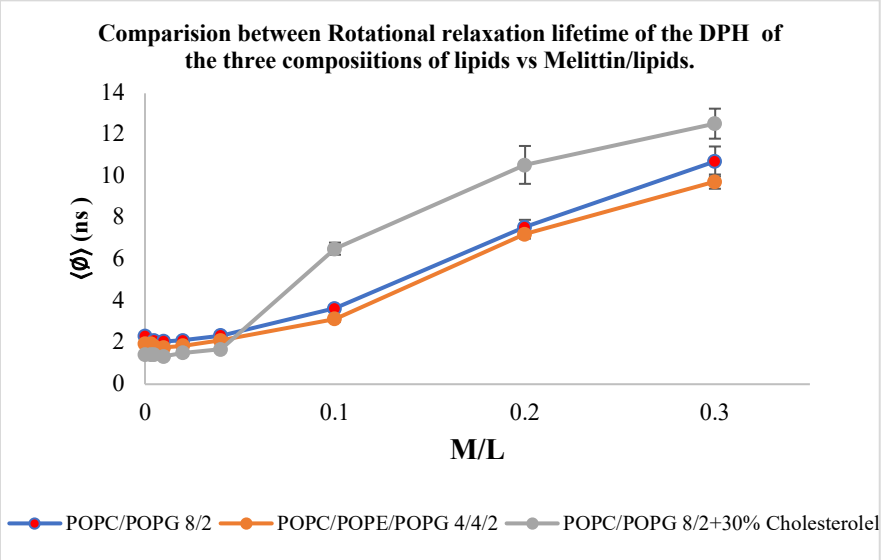

Figure 3. 13 Comparison between Rotational relaxation lifetime of the DPH of the three compositions of lipids vs Melittin molar ratio to lipids.

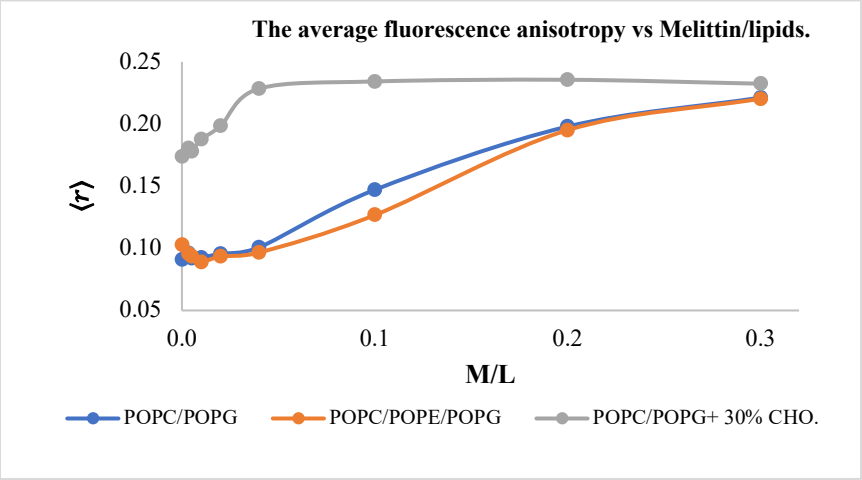

Figure 3. 14 The average fluorescence anisotropy $\langle r \rangle$ of the DPH of the three compositions vs melittin to lipids molar ratio.

3.5. DPH Orientational probability distribution function as a function of added melittin

One goal of this study was to assess the changes in the bilayer interior as the peptides proceed through the process of binding to the bilayer surface, penetrate deeper into the bilayer, intercalate between the phospholipid acyl chains, and finally produce bilayer-spanning pores. Because it is a free-tumbling fluorescent probe, DPH provides a unique tool to assess the overall ensemble packing of the acyl chains. Its size is 1.41 nm from C4 of one phenyl ring to the C4 of the opposite phenyl ring. The depth of the nonpolar, hydrophobic part of the bilayer, roughly from the glycerol backbone on one side of the bilayer to the glycerol backbone on the opposite leaflet of the bilayer, is about 3 nm. This means that DPH is about the length of the acyl chain region of one leaflet of a phospholipid bilayer. In other words, if DPH is roughly parallel to the bilayer normal it fits in one leaflet of the bilayer. Most methods of analyzing the orientation of DPH in a phospholipid bilayer assume that the principal orientation is more or less parallel to the phospholipid acyl chains. An example of this type of model is the popular wobbling-in-cone model of Kinoshita [24][103][112]. The Brownian Rotational Diffusion (BRD) model makes no assumptions about the orientation of DPH and explicitly allows for orientations that are at any angle from the bilayer normal. This is possible because it analyzes dynamic anisotropy decay in terms of contributions from both probe motion and probe orientational heterogeneity. It explicitly separates fluorophore motion from fluorophore equilibrium orientation. In general, fluorescence anisotropy is a result of both fluorophore motion on the time scale of the excited state lifetime, and non-random fluorophore orientation.

BRD model analyzes the anisotropy decay in terms of an explicit orientational distribution function, $f(\theta)$, based on the 2^{nd} and 4^{th} Legendre polynomials and rotation of the fluorophore about its long axis [24][103]. This rotational motion is the principal motion available to DPH over its excited state lifetime of about 10 nanoseconds in the hindered, highly viscous environment afforded by phospholipid acyl chains. Thus, the BRD analysis yields two related but distinct ways to characterize the bilayer acyl chain environment: motion of a fluorescent probe molecule, and equilibrium orientation of that molecule. The equilibrium orientational probability distribution provides a measure of the bilayer location of a large probe molecule like DPH.

Fig.3.15 shows the effect of the temperature on the angular orientational probability distribution function of DPH in interior bilayer (POPC). At both temperatures the probability distribution consists of two broad populations, one centered at about 15^0 and one centered at 90^0. The population at 15^0 consists of DPH molecules oriented essentially parallel to the phospholipid acyl chains. The basic structure of the phospholipid bilayer means that the population at 90^0 to the membrane normal must be in the bilayer midplane, between the two leaflets. At 10^0C the two distributions are about the same size; the probability from 0 to 45^0 is 48%. Also, the probability of orientations at high angles from the two main orientations, between 30^0 and 60^0, are low, but not zero. Raising the temperature to 37^0 shifts a significant amount of the 'acyl chain parallel' population to the population in midplane. This is consistent with a number of studies showing that temperature increases the motion of the highly flexible acyl chains, increasing the amount of time when they curl up and leave room in the bilayer midplane. This temperature-

induced shift in the two populations produces essentially no change in the small population of DPH at intermediate orientations [103].

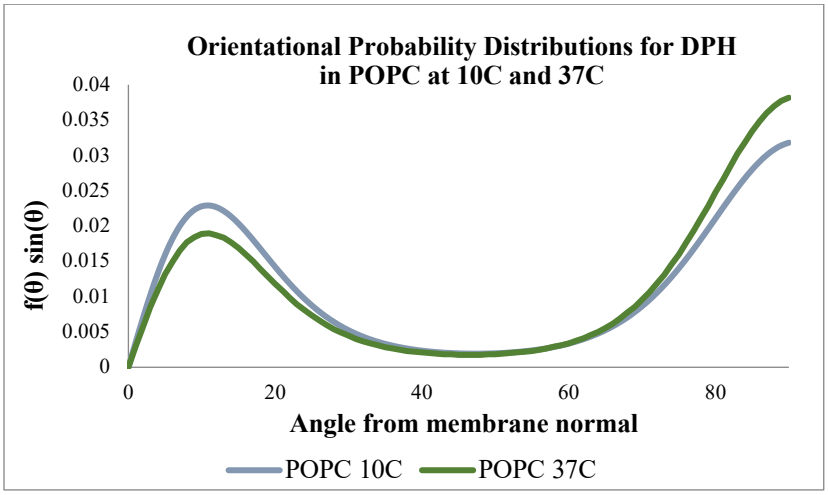

Figure 3. 15 The angular orientational probability distribution function $f(\theta)\,sin(\theta)$ of DPH with respect to bilayer normal for Vs the temperature for PC vesicles.

The equilibrium orientational distribution function, $f(\theta)\sin(\theta)$, for DPH in the three bilayers investigated in this study is shown in Fig 3.19, 3.20. The anisotropy decay analysis leads to the angular orientational probability distribution of DPH, $f(\theta)\sin(\theta)$. This angular distribution function summarizes the orientation of DPH in the absence of motion. The point of the BRD analysis of the DPH anisotropy decay is to separate anisotropy due to motion from anisotropy due to heterogenous orientation.

Fig. 3.18 shows the effect of the peptides on the angular orientational probability distribution function of DPH in the bilayer interior. These are orientational probability distributions, so the area under each curve is identical. In general, the probability distribution consists of two broad populations, one centered at about 12^0 and one centered at 90^0 from the bilayer normal. The population at 12^0 consists of DPH molecules oriented essentially parallel to the phospholipid acyl chains. The distribution centered at 90^0 from

the bilayer normal reflects a population of DPH in the bilayer midplane, oriented essentially parallel to the surface of the bilayer. As one might expect, the $f(\theta)\sin(\theta)$ of DPH molecules is clearly affected by the composition of the phospholipid bilayer, see Fig.3.18. In the case of cholesterol-containing lipid vesicles with no peptides, the distribution is generally divided in two populations; the probability density from 0 to 45^0 is about 76%, and it is very low (about ~9%) from 30 to 60^0. The effect of the cholesterol on the distribution of DPH increases the population of DPH oriented parallel to the acyl chains, which is similar to the change induced by a decrease in temperature.

The angular orientation probability distribution was also examined to figure out the effect of melittin concentration (Mel/L 1/100 and Mel/L 1/10) on DPH orientation in the interior of the bilayer of cholesterol-containing lipid vesicles. I have found that at Mel/L 1/100 the distribution of DPH from 0 to 45^0 increases to 78% and at high concentrations of Mel/L 1/10 it decreases to 70% in comparison with no melittin. Intermediate orientations, between 30 and 60^0 at Mel/L 1/100 is lower than with no melittin which is about 8% and almost completely eliminated at high concentration Mel/L 1/10 as shown in Fig. 3.19.

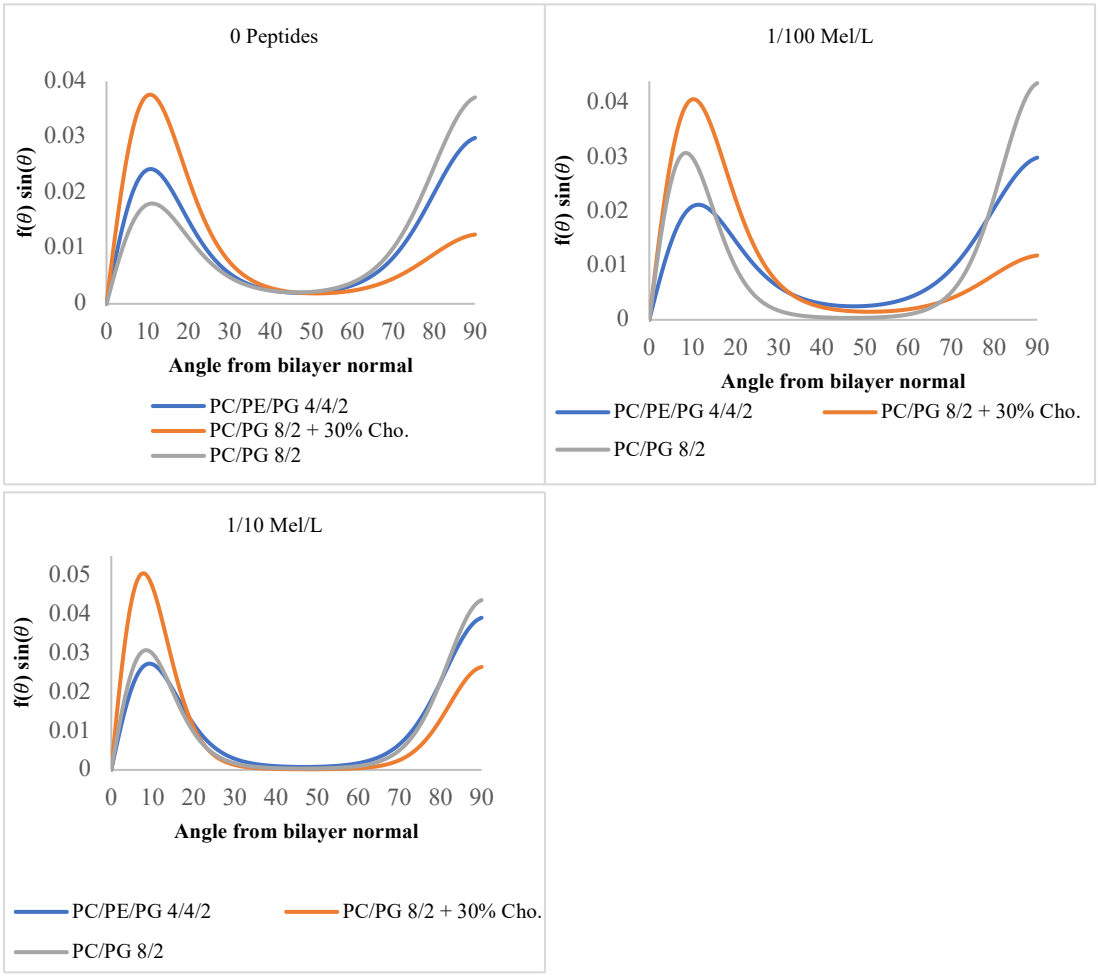

Figure 3. 16 The angular orientational probability distribution function $f(\theta)\,sin(\theta)$ of DPH with respect to bilayer normal for the three compositions for different melittin to lipids concentrations melittin/L.

In case of POPC/POPG with no peptides, the distribution is different in size; the probability from 0 to 45^0 is about 40%, and it is very low from 30 to 60^0 at about ~9%. In the absence of the cholesterol in the interior bilayer the distribution of DPH decreases the population of DPH oriented parallel to the acyl chains, which is similar to the change induced by an increase in temperature. The angular orientation probability distribution was also examined to figure out the effect of melittin concentration (Mel/L 1/100 and Mel/L 1/10) on DPH

orientation in the interior of the bilayer of POPC/POPE/POPG. I found that the distribution of DPH from 0 to 45^0 increases to 42% and 47% at concentrations of Mel/L 1/100 and Mel/L 1/10 in comparison with no melittin, respectively.

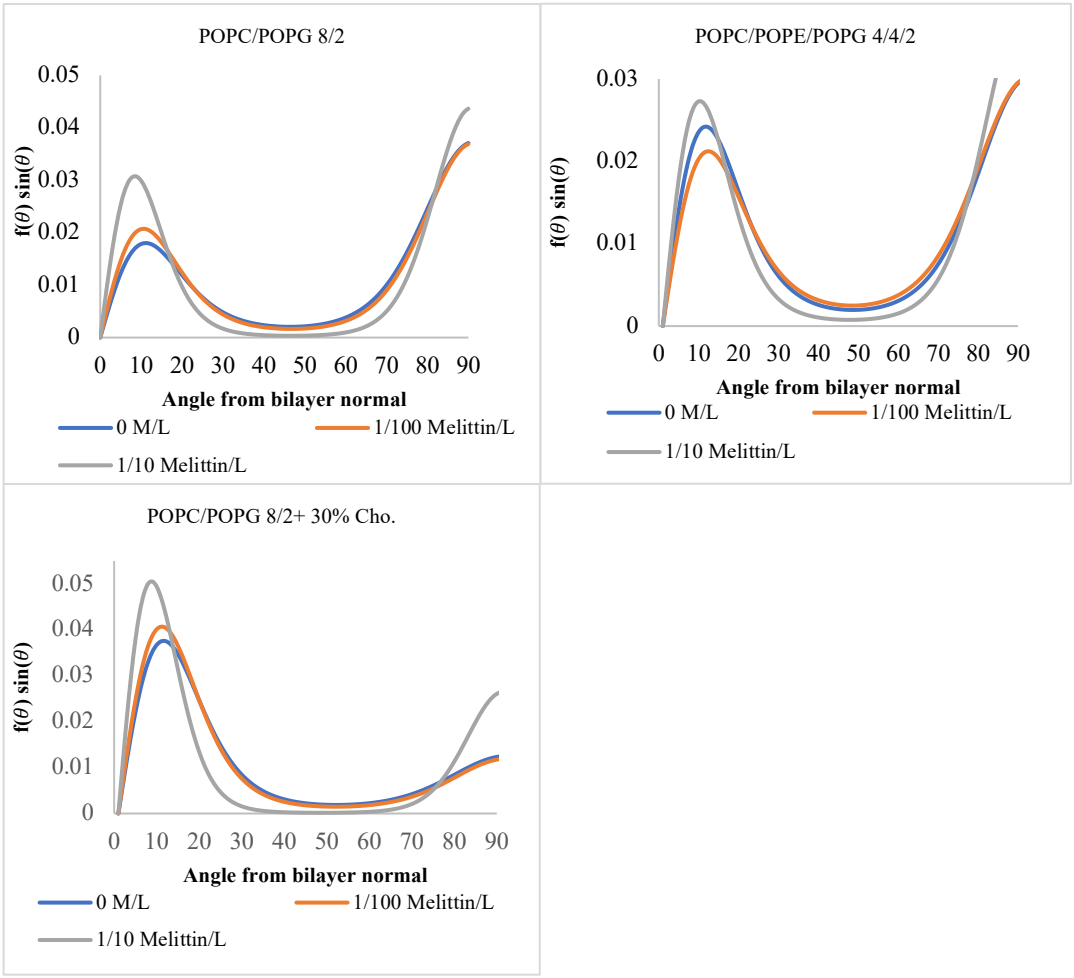

Figure 3. 17 The orientational probability distribution function $f(\theta)\,sin(\theta)$ of DPH with respect to bilayer normal for the three compositions for different melittin to lipids concentrations Mel/L.

The orientational distribution function, $f(\theta)\sin(\theta)$, for DPH shows how each bilayer is different. The most space in the midplane is found in PC/PG lipid vesicles, and the least is

in cholesterol-containing lipid vesicles. At 1/100 the intermediate orientations in PC/PG are already eliminated indicating that the two DPH populations have already been separated from each other. On the other hand, at 1/10 this is true for all three lipid compositions. This figure also shows that the fluorescence lifetime of DPH is shorter when there is more DPH in the midplane, and longer when there is more DPH parallel to the acyl chains (close to bilayer normal).

The orientational distribution function, $f(\theta)\sin(\theta)$, for DPH shows that how each bilayer is different. The most space in the midplane was in case of PC/PG lipid vesicles, and the least was in cholesterol-containing lipid vesicles. At 1/100 the intermediate orientations in PC/PG are already eliminated indicating that the two DPH populations have already been separated from each other. On the other hand, at 1/10 this is true for all three lipid compositions.

The parameter f_{random} is the overlap of the random orientational distribution, $f(\theta)_{rand}\sin(\theta)$ and the orientational probability distribution, $f(\theta)\sin(\theta)$, can be defined according:

$$f_{random} = 1 - \frac{1}{2}\int_0^{\pi} |f(\theta) - f(\theta)_{rand}|\ \sin(\theta)\ \mathrm{d}\,\theta$$

Where $f(\theta)$ is defined as a normalized distribution function according to Eq. 2.37.

$f(\theta)_{rand}$ is given by Eq. 2.33, with $L_2 = L_4 = 0$

This parameter f_{random} has the advantage that it results from a direct comparison with a random orientational distribution over the entire angular range from 0 to π.The parameter f_{random} provides information on changes in the degree of orientational freedom of DPH

due to changes in melittin concentration. The results of f_{random} DPH were determined using the BRD model for all of the phospholipid bilayers with respect to Mel/L and are summarized in table 3.12.

The Fig. 3.21 show that f_{random} of DPH has the lowest values when embedded in cholesterol-containing lipid vesicles, and it also decreases as Mel/L increasing. This effect of increasing Mel/L on f_{random} is similar to the effect of decreeing the temperature.

Table 3. 12 The parameter f_{random} of DPH embedded in all the three bilayer compositions.

M/L	PPC/POPG		POPC/POPE/POPG		POPC/POPG+30% Cho	
	f_{random}	σ	f_{random}	σ	f_{random}	σ
0	0.603	±0.01	0.572	±0.008	0.388	±0.007
1/300	0.596	±0.011	0.587	±0.007	0.375	±0.013
1/100	0.591	±0.01	0.605	±0.008	0.355	±0.004
1/25	0.568	±0.012	0.599	±0.005	0.274	±0.003

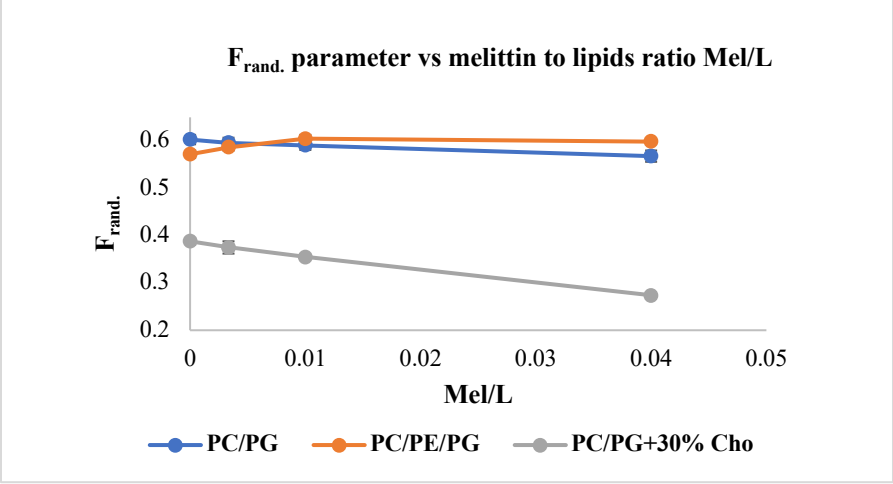

Figure 3. 18 $F_{rand.}$ parameter vs melittin to lipids ratio Mel/L.

By comparison between the f_{random} and distribution function, the results of f_{random} correspond to the angular orientational probability distribution function $f(\theta)\,sin(\theta)$ of DPH when DPH population shifted toward the bilayer normal, see Fig. 3.17. Instance, the f_{random} in the case of PC/PG slightly decreases when Mel/l decreases which is also corresponding to the angular orientational probability distribution function $f(\theta)\,sin(\theta)$ of DPH when DPH population shifted toward the bilayer normal, see Fig. 3.19. Interestingly, f_{random} in the case of PC/PE/PG increases a little as Mel/L increasing and the effect of Mel/L in this case as the effect of increasing the temperature, which supports the results of angular orientational probability distribution function $f(\theta)\,sin(\theta)$ of DPH when DPH population shifted down to midplane from the bilayer normal, see Fig. 3.20. In general, the parameter f_{random} summarizes the differences in acyl chain packing of the bilayer interior of the three-phospholipid bilayer as a function of Mel/L.

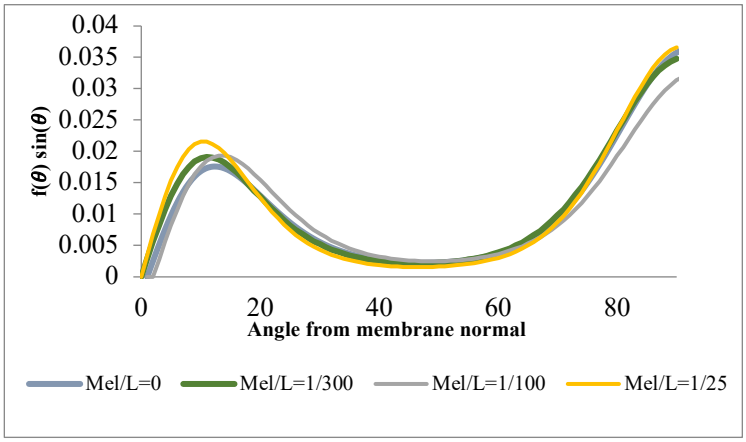

Figure 3. 19 The orientational probability distribution function $f(\theta)\,sin(\theta)$ of DPH with respect to bilayer normal for the PC//PG composition for different melittin to lipids concentrations Mel/L.

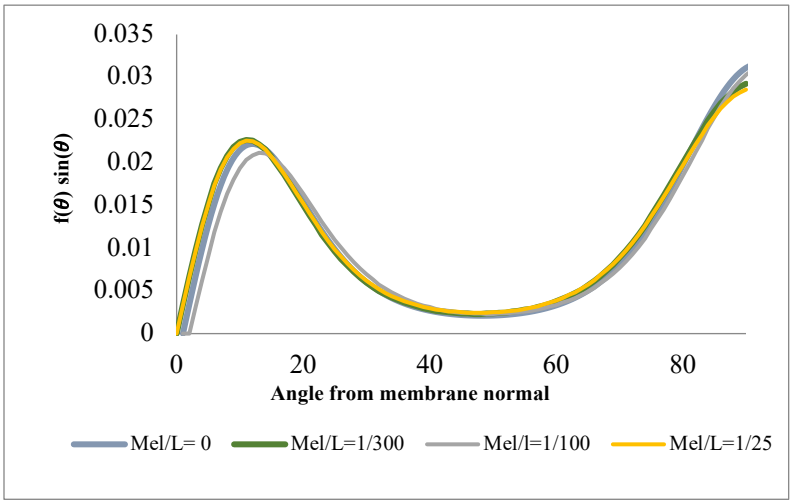

Figure 3. 20 The orientational probability distribution function $f(\theta)\,sin(\theta)$ of DPH with respect to bilayer normal for the PC/PE/PG composition for different melittin to lipids concentrations Mel/L.

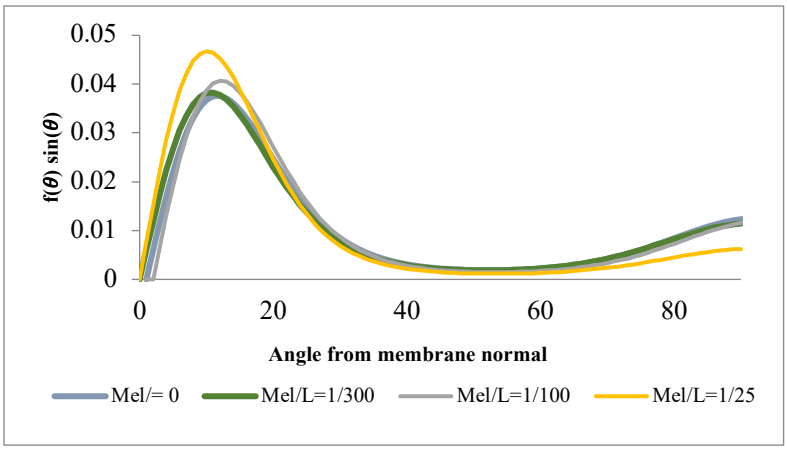

Figure 3. 21 The angular orientational probability distribution function $f(\theta)\,sin(\theta)$ of DPH with respect to bilayer normal for PC/PG+30% Cho composition for different melittin to lipids concentrations Mel/L.

3.6. Time-resolved fluorescence measurements of DPH as a function of added magainin 2

One goal of studying magainin 2 with the three compositions is to compare the different mechanism actions of the two AMPs that were used in this research (magainin 2 and melittin) with the three phospholipid bilayer compositions. The question of the last part of this dissertation is: What is the effect of the positive charges of peptides on the peptides-lipid interaction, and how is this interaction affected by the lipid composition? Magainin 2 does not have intrinsic fluorophore like melittin. Thus, the steady–state measurements to study magainin–bound lipids bilayers cannot be obtained by using intrinsic probes as a first step to study the binding of magainin 2 to phospholipids bilayer. Time-resolved fluorescence lifetime and anisotropy decay of DPH were used to study magainin 2–lipid bilayer interaction. Similarly, to time-resolved fluorescence measurements of melittin-lipid interaction, DPH fluorescence lifetime and anisotropy decay parameters were measured with respect to magainin 2 to lipids (Mag2/L) for each bilayer composition, and the results are summarized in tables 3.12-3.17. In contrast to melittin where the water penetration was induced above the critical ratio (Mel/L~1/50), water penetration was not induced at this ratio with magainin 2. Even at a concentration fifteen times higher than that (Mag2/L=3/10), it was not sufficient to allow to water molecules to penetrate to the bilayer, see Fig. 3.22. The evidence of no water penetration is that the increase of DPH lifetime $\langle\tau\rangle$ corresponds to an increase in magainin 2. The magainin 2 concentrations required to induce water penetration greatly depend on the surface charge density [21]. From the DPH lifetime $\langle\tau\rangle$ results reported in this experiment, the surface charge density (20% PG) is not enough for

magainin 2 to induce water penetration on the three studied phospholipid bilayers over the same range that were studied with the melittin-lipid bilayer interaction. Interestingly, the behavior of DPH $\langle\tau\rangle$ at high concentrations of magainin 2 to lipids (Mag2/L= 1/10, 1/5 and 3/10) is similar to the behavior of Mel/L at low concentration (1/300 and1/200). The data in tables 3.12 and 3.14 show that there is an observable increase in $\langle\tau\rangle$ of DPH of both lipid vesicles, POPC/POPG and cholesterol-containing PC/PG compared to magainin-free.

Table. 13 Effect of magainin 2 on fluorescence lifetime ⟨τ⟩ of DPH embedded in POPC /POPG 8/2 at 30 ºC

M/L	α_1	τ_1 (ns)	α_2	τ_2 (ns)	$\langle\tau\rangle$ (ns)
0	0.15±0.03	4.89±0.31	0.85±0.03	8.38±0.05	8.07±0.030
1/300	0.18±0.03	5.70±0.87	0.82±0.14	8.34±0.29	8.03±0.09
1/200	0.03±0.00	0.60±0.07	0.99±0.00	7.93±0.01	7.91±0.01
1/100	0.05±0.01	0.56±0.09	0.98±0.00	8.0±0.01	7.97±0.04
1/50	0.02±0.00	1.67±0.02	0.98±0.01	8.37±0.01	8.20±0.01
1/25	0.14±0.02	4.74±0.22	0.86±0.02	8.54±0.18	8.29±0.07
1/10	0.56±0.04	6.98±0.14	0.47±0.07	9.96±0.25	8.64±0.04
1/5	0.18±0.03	5.80±0.24	0.72±0.10	9.60±0.55	8.89±0.05
3/10	0.55±0.02	7.26±0.41	0.58±0.02	6.61±0.1	9.08±0.14

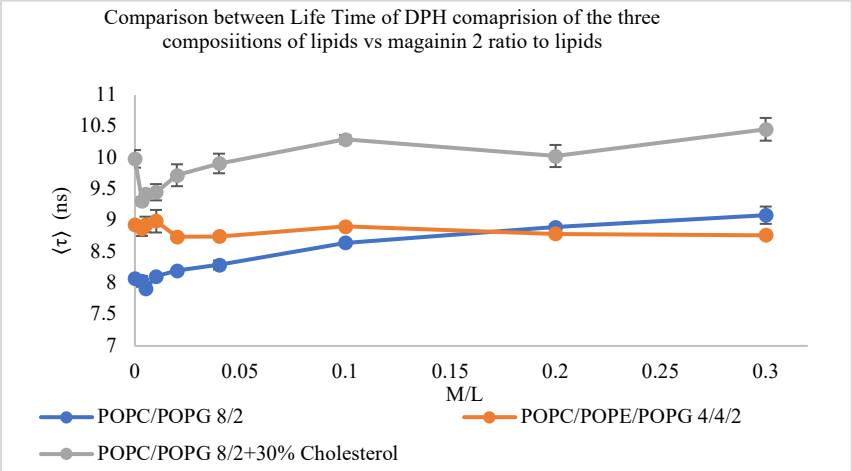

Figure 3.22 Comparison between the Lifetime of DPH in three compositions of lipids vs Magainin 2 to lipids molar ratio.

Table 3. 14 Effect of magainin 2 on fluorescence lifetime ⟨τ⟩ of DPH embedded in POPC/POPE/POPG 4/4/2 at 30 ºC

M/L	α_1	τ_1 (ns)	α_2	τ_2 (ns)	$\langle\tau\rangle$ (ns)
0	0.41±0.01	10.28±0.13	0.58±0.01	7.62±0.10	8.93±0.02
1/300	0.16±0.15	12.61±2.29	0.84±0.15	8.17±0.24	8.87±0.11
1/200	0.80±0.23	7.91±0.50	0.20±0.23	13.42±3.68	8.94±0.12
1/100	0.62±0.28	7.37±0.65	0.38±0.28	11.50±2.25	8.99±0.18
1/50	0.26±0.10	6.33±0.57	0.74±0.10	9.32±0.23	8.74±0.04
1/25	0.15±0.06	5.56±0.43	0.85±0.06	9.09±0.16	8.75±0.03
1/10	0.37±0.03	6.71±1.28	0.63±0.03	9.79±0.36	8.91±0.04
1/5	0.17±0.14	5.20±0.36	0.83±0.14	9.18±0.04	8.79±0.04
3/10	0.06±0.02	3.73±0.06	0.94±0.02	8.90±0.02	8.76±0.02

Table 3. 15 Effect of magainin 2 on fluorescence lifetime ⟨τ⟩ of DPH embedded in POPC/POPG 8/2+ 30% of Cholesterol at 30 ºC

M/L	α_1	τ_1 (ns)	α_2	τ_2 (ns)	$\langle\tau\rangle$ (ns)
0	0.19±0.13	8.45±0.56	0.80±0.14	10.28±0.312	9.98±0.14
1/300	0.70±0.23	9.00±0.31	0.30±0.23	9.80±0.465	9.30±0.06
1/200	0.78±0.33	9.41±0.10	0.22±0.33	9.75±0.372	9.42±0.06
1/100	0.32±0.01	8.95±0.16	0.68±0.01	9.67±0.204	9.45±0.13
1/50	0.57±0.49	6.19±0.88	0.44±0.49	12.22±2.931	9.72±0.18
1/25	0.56±0.27	8.42±0.87	0.44±0.27	11.29±0.760	9.91±0.16
1/10	0.90±0.05	9.29±0.12	0.10±0.05	16.05±1.93	10.29±0.07
1/5	0.75±0.19	9.17±1.93	0.25±0.19	12.75±0.18	10.03±0.18
3/10	0.56±0.14	8.53±0.62	0.44±0.14	12.21±0.18	10.45±0.18

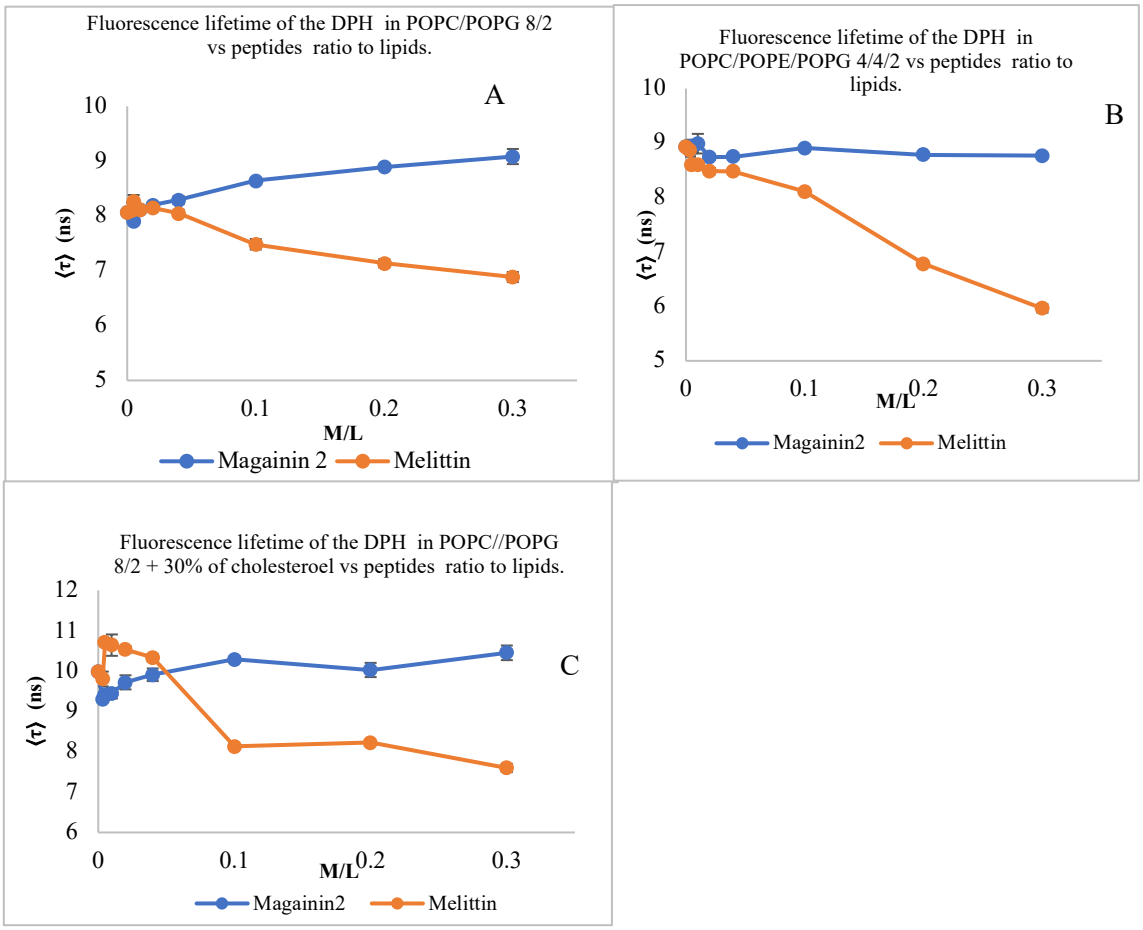

Figure 3. 22 Comparison between excited state lifetime of DPH with two peptides (melittin and magainin 2) as a function of peptides to lipids molar ratio. A) PC/PG, B) PC/PE C) PC/PG+ Chol.

At the same high ratio, the data in table 3.13 shows that $\langle\tau\rangle$ of DPH decreases as Mag2/L increases in the case of PE-containing lipids. This is most likely due to the same reason as the melittin analyses in the case of low concentrations described previously. These results agree with the results of the angular orientational probability distribution reported for DPH, $f(\theta)\sin(\theta)$, see Fig. 3.22. DPH orientation in the bilayer interior of POPC/POPG, and cholesterol-containing PC/PG was shifted toward the distribution centered at θ =15^0 from the bilayer normal. As a result, the $\langle\tau\rangle$ of DPH increases which is similar to the effect of

decreasing the temperature. However, for the PE-containing lipid vesicles, DPH orientation in the interior of the bilayer shifted toward the distribution centered at $\theta = 90^0$ from the normal on the surface of bilayer. Thus, the $\langle\tau\rangle$ of DPH decreases which is similar to the effect of increasing the temperature. The rotational correlation lifetime $\langle\emptyset\rangle$ from anisotropy decay analyses of DPH shows that $\langle\emptyset\rangle$ is essentially constant for cholesterol-containing, and PE-containing bilayers but increases in PC/PG above Mel/L~1/50 as shown in Fig. 3.23.

Table 3. 16 Effect of magainin 2 on fluorescence anisotropy of DPH embedded in POPC/ POPG 8/2 at 30 ºC

M/L	r_0	$\langle\emptyset\rangle$ (ns)	P_2	P_4	$D_\perp$	S	$\langle r\rangle$
0	0.367±0.007	2.325±0.051	0.177±0.004	0.352±0.016	0.153±0.007	0.177±0.004	0.012
1/300	0.377±0.006	2.047±0.141	0.225±0.014	0.374±0.006	0.179±0.012	0.226±0.016	0.019
1/200	0.380±0.005	1.804±0.020	0.238±0.013	0.352±0.006	0.181±0.006	0.245±0.015	0.023
1/100	0.383±0.001	1.772±0.172	0.248±0.006	0.345±0.015	0.178±0.007	0.254±0.008	0.025
1/50	0.383±0.003	1.886±0.127	0.229±0.010	0.378±0.027	0.197±0.011	0.234±0.009	0.021
1/25	0.374±0.003	2.188±0.020	0.244±0.019	0.395±0.008	0.178±0.012	0.244±0.019	0.022
1/10	0.366±0.013	3.756±0.183	0.2943.015	0.478±0.073	0.212±0.111	0.298±0.011	0.033
1/5	0.380±0.003	3.861±0.034	0.337±0.012	0.514±0.022	0.200±0.009	0.339±0.015	0.044
3/10	0.368±0.002	3.788±0.067	0.332±0.016	0.513±0.013	0.160±0.018	0.332±0.016	0.041

Table 3. 17 Effect of magainin 2 on fluorescence anisotropy of DPH embedded in POPC/POPE/POPG 4/4/2 at 30 ºC

M/L	r_0	⟨∅⟩ (ns)	P_2	P_4	$D_\perp$	S	⟨*r*⟩
0	0.388±0.003	1.949±0.036	0.324±0.003	0.421±0.008	0.193±0.009	0.324±0.003	0.103
1/300	0.380±0.002	1.977±0.035	0.318±0.005	0.418±0.005	0.190±0.008	0.318±0.005	0.101
1/200	0.375±0.006	1.966±0.038	0.325±0.010	0.412±0.013	0.183±0.011	0.325±0.010	0.100
1/100	0.379±0.001	1.929±0.011	0.320±0.010	0.420±0.008	0.196±0.012	0.320±0.009	0.099
1/50	0.380±0.001	2.006±0.031	0.315±0.012	0.416±0.006	0.187±0.012	0.315±0.012	0.102
1/25	0.383±0.004	1.988±0.023	0.307±0.009	0.421±0.009	0.196±0.013	0.307±0.009	0.100
1/10	0.372±0.007	2.173±0.056	0.293±0.013	0.415±0.006	0.179±0.007	0.293±0.013	0.099
1/5	0.396±0.005	2.089±0.022	0.277±0.011	0.461±0.015	0.244±0.017	0.277±0.011	0.101
3/10	0.371±0.007	2.422±0.054	0.294±0.012	0.405±0.013	0.154±0.012	0.294±0.012	0.105

Table 3. 18 Effect of magainin 2 on fluorescence anisotropy of DPH embedded in POPC/POPG 8/2+ 30% of Cholesterol at 30 ºC

M/L	r_0	⟨∅⟩ (ns)	P_2	P_4	$D_\perp$	S	⟨*r*⟩
0	0.376±0.016	1.410±0.183	0.622±0.004	0.525±0.025	0.165±0.043	0.622±0.004	0.174
1/300	0.383±0.003	1.536±0.004	0.610±0.004	0.532±0.003	0.161±0.001	0.610±0.004	0.176
1/200	0.384±0.004	1.486±0.032	0.615±0.002	0.535±0.003	0.166±0.007	0.616±0.002	0.178
1/100	0.387±0.004	1.519±0.010	0.615±0.003	0.539±0.005	0.165±0.003	0.615±0.003	0.180
1/50	0.391±0.024	1.501±0.202	0.608±0.011	0.519±0.012	0.158±0.022	0.608±0.011	0.178
1/25	0.380±0.006	1.590±0.016	0.613±0.004	0.532±0.008	0.154±0.007	0.613±0.004	0.175
1/10	0.379±0.001	1.679±0.003	0.621±0.002	0.545±0.005	0.150±0.006	0.621±0.002	0.178
1/5	0.378±0.011	1.840±0.148	0.626±0.012	0.551±0.004	0.139±0.024	0.626±0.012	0.184
3/10	0.382±0.00	1.839±0.086	0.643±0.006	0.568±0.012	0.138±0.011	0.643±0.006	0.192

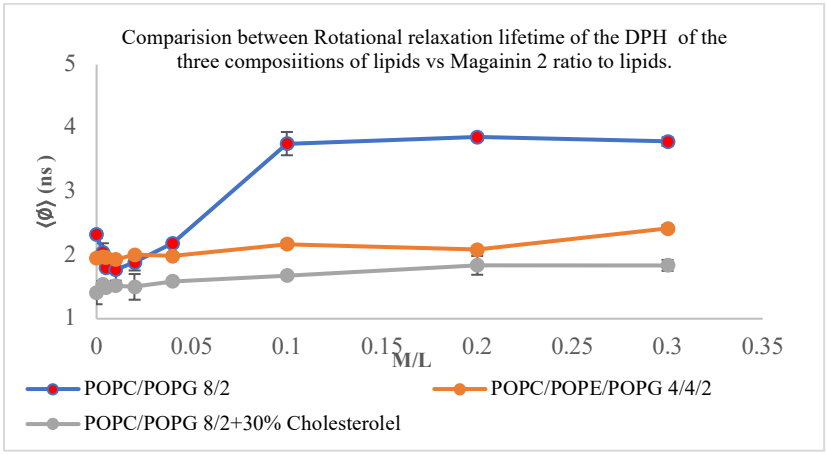

Figure 3. 23 Comparison between Rotational relaxation lifetime ⟨Ø⟩ of the DPH of the three compositions of lipids vs Magainin molar ratio to lipids.

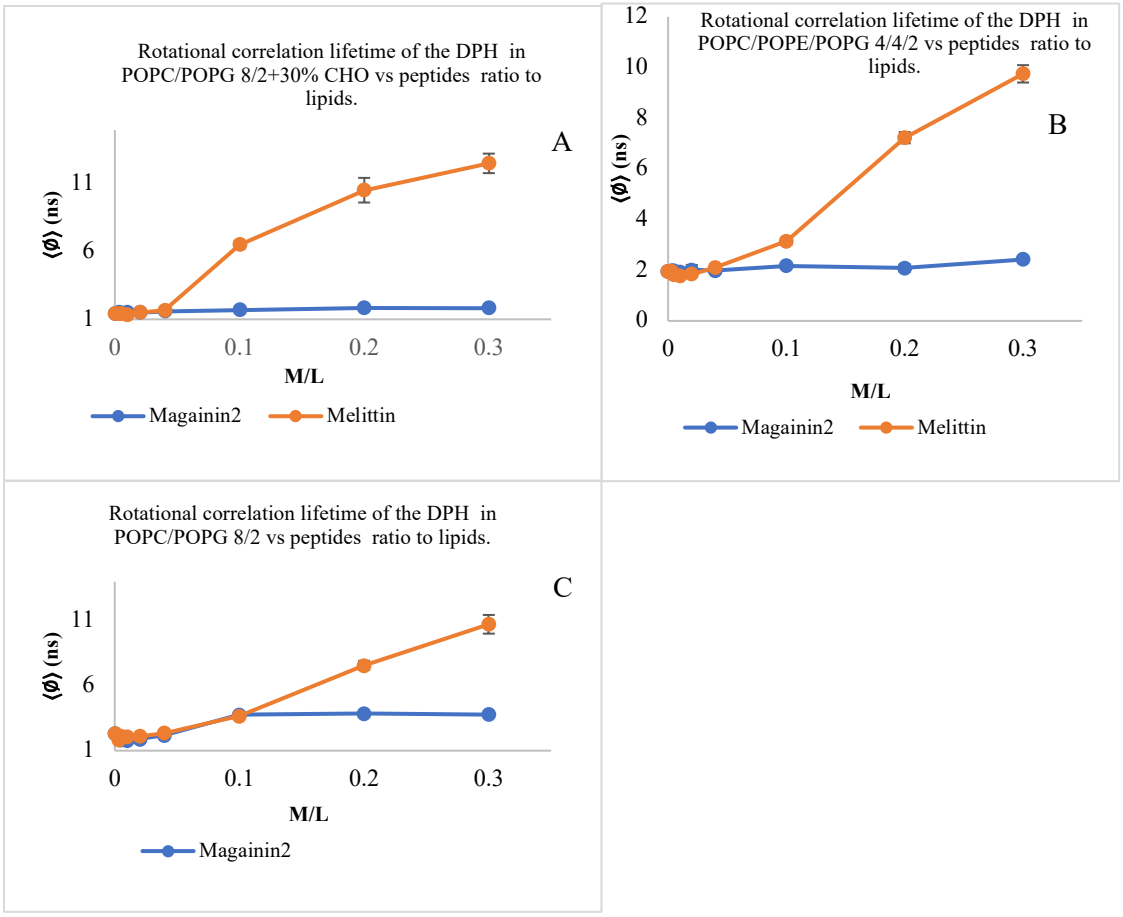

Figure 3. 24 Comparison between correlation rotational lifetime ⟨Ø⟩ of DPH with two peptides (melittin and magainin 2) as a function of peptides to lipids molar ratio. A) PC/PG, B) PC/PE C) PC/PG+ Chol.

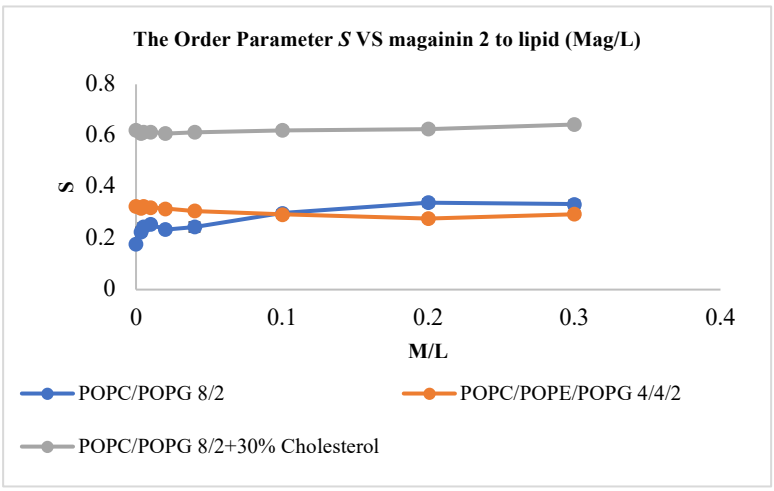

Figure 3. 25 The average fluorescence anisotropy $\bar{r}$ of the DPH of the three compositions vs magainin 2 to lipids molar ratio.

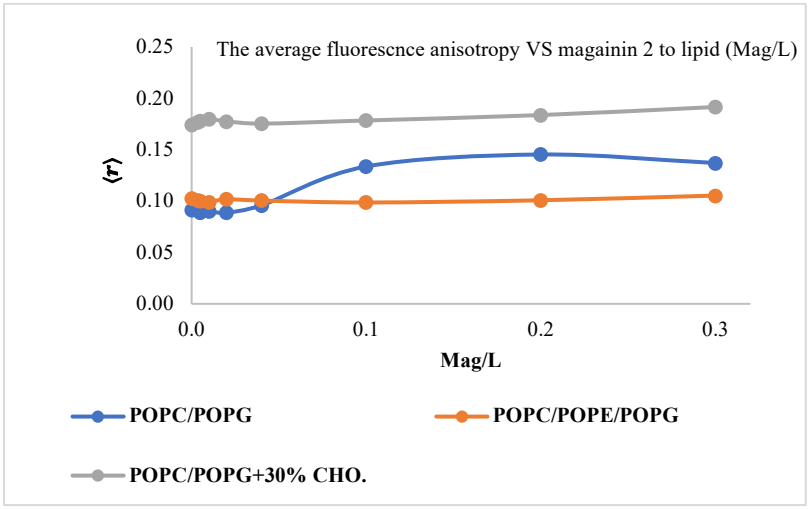

Figure 3. 26 The average fluorescence anisotropy $\bar{r}$ of the DPH of the three compositions vs magainin 2 to lipids molar ratio.

The lipid order parameter S and the motion parameter average anisotropy $\langle r \rangle$ of the DPH fluorophore were evaluated from the anisotropy decay results as described before in section 3.2.3. The parameters S and the$\langle r \rangle$ are essentially unchanged for cholesterol-containing and PE-containing lipid vesicles. The consistency of these fluorescence anisotropy decay parameters of DPH indicates no observable changes into the bilayer interior induced by

magainin 2 over the range of Mag2/L studied in this research. These results support the consistency of the excited state lifetime $\langle\tau\rangle$ and angular orientational probability distribution results of DPH as shown in Fig. 3.23 and 3.27. On the other hand, in the case of PC/PG phospholipids bilayer, S and $\langle r\rangle$ increase when Mag2/L increase above 1/25. Angular orientational probability distribution results of DPH embedded to POPC/POPG show that at high concentrations of Mag2/L~1/10 the DPH shifted to the midplane between the two leaflets as shown in Fig. 3.27. This result agrees with increasing of excited state lifetime $\langle\tau\rangle$ of DPH at any Mag2/L above 1/25 as shown in Fig. 3.23.

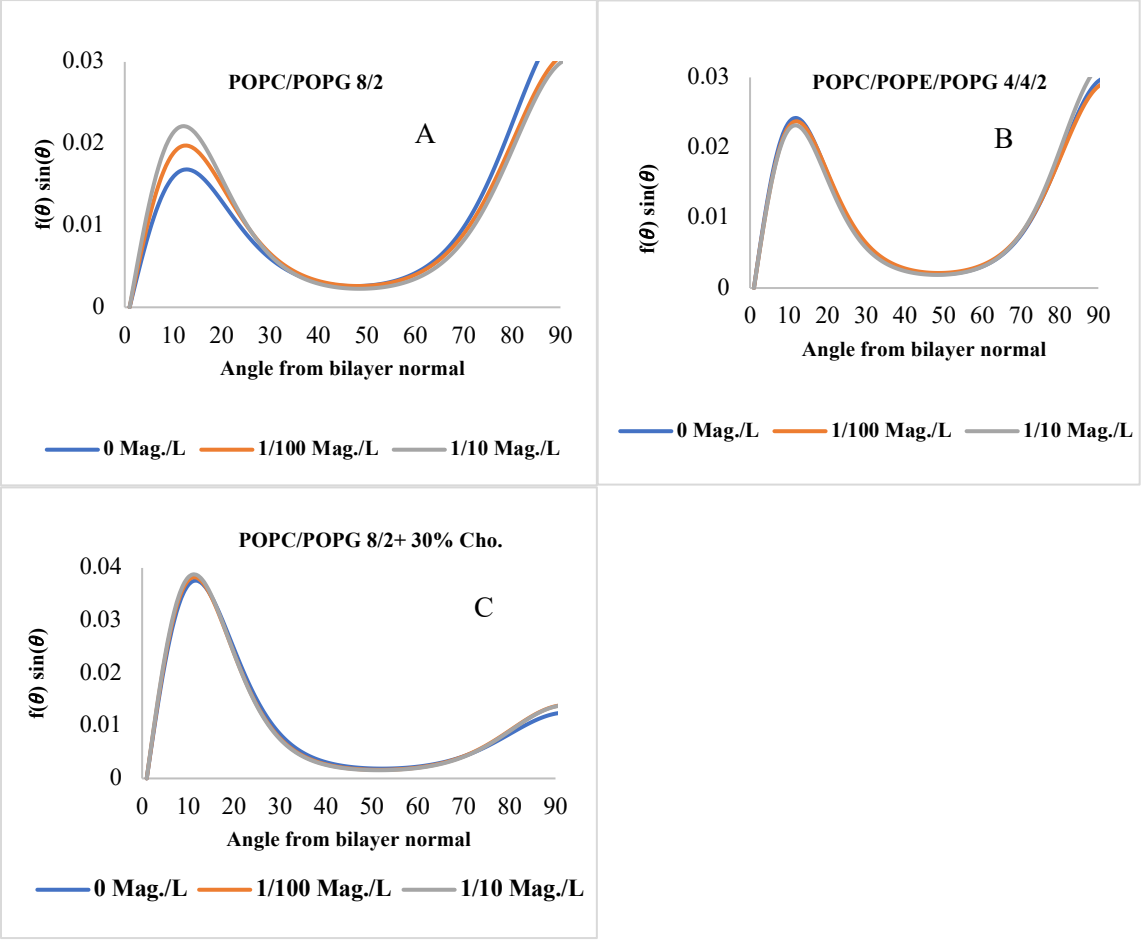

Figure 3. 27 Shows the angular orientational probability distribution function $f(\theta)\,sin(\theta)$ of DPH with respect to bilayer normal for both compositions for different magainin 2 to lipids concentrations Mag2/L. A) PC/PG, B) PC/PE C) PC/PG+ Chol.

The results of angular orientational the probability distribution of DPH, $f(\theta)\sin(\theta)$ for both molar ratios 1/100 and 1/10 are almost the same for all of cases with no. This is supported by fluorescence lifetime measurements where there are no big changes in the lifetime as shown in figure 3.23. This is evidence that the magainin 2 does not let water penetrate the bilayer at these concentrations see Fig. 3.27.

4. Discussion

Tryptophan Fluorescence - aqueous The tryptophan residue at position 19 (W19) of melittin was used as a fluorescent probe. The sensitivity of W19 fluorescence lifetime $\langle \boldsymbol{\tau} \rangle$ in aqueous buffer (lipid-free) was investigated as a function of temperature. It was found that the lifetime parameters are highly sensitive to changes in the temperature and local environment like the dielectric constant and the polarity. The results show that the Trp lifetime is increased by about 100% when the temperature decreased from 40 to 10°C, see table 2. The dielectric constant in water increases continuously as a temperature increases. The values of the polarity parameter ($\Delta \boldsymbol{f}$) as a function of temperature were calculated, and I found that $\Delta \boldsymbol{f}$ decreases linearly as the temperature increases, see Fig. 3.4. Analysis in terms of the Lippert-Mataga equation and the polarity parameter ($\Delta \boldsymbol{f}$) show that, the shifts of the 0-0 absorption and fluorescence transition energies ($\langle \Delta \boldsymbol{E} \rangle = \langle \Delta \boldsymbol{E_A} \rangle - \langle \Delta \boldsymbol{E_B} \rangle$) decrease as the polarity parameter decreases. The fluorescence lifetime of tryptophan is known to be reduced as the polarity of the tryptophan environment increases due to accelerated deactivation processes in polar environments [118][126]. Decrease in dielectric constant is correlated with a decrease in the Trp fluorescence lifetime as shown by Fig 3.3. I conclude that the decreased dielectric constant enhances either triplet state production or intersystem crossing as both would reduce the number of excited states that decay via photon emission.

Tryptophan Fluorescence – bilayer interactions The tryptophan residue at position 19 (W19) of melittin was used as a fluorescent probe to follow melittin binding to three

phospholipid bilayers measuring both steady-state and time-resolved fluorescence. Previous studies have observed a blue shift of the fluorescence emission maximum and a reduction in fluorescence intensity of W19 due to bilayer-bound melittin [126] [146]. The steady state results in this research confirmed that addition of melittin gradually moved λ_{max} to lower wavelengths, then it stayed constant. The changes in lifetime of W19 with added melittin showed different behavior, and the effect depended on bilayer composition. For all three bilayers the lowest dose of melittin (Mel/L=1/400), corresponding to initial binding to the surface, caused a large drop in W19 lifetime. This drop would be consistent with a slight reduction in the local dielectric constant around W19 upon binding to the bilayer. However, alternative mechanisms such as increased vibrational deexcitation (non-radiative), triplet state production or intersystem crossing are also possible.

At higher ratios of melittin to lipid the changes in W19 fluorescence lifetime were similar in the two bilayers without cholesterol, but quite different in the cholesterol-containing bilayer. In the two bilayers without cholesterol the shifts in W19 lifetime at the lowest dose at 30^0C were essentially identical; from (2.57±0.01) ns in the aqueous phase to (1.13±0.03) bound to PC/PG and (1.15±0.00) ns bound to PC/PG/PE. In both bilayers addition of melittin to 1/100 (Mel/lipid) raised the fluorescence lifetime to a statistically significant extent; (1.68±0.02) ns in PC/PG and (1.46±0.00) ns in PC/PG/PE. In both bilayers this value was essentially unchanged at higher doses of melittin. This pattern suggests that in these two bilayers W19 undergoes a similar change in local environment during the transition from initial binding to intermediate formation and final pore formation. It seems unlikely that the changes in W19 lifetime are solely due to differing local dielectric as this

would imply that W19 is most imbedded in the membrane in the surface bound state and becomes less deeply buried as pore formation proceeds. The multiple mechanisms that could reduce W19 lifetime make it impossible to assign a specific mechanism without further studies. However, it is clear from the results that in these two bilayers melittin, or at least W19, experiences two distinct environments when bound to the bilayer.

At the lowest dose of melittin in the cholesterol-containing bilayer W19 lifetime was reduced less than in the other two bilayers; from (2.57±0.01) ns aqueous to (1.54±0.01) ns. Surprisingly this value was essentially unchanged as the ratio of melittin to lipid was increased above ~1/400. Previous studies showed that over the range of added melittin examined in the current work melittin induces leakage in cholesterol-containing bilayers, which is cited by most investigators as evidence of transient pore formation [147]. The fact that W19 fluorescence lifetime was unchanged over this wide range of melittin strongly suggests that the W19 stays in the same environment as melittin binds to the membrane, likely forms pre-pore intermediate structures, and eventually forms trans bilayer pores. This implies that the enhanced van der Waals interactions between the acyl chains due to cholesterol inhibit the changes of W19 location during the process of binding and pore formation. The experimental data on pore structure are important and proportional to concentrations of melittin to lipids [145]. In the literature the ratio of melittin to lipid in the absence of cholesterol to form pores is about Mel/L = 1/100 [145]. In presence of cholesterol, approximately three times more melittin is required to make pores [118][126]. The differences between the measured Trp lifetimes in the three bilayers is evidence that

the local environment of W19 when melittin is bound to the bilayer surface is different in the three compositions.

Characterization of the bilayer interiors A combination of time-resolved study of the fluorescence intensity and anisotropy decay of the embedded DPH fluorophore at 30 ºC were applied to provide details regarding the effect of the peptides on the interior of the phospholipid bilayer. The high sensitivity of fluorescence decay parameters of DPH to the polarity and acyl chain packing density of the bilayer provide detailed information about the bilayer interior [148]. The DPH fluorescence lifetime is especially sensitive to water molecules which makes it a valuable sensor of dynamic water penetration into the lipid bilayer [149]. The dynamic quenching by water molecules is responsible for the deactivation of DPH excited states [150]. Therefore, If the amount of water is increased the DPH lifetime decreases [80]. Previous studies observed that addition of cholesterol to large unilamellar vesicles composed of di-18:1 PC (DOPC) increases the lifetime of DPH [151][148]. The average lifetimes of the DPH measured in strongly packed lipids in the liquid-ordered phase, L_o is greater than the loosely packed lipids in the liquid-disordered L_d phase[148].

In the absence of peptides, the present results showed that the DPH fluorescence lifetime value was lowest in the POPC/POPG bilayer (8.07±0.03) ns intermediate in the PE-containing bilayer (8.93±0.02) ns, and greatest in the cholesterol-containing bilayer (9.98±0.14) ns. This demonstrates that in the cholesterol-containing bilayer the enhanced van der Waals interactions between the acyl chains resulted in tighter headgroup packing, and this allowed less water penetration into the bilayer interior. It also shows that adding

the smaller PE to the base PC/PG bilayer increases the headgroup packing and therefore water penetration into the bilayer will be reduced. [152]. I concluded that the increase of fluorescence lifetime of DPH indicates both cholesterol and PE reduce the water penetration into the bilayers by comparison to the base bilayer, see Fig 3-12.

Rotational relaxation lifetime, $\langle\emptyset\rangle$, of DPH was used to summarize the motion of embedded DPH in the bilayers. In the absence of peptides, the DPH anisotropy results showed that the motion of DPH is different in the three bilayers. DPH rotational relaxation time reflects only the motion of DPH but not the order of the bilayers interior, and $\langle\emptyset\rangle$ was largest in the PC/PG bilayer (2.325±0.051) ns, intermediate in the PE-containing bilayer (1.949±0.036) ns, and smallest in the cholesterol-containing bilayer (1.410±0.183). Interestingly, both cholesterol and the PE head groups restrict the motion of DPH less by comparison to the base bilayer. The rotational relaxation lifetime, $\langle\emptyset\rangle$, is a time constant, thus smaller values correspond to faster motion. I concluded that, the rotational relaxation time results of DPH showed the behavior of the embedded DPH depends on the bilayer interior and headgroup composition, and $\langle\emptyset\rangle$ is significantly affected by both PE headgroups and cholesterol.

The anisotropy decay measurements were analyzed in terms of the Brownian Rotational Diffusion model which summarizes orientational order in terms of the angular orientational probability distribution, $f(\theta)\sin(\theta)$ of DPH. The results of $f(\theta)\sin(\theta)$ showed that DPH molecules in the bilayer consisted of two populations, one approximately parallel to bilayer normal and one parallel to the plane of bilayer, presumably in the bilayer midplane between the two leaflets where free volume is largest, see Fig. 3-16. One way to compare

orientational probability distributions, like those shown in Fig. 3-16, is in terms of the relative size of these two populations. F_{perp} is the fraction of the DPH in the population centered at 90^0 form the bilayer normal, the fraction of DPH oriented about the bilayer midplane. Previous studies show that an increase in temperature increases this population, thus it is a good measure of overall ensemble acyl chain order [7]. In the absence of peptide F_{perp} was largest in PC/PG (0.54 ± 0.01), intermediate in PE-containing bilayer (0.428 ± 0.007) and lowest with cholesterol (0.201 ± 0.007). Cholesterol greatly increases the population of DPH oriented parallel to the acyl chains, similar to the change induced by a decrease in temperature. In the presence of PE DPH molecules prefer to be accommodated in the direction of the bilayer normal by comparison into the base bilayer but less so than in the cholesterol-containing bilayer. These results of the DPH orientational distribution as a function of lipid composition reflect the order of the bilayer interior and the overall ensemble packing of the bilayer acyl chains [153].

Melittin effects on the bilayer interior The addition of peptides to the three bilayers produced changes in both DPH fluoresce lifetime and anisotropy decays that were dose-dependent and distinct for each bilayer. In the PC/PG bilayer melittin caused no statistically significant change in the DPH fluoresce lifetime, $\langle\tau\rangle$, until the ratio of melittin to the lipids reached 1/10 (Mel/L). At this high ratio of melittin to lipid $\langle\tau\rangle$ decreased from (8.07±0.03) ns to (7.48±0.10) ns, indicating that melittin disrupted headgroup packing with respect to water penetration. This level of melittin is well into the range where previous studies report melittin-induced trans-bilayer leakage, presumably through melittin pores. This the first report that the early stages of melittin-bilayer interaction, initial binding and

pre-pore intermediate formation, have no effect on headgroup packing, at least in a PC/PG bilayer.

In the presence of the cholesterol the DPH lifetime response to melittin was dramatically different. At the lowest dose of melittin, 1/300, where all binding is to the surface of the bilayer, there was no change in ⟨τ⟩. The next highest dose of melittin, 1/100, caused a statistically significant increase from (9.98±0.14) ns to (10.64±0.27) ns, indicating that melittin had induced tighter headgroup packing, which is the opposite of the effect in PC/PG with no cholesterol. At a high dose of melittin, 1/10, ⟨τ⟩ was reduced, below the value in the absence of melittin to (8.13±0.02) ns. This reversing of melittin's effects in the cholesterol membrane, sealing the membrane at intermediate melittin concentrations, and increasing water permeability at a high concentration is another demonstration that melittin-bilayer interaction for cholesterol-containing bilayer is distinct from cholesterol-free bilayers. I concluded that, the behavior of the DPH lifetime at a ratio of Mel/L less than 1/25 is totally different in the presence of cholesterol by comparison to the presence of POPE and the base bilayer.

The fluorescence intensity decays of DPH results show that fluorescence lifetime ⟨τ⟩ decreases at about Mel/L~1/25 in the case of POPE and base bilayer, and at about Mel/L~1/10 in case of cholesterol-containing bilayer.

In the PE-containing bilayer the effect of melittin on ⟨τ⟩ was unique at the two intermediate concentrations of melittin. At both 1/100 and 1/25 (melittin/lipid) ⟨τ⟩ was significantly reduced, from (8.93±0.020) ns to (8.59±0.03) ns and (8.48±0.05) ns, respectively. This suggests that PE causes a weakening of headgroup packing during the intermediate phase

between initial bilayer binding and pore formation. This is in contrast with both PC/PG, where there was no change over this concentration range, and PC/PG/cholesterol where the opposite change in headgroup packing was observed. This is evidence that melittin interacts with a PE-containing bilayer that is distinct from a PC/PG bilayer which has been used in the vast majority of studies.

The effects of melittin on DPH rotational relaxation time ⟨∅⟩ was unique in each bilayer and demonstrates that each bilayer interior undergoes distinct changes in response to melittin binding to the bilayer surface and proceeding pore formation. In the PC/PG bilayer the smallest dose of melittin, 1/300, caused a significant increase in the rate DPH rotation, ⟨∅⟩ deceased from (2.33±0.05) ns to (1.81±0.134) ns. This surprising result suggests that melittin on the surface of a PC/PG bilayer induces more rapid motion of DPH in the bilayer interior. This increase in motion was also observed at higher melittin concentrations, but at 1/10 ⟨∅⟩ increased to (3.65±0.11) ns, indicating a large reduction in DPH motion at this high melittin concentration. The effects of melittin in the PE-containing bilayer were qualitatively similar, but there was no effect at 1/300, and the melittin-induced increase in DPH rotation was observed at 1/100 (melittin/lipid). Similar to the effects observed in PC/PG the high ratio of 1/10 caused significant reduction in DPH rotation as ⟨∅⟩ was increased from (1.95±0.04) ns to (3.15±0.14) ns. In contrast, melittin in the cholesterol-containing bilayer had no effect on ⟨∅⟩ for DPH at the concentrations below 1/25. At 1/25 it increased ⟨∅⟩ from (1.41±0.18) ns to (1.67±0.06) ns, indicating a reduction in DPH motion. Further addition of melittin to a ratio of 1/10 dramatically slowed DPH motion as ⟨∅⟩ increased to (6.52+±0.292) ns.

Adding melittin to the bilayers had a big effect on the population of DPH in the bilayer interior, although the melittin-induced effects were distinct in each composition. Increasing the concentration of melittin reduced the population of DPH molecules oriented about the membrane bilayer normal in both PC/PG and PC/PG/cholesterol. This trend was essentially monotonic over the melittin concentration range from 1/300 to 1/25. At 1/25 F_{perp} in PC/PG was reduced from 0.54 to 0.49, while in cholesterol it was reduced from 0.20 to 0.10, suggesting a more dramatic change in the cholesterol bilayer. Surprisingly the changes in F_{perp} observed in the PE-containing bilayer were distinct, and in the opposite direction. In this bilayer the smallest dose of melittin, 1/300, caused an increase in F_{perp} from 0.42 to 0.44, which was statistically significant. This increase in F_{perp} was essentially unchanged at higher concentrations of melittin. These results clearly suggest the presence of PE headgroups reverses the effect of melittin binding on acyl chain packing in the core, the midplane region, of the bilayer. This is a surprising result, and the paucity of studies in the literature of melittin interaction with PE-containing bilayers does little to suggest an explanation. As a result, adding melittin to the bilayers increases the order of the bilayer interior which is like the effect of decreasing the temperature. Adding melittin apparently extends the acyl chains tails in of the bilayer midplane and make less room for the DPH in this region.

Magainin 2 effects on the bilayer interior Magainin 2 (Mag2) has been found to be less active than melittin in previous research [154]. These studies also showed that Mag2 cationic residues are distributed along its length and form a large angle on the helical face, see Fig 1.8 [154]. Mag2 acts as a positive curvature inducing bilayer wedge, thus Mag2 is

unable to fully insert into the core of hydrophobic lipid bilayers due to its large polar angle [154][155] [156].

In the PC/PG bilayer Mag2 had only negligible effect on the DPH fluorescence lifetime, ⟨τ⟩ at concentrations below 1/25 (Mag2/lipid). Above this concentration it gradually raised ⟨τ⟩ indicating that very high levels of Mag2 reduce transient water penetration into the bilayer. The effects of Mag2 on DPH rotational motion, ⟨∅⟩, were also modest. At magainin concentrations up to 1/25 ⟨∅⟩ was gradually increased by a few tenths of a nanosecond, indicating that the DPH rotational rate was increased. The largest effect of Mag2 in the PC/PG bilayer was a shift in the orientational probability distribution, where population was shifted away from the distribution centered about the bilayer midplane, as shown in Fig. 3.28. This figure shows that Mag2 at a level of 1/100 shifts the fractional population in the midplane distribution, F_{perp}, from 0.54 to 0.49, and the addition of Mag2 to a ratio of 1/10 reduces F_{perp} further to 0.44. These are larger than the changes in the orientational order of DPH induced by melittin binding to the bilayer. These results are somewhat surprising given the modest changes in DPH fluorescence lifetime and rotational motion. This suggests that Mag2 bound to the surface of a PC/PG bilayer induces changes in acyl order that propagate to the midplane of the bilayer and reduce the free volume available to DPH.

In the POPE-containing bilayer Mag2 produced only small changes in any of the DPH fluorescence parameters below very high concentrations of Mag2. Mag2 produced no noticeable changes on the DPH lifetime up to about 1/10 Mag2/L, where there was a statistically significant decrease in lifetime. The rotational motion parameter for DPH, ⟨∅⟩,

was not significantly changed by any concentration of Mag2. Likewise, magainin had no significant effect on the DPH orientational probability distribution, $f(\theta)\sin(\theta)$, at any ratio of Mag2 to lipids, as shown in Fig. 3.28.

In the cholesterol-containing bilayer changes in lifetime, $\langle\tau\rangle$ of the embedded DPH in the bilayer interior did not appear until the ratio of Mag2 to lipids reached Mag2/L~>1/25, and the DPH lifetime increases as the ratio of Mag2 to lipids increases. This increase of DPH lifetime indicates a reduction in water entering the hydrophobic core of the bilayer interior caused by magainin 2. Similar to the cholesterol-containing bilayer, in presence of PE, Mag2 had no effect on DPH rotational motion, $\langle\emptyset\rangle$, or the orientational probability distribution, $f(\theta)\sin(\theta)$, at any ratio of Mag2 to lipids. There is no change in $f(\theta)\sin(\theta)$ of DPH as Mag2 added implies that Mag2 added to the bilayers in presence of of PE and cholesterol did not change the order of the bilayer interior.

Several structural aspects make melittin more active than Mag2 with respect to disrupting the bilayer in the range of the peptide to lipids studied in this research. Melittin has about twice the number of cationic residues as Mag2, therefore the electrostatic interaction between the cationic residues of peptides and zwitterionic lipid bilayers is stronger in the case of melittin [154]. The helical face of Mag2 is more free to interact with zwitterionic lipid bilayers because the charged and sterically bulky residues of melittin are clustered at one end of the helix [154]. As a result, melittin is more sensitive to zwitterionic lipid bilayer than Mag2, which has cationic residues distributed along its helical length [154].

5. Conclusions

This study was undertaken with two broad goals; 1) to examine the effects of peptide binding on the bilayer interior, and 2) to examine the effects on peptide binding of two biologically relevant lipid components that are generally omitted from investigations of peptide-bilayer interactions. One of these was a modification in the bilayer headgroup via introduction of phosphatidyl ethanolamine in the form of POPE, which is common in many biological membranes, particularly those involved in any signaling process. The second was a modification in the bilayer hydrophobic core via introduction of cholesterol, which is found in nearly all biological membranes. The effects of the peptides examined were found to be unique in each of the three bilayer compositions.

Melittin binding Melittin, or at least W19, experiences exactly two distinct environments when bound to the bilayer. This was found to be true over the entire range of melittin concentration from initial binding to intermediate structure, to pore formation. An exception to this was found in the cholesterol-containing bilayer where W19 stays in the same environment as melittin binds to the membrane, likely forms pre-pore intermediate structures, and eventually forms trans bilayer pores.

Effects of peptide binding on the bilayer interior These effects were found to vary widely across the two peptides examined and the three bilayer compositions. However, it is possible to draw to general conclusions. One of these conclusions is that cholesterol in the bilayer hydrophobic core has measurable and distinct effects on the ways peptides alter processes generally associated with the bilayer headgroup region, such as water permeability. The second is that the addition of PE to the bilayer headgroup has

distinct effects on the ability of peptides to alter aspects of the bilayer interior such as ensemble acyl chain order and the relative motion of an embedded molecule like DPH.

6. Future studies

Steady-state fluorescence measurements can be used to study the leakage of entrapped fluorophores into lipid bilayer interior as function of ratio of peptide to lipid. Fluorescein, rhodamine or calcein leakage assay are suggested to probe lipid bilayer leakage.

More details about the interaction of melittin and magainin 2 with different bilayer compositions and different temperatures can be obtained by using time-resolved fluorescence intensity and anisotropy decays of the embedded DPH. I suggest changing the percentage of cholesterol to phospholipids to study the effect of the bilayer interior on peptide-bilayer interaction and change the ratio of POPE to phospholipids to study the effect of different headgroups on the peptide-bilayer interaction.

References

[1] J. Lei *et al.*, "The antimicrobial peptides and their potential clinical applications," *American journal of translational research*, vol. 11, pp. 3919–3931, Jul. 2019.

[2] A. Lewies, L. H. Du Plessis, and J. F. Wentzel, "Antimicrobial Peptides: the Achilles' Heel of Antibiotic Resistance?," *Probiotics Antimicrob Proteins*, vol. 11, no. 2, pp. 370–381, Jun. 2019, doi: 10.1007/s12602-018-9465-0.

[3] P. L. Ho, H. K. Ong, J. Teo, D. S.-W. Ow, and S.-H. Chao, "HEXIM1 Peptide Exhibits Antimicrobial Activity Against Antibiotic Resistant Bacteria Through Guidance of Cell Penetrating Peptide," *Front. Microbiol.*, vol. 10, 2019, doi: 10.3389/fmicb.2019.00203.

[4] J. Hong, X. Lu, Z. Deng, S. Xiao, B. Yuan, and K. Yang, "How Melittin Inserts into Cell Membrane: Conformational Changes, Inter-Peptide Cooperation, and Disturbance on the Membrane," *Molecules*, vol. 24, no. 9, p. 1775, Jan. 2019, doi: 10.3390/molecules24091775.

[5] M. Mahlapuu, J. Håkansson, L. Ringstad, and C. Björn, "Antimicrobial Peptides: An Emerging Category of Therapeutic Agents," *Front Cell Infect Microbiol*, vol. 6, Dec. 2016, doi: 10.3389/fcimb.2016.00194.

[6] R. Seyfi *et al.*, "Antimicrobial Peptides (AMPs): Roles, Functions and Mechanism of Action," *Int J Pept Res Ther*, Oct. 2019, doi: 10.1007/s10989-019-09946-9.

[7] L. Zhang and R. L. Gallo, "Antimicrobial peptides," *Current Biology*, vol. 26, no. 1, pp. R14–R19, Jan. 2016, doi: 10.1016/j.cub.2015.11.017.

[8] A. Marquette and B. Bechinger, "Biophysical Investigations Elucidating the Mechanisms of Action of Antimicrobial Peptides and Their Synergism," *Biomolecules*, vol. 8, no. 2, Apr. 2018, doi: 10.3390/biom8020018.

[9] S. Galdiero, A. Falanga, M. Cantisani, M. Vitiello, G. Morelli, and M. Galdiero, "Peptide-Lipid Interactions: Experiments and Applications," *Int J Mol Sci*, vol. 14, no. 9, pp. 18758–18789, Sep. 2013, doi: 10.3390/ijms140918758.

[10] B. Bechinger and S.-U. Gorr, "Antimicrobial Peptides: Mechanisms of Action and Resistance," *J Dent Res*, vol. 96, no. 3, pp. 254–260, Mar. 2017, doi: 10.1177/0022034516679973.

[11] A. A. Bahar and D. Ren, "Antimicrobial Peptides," *Pharmaceuticals (Basel)*, vol. 6, no. 12, pp. 1543–1575, Nov. 2013, doi: 10.3390/ph6121543.

[12] H. Zhao, J. P. Mattila, J. M. Holopainen, and P. K. Kinnunen, "Comparison of the membrane association of two antimicrobial peptides, magainin 2 and indolicidin," *Biophys J*, vol. 81, no. 5, pp. 2979–2991, Nov. 2001, doi: 10.1016/S0006-3495(01)75938-3.

[13] P. Kumar, J. N. Kizhakkedathu, and S. K. Straus, "Antimicrobial Peptides: Diversity, Mechanism of Action and Strategies to Improve the Activity and Biocompatibility In Vivo," *Biomolecules*, vol. 8, no. 1, Jan. 2018, doi: 10.3390/biom8010004.

[14] F. G. Avci, B. S. Akbulut, and E. Ozkirimli, "Membrane Active Peptides and Their Biophysical Characterization," *Biomolecules*, vol. 8, no. 3, Aug. 2018, doi: 10.3390/biom8030077.

[15] S. T. Henriques, M. N. Melo, and M. A. R. B. Castanho, “How to address CPP and AMP translocation? Methods to detect and quantify peptide internalization in vitro and in vivo (Review),” *Molecular Membrane Biology*, vol. 24, no. 3, pp. 173–184, Jan. 2007, doi: 10.1080/09687860601102476.
[16] Y. H. Nan, I.-S. Park, K.-S. Hahm, and S. Y. Shin, “Antimicrobial activity, bactericidal mechanism and LPS-neutralizing activity of the cell-penetrating peptide pVEC and its analogs,” *J Pept Sci*, vol. 17, no. 12, pp. 812–817, Dec. 2011, doi: 10.1002/psc.1408.
[17] I. Zelezetsky and A. Tossi, “Alpha-helical antimicrobial peptides—Using a sequence template to guide structure–activity relationship studies,” *Biochimica et Biophysica Acta (BBA) - Biomembranes*, vol. 1758, no. 9, pp. 1436–1449, Sep. 2006, doi: 10.1016/j.bbamem.2006.03.021.
[18] K. T. Nguyen, S. V. Le Clair, S. Ye, and Z. Chen, “Molecular Interactions between Magainin 2 and Model Membranes in Situ,” *J. Phys. Chem. B*, vol. 113, no. 36, pp. 12358–12363, Sep. 2009, doi: 10.1021/jp904154w.
[19] K. Zeth, “Structure and mechanism of human antimicrobial peptide dermcidin and its antimicrobial potential,” p. 9.
[20] F. G. Avci, B. S. Akbulut, and E. Ozkirimli, “Membrane Active Peptides and Their Biophysical Characterization,” *Biomolecules*, vol. 8, no. 3, Aug. 2018, doi: 10.3390/biom8030077.
[21] T. Y and Y. M, “Magainin 2-induced pore formation in the lipid membranes depends on its concentration in the membrane interface.,” *J Phys Chem B*, vol. 113, no. 14, pp. 4846–4852, Apr. 2009, doi: 10.1021/jp8109622.
[22] “Use of fluorescent probes to monitor molecular order and motions within liposome bilayers - Google Search.” https://www.google.com/search?client=firefox-b-1-d&q=Use+of+fluorescent+probes+to+monitor+molecular+order+and+motions+within+liposome+bilayers (accessed Feb. 19, 2021).
[23] C. Poojari *et al.*, “Behavior of the DPH fluorescence probe in membranes perturbed by drugs,” *Chemistry and Physics of Lipids*, vol. 223, p. 104784, Sep. 2019, doi: 10.1016/j.chemphyslip.2019.104784.
[24] D. C. Mitchell and B. J. Litman, “Molecular Order and Dynamics in Bilayers Consisting of Highly Polyunsaturated Phospholipids,” *Biophysical Journal*, vol. 74, no. 2, pp. 879–891, Feb. 1998, doi: 10.1016/S0006-3495(98)74011-1.
[25] J. Ce, M. K, K. Y, W. H, and S.-W. Ig, “Efficacy of a proapoptotic peptide towards cancer cells.,” *In Vivo*, vol. 26, no. 3, pp. 419–426, May 2012.
[26] H. Raghuraman and A. Chattopadhyay, “Melittin: a Membrane-active Peptide with Diverse Functions,” *Biosci Rep*, vol. 27, no. 4–5, pp. 189–223, Aug. 2007, doi: 10.1007/s10540-006-9030-z.
[27] A. Kurek-Górecka, K. Komosinska-Vassev, A. Rzepecka-Stojko, and P. Olczyk, “Bee Venom in Wound Healing,” *Molecules*, vol. 26, no. 1, Art. no. 1, Jan. 2021, doi: 10.3390/molecules26010148.
[28] M. Pincus, “Physiological Structure and Function of Proteins,” in *Cell Physiology Source Book*, 2001, pp. 19–42. doi: 10.1016/B978-012656976-6/50094-9.

[29] H. Raghuraman and A. Chattopadhyay, “Melittin: a membrane-active peptide with diverse functions,” *Biosci Rep*, vol. 27, no. 4–5, pp. 189–223, Oct. 2007, doi: 10.1007/s10540-006-9030-z.
[30] G. Klocek and J. Seelig, “Melittin interaction with sulfated cell surface sugars,” *Biochemistry*, vol. 47, no. 9, pp. 2841–2849, Mar. 2008, doi: 10.1021/bi702258z.
[31] “Quantitative Studies on the Melittin-Induced Leakage Mechanism of Lipid Vesicles | Biochemistry.” https://pubs.acs.org/doi/10.1021/bi971009p (accessed Apr. 30, 2021).
[32] “Binding of Antibacterial Magainin Peptides to Electrically Neutral Membranes: Thermodynamics and Structure | Biochemistry.” https://pubs.acs.org/doi/10.1021/bi990913%2B (accessed Apr. 30, 2021).
[33] J. Seelig, S. Nebel, P. Ganz, and C. Bruns, “Electrostatic and nonpolar peptide-membrane interactions. Lipid binding and functional properties of somatostatin analogues of charge z = +1 to z = +3,” *Biochemistry*, vol. 32, no. 37, pp. 9714–9721, Sep. 1993, doi: 10.1021/bi00088a025.
[34] R. A. Cox, “Biophysical Chemistry Part III: The Behavior of Biological Macromolecules,” *FEBS Letters*, vol. 124, no. 1, pp. 126–127, 1981, doi: https://doi.org/10.1016/0014-5793(81)80070-1.
[35] L. Yang, T. A. Harroun, T. M. Weiss, L. Ding, and H. W. Huang, “Barrel-Stave Model or Toroidal Model? A Case Study on Melittin Pores,” *Biophysical Journal*, vol. 81, no. 3, pp. 1475–1485, Sep. 2001, doi: 10.1016/S0006-3495(01)75802-X.
[36] D. Sengupta, H. Leontiadou, A. E. Mark, and S.-J. Marrink, “Toroidal pores formed by antimicrobial peptides show significant disorder,” *Biochim Biophys Acta*, vol. 1778, no. 10, pp. 2308–2317, Oct. 2008, doi: 10.1016/j.bbamem.2008.06.007.
[37] H. W. Huang, “Molecular mechanism of antimicrobial peptides: The origin of cooperativity,” *Biochimica et Biophysica Acta (BBA) - Biomembranes*, vol. 1758, no. 9, pp. 1292–1302, Sep. 2006, doi: 10.1016/j.bbamem.2006.02.001.
[38] G. van den Bogaart, J. V. Guzmán, J. T. Mika, and B. Poolman, “On the mechanism of pore formation by melittin,” *J Biol Chem*, vol. 283, no. 49, pp. 33854–33857, Dec. 2008, doi: 10.1074/jbc.M805171200.
[39] T. Benachir and M. Lafleur, “Study of vesicle leakage induced by melittin,” *Biochim Biophys Acta*, vol. 1235, no. 2, pp. 452–460, May 1995, doi: 10.1016/0005-2736(95)80035-e.
[40] P. Wessman, A. A. Strömstedt, M. Malmsten, and K. Edwards, “Melittin-Lipid Bilayer Interactions and the Role of Cholesterol,” *Biophys J*, vol. 95, no. 9, pp. 4324–4336, Nov. 2008, doi: 10.1529/biophysj.108.130559.
[41] A. A. Strömstedt, P. Wessman, L. Ringstad, K. Edwards, and M. Malmsten, “Effect of lipid headgroup composition on the interaction between melittin and lipid bilayers,” *J Colloid Interface Sci*, vol. 311, no. 1, pp. 59–69, Jul. 2007, doi: 10.1016/j.jcis.2007.02.070.
[42] Y. Lyu, N. Xiang, X. Zhu, and G. Narsimhan, “Potential of mean force for insertion of antimicrobial peptide melittin into a pore in mixed DOPC/DOPG lipid bilayer by molecular dynamics simulation,” *J. Chem. Phys.*, vol. 146, no. 15, p. 155101, Apr. 2017, doi: 10.1063/1.4979613.

[43] Y. Miyazaki, S. Okazaki, and W. Shinoda, “Free energy analysis of membrane pore formation process in the presence of multiple melittin peptides,” *Biochimica et Biophysica Acta (BBA) - Biomembranes*, vol. 1861, no. 7, pp. 1409–1419, Jul. 2019, doi: 10.1016/j.bbamem.2019.03.002.
[44] C. Münster, A. Spaar, B. Bechinger, and T. Salditt, “Magainin 2 in phospholipid bilayers: peptide orientation and lipid chain ordering studied by X-ray diffraction,” *Biochim Biophys Acta*, vol. 1562, no. 1–2, pp. 37–44, May 2002, doi: 10.1016/s0005-2736(02)00357-7.
[45] S. M. Gregory, A. Pokorny, and P. F. F. Almeida, “Magainin 2 Revisited: A Test of the Quantitative Model for the All-or-None Permeabilization of Phospholipid Vesicles,” *Biophys J*, vol. 96, no. 1, pp. 116–131, Jan. 2009, doi: 10.1016/j.bpj.2008.09.017.
[46] B. Bechinger, D. W. Juhl, E. Glattard, and C. Aisenbrey, “Revealing the Mechanisms of Synergistic Action of Two Magainin Antimicrobial Peptides,” *Frontiers in Medical Technology*, vol. 2, 2020, doi: 10.3389/fmedt.2020.615494.
[47] A. Pino-Angeles, J. M. L. Iii, and T. Lazaridis, “Pore Structure and Synergy in Antimicrobial Peptides of the Magainin Family,” *PLOS Computational Biology*, vol. 12, no. 1, p. e1004570, Jan. 2016, doi: 10.1371/journal.pcbi.1004570.
[48] Y. Tamba and M. Yamazaki, “Magainin 2-induced pore formation in the lipid membranes depends on its concentration in the membrane interface,” *J Phys Chem B*, vol. 113, no. 14, pp. 4846–4852, Apr. 2009, doi: 10.1021/jp8109622.
[49] A. Som, S. Vemparala, I. Ivanov, and G. N. Tew, “Synthetic mimics of antimicrobial peptides,” *Peptide Science*, vol. 90, no. 2, pp. 83–93, 2008, doi: https://doi.org/10.1002/bip.20970.
[50] “Structure of the plasma membrane (article),” *Khan Academy*. https://www.khanacademy.org/science/high-school-biology/hs-cells/hs-the-cell-membrane/a/structure-of-the-plasma-membrane (accessed Mar. 05, 2020).
[51] “Pekker and Shneider - The surface charge of a cell lipid membrane.pdf.”
[52] “Interaction of POPC, DPPC, and POPE with the μ opioid receptor: A coarse-grained molecular dynamics study.” https://journals.plos.org/plosone/article?id=10.1371/journal.pone.0213646 (accessed May 01, 2021).
[53] H. C. Berg, *Random Walks in Biology*, REV-Revised. Princeton University Press, 1993. doi: 10.2307/j.ctv7r40w6.
[54] R. Koynova and B. Tenchov, “Phase Transitions and Phase Behavior of Lipids,” 2012. doi: 10.1007/978-3-642-16712-6_542.
[55] D. A. Brown and E. London, “Structure and Origin of Ordered Lipid Domains in Biological Membranes,” *J. Membrane Biol.*, vol. 164, no. 2, pp. 103–114, Jul. 1998, doi: 10.1007/s002329900397.
[56] W. Rawicz, K. C. Olbrich, T. McIntosh, D. Needham, and E. Evans, “Effect of Chain Length and Unsaturation on Elasticity of Lipid Bilayers,” *Biophysical Journal*, vol. 79, no. 1, pp. 328–339, Jul. 2000, doi: 10.1016/S0006-3495(00)76295-3.

[57] S. Uran, Å. Larsen, P. B. Jacobsen, and T. Skotland, “Analysis of phospholipid species in human blood using normal-phase liquid chromatography coupled with electrospray ionization ion-trap tandem mass spectrometry,” *Journal of Chromatography B: Biomedical Sciences and Applications*, vol. 758, no. 2, pp. 265–275, Jul. 2001, doi: 10.1016/S0378-4347(01)00188-8.
[58] W. Dowhan, “Molecular basis for membrane phospholipid diversity: why are there so many lipids?,” *Annu Rev Biochem*, vol. 66, pp. 199–232, 1997, doi: 10.1146/annurev.biochem.66.1.199.
[59] K. Murzyn, T. Róg, and M. Pasenkiewicz-Gierula, “Phosphatidylethanolamine-phosphatidylglycerol bilayer as a model of the inner bacterial membrane,” *Biophys J*, vol. 88, no. 2, pp. 1091–1103, Feb. 2005, doi: 10.1529/biophysj.104.048835.
[60] J. Soussi and Y. Chalopin, “Electric polarizability of lipid bilayers: The influence of the structure,” *The Journal of Chemical Physics*, vol. 143, no. 14, p. 144904, Oct. 2015, doi: 10.1063/1.4932340.
[61] H. Huang *et al.*, “Using Fluorescence Quenching Titration to Determine the Orientation of a Model Transmembrane Protein in Mimic Membranes,” *Materials (Basel)*, vol. 12, no. 3, Jan. 2019, doi: 10.3390/ma12030349.
[62] J. A. Urbina, B. Moreno, W. Arnold, C. H. Taron, P. Orlean, and E. Oldfield, “A carbon-13 nuclear magnetic resonance spectroscopic study of inter-proton pair order parameters: a new approach to study order and dynamics in phospholipid membrane systems,” *Biophys J*, vol. 75, no. 3, pp. 1372–1383, Sep. 1998, doi: 10.1016/S0006-3495(98)74055-X.
[63] R. L. Thurmond, S. W. Dodd, and M. F. Brown, “Molecular areas of phospholipids as determined by 2H NMR spectroscopy. Comparison of phosphatidylethanolamines and phosphatidylcholines,” *Biophys J*, vol. 59, no. 1, pp. 108–113, Jan. 1991, doi: 10.1016/S0006-3495(91)82203-2.
[64] O. Engberg *et al.*, “Lipid Interactions and Organization in Complex Bilayer Membranes,” *Biophysical Journal*, vol. 110, no. 7, pp. 1563–1573, Apr. 2016, doi: 10.1016/j.bpj.2015.12.043.
[65] C. Caianiello, M. D’Avino, D. Cavasso, L. Paduano, and G. D’Errico, “Bioinspired Nanoemulsions Stabilized by Phosphoethanolamine and Phosphoglycerol Lipids,” *Nanomaterials (Basel)*, vol. 10, no. 6, Jun. 2020, doi: 10.3390/nano10061185.
[66] L. de Oliveira Andrade, “Understanding the role of cholesterol in cellular biomechanics and regulation of vesicular trafficking: The power of imaging,” *BSI*, vol. 5, no. s1, pp. S101–S117, Dec. 2016, doi: 10.3233/BSI-160157.
[67] W. J. Van Blitterswijk, R. P. Van Hoeven, and B. W. Van der Meer, “Lipid structural order parameters (reciprocal of fluidity) in biomembranes derived from steady-state fluorescence polarization measurements,” *Biochim Biophys Acta*, vol. 644, no. 2, pp. 323–332, Jun. 1981, doi: 10.1016/0005-2736(81)90390-4.
[68] S. Kawato, K. Kinosita, and A. Ikegami, “Effect of cholesterol on the molecular motion in the hydrocarbon region of lecithin bilayers studied by nanosecond fluorescence techniques,” *Biochemistry*, vol. 17, no. 23, pp. 5026–5031, Nov. 1978, doi: 10.1021/bi00616a026.

[69] H. Raghuraman and A. Chattopadhyay, “Interaction of Melittin with Membrane Cholesterol: A Fluorescence Approach,” *Biophys J*, vol. 87, no. 4, pp. 2419–2432, Oct. 2004, doi: 10.1529/biophysj.104.043596.
[70] E. Bastiaanse, “The effect of membrane cholesterol content on ion transport processes in plasma membranes,” *Cardiovascular Research*, vol. 33, no. 2, pp. 272–283, Feb. 1997, doi: 10.1016/S0008-6363(96)00193-9.
[71] K. Bloch, “Chapter 12 Cholesterol: evolution of structure and function,” in *New Comprehensive Biochemistry*, vol. 20, D. E. Vance and J. E. Vance, Eds. Elsevier, 1991, pp. 363–381. doi: 10.1016/S0167-7306(08)60340-3.
[72] P. L. Yeagle, “Cholesterol and the cell membrane,” *Biochim Biophys Acta*, vol. 822, no. 3–4, pp. 267–287, Dec. 1985, doi: 10.1016/0304-4157(85)90011-5.
[73] F. A. Nezil and M. Bloom, “Combined influence of cholesterol and synthetic amphiphillic peptides upon bilayer thickness in model membranes.,” *Biophys J*, vol. 61, no. 5, pp. 1176–1183, May 1992.
[74] R. A. Demel and B. De Kruyff, “The function of sterols in membranes,” *Biochim Biophys Acta*, vol. 457, no. 2, pp. 109–132, Oct. 1976, doi: 10.1016/0304-4157(76)90008-3.
[75] B. Ramstedt and J. P. Slotte, “Membrane properties of sphingomyelins,” *FEBS Lett*, vol. 531, no. 1, pp. 33–37, Oct. 2002, doi: 10.1016/s0014-5793(02)03406-3.
[76] J. R. Silvius, “Role of cholesterol in lipid raft formation: lessons from lipid model systems,” *Biochimica et Biophysica Acta (BBA) - Biomembranes*, vol. 1610, no. 2, pp. 174–183, Mar. 2003, doi: 10.1016/S0005-2736(03)00016-6.
[77] B. Alberts, A. Johnson, J. Lewis, M. Raff, K. Roberts, and P. Walter, *Molecular Biology of the Cell*, 4th ed. Garland Science, 2002.

[78] D. Dzebo, “Photon Upconversion through Triplet-Triplet Annihilation: Towards Higher Efficiency and Solid State Applications,” Ph.D., Chalmers Tekniska Hogskola (Sweden), Sweden. Accessed: Jun. 22, 2021. [Online]. Available: https://www.proquest.com/docview/2401896770/abstract/51FDCB6F64994DFFPQ/1
[79] J. Plášek and P. Jarolím, “Interaction of the Fluorescent Probe 1,6-Diphenyl- 1, 3, 5-Hexatriene with Biomembranes,” p. 24.
[80] E. Gratton and T. Parasassi, “Fluorescence lifetime distributions in membrane systems,” *J Fluoresc*, vol. 5, no. 1, pp. 51–57, Mar. 1995, doi: 10.1007/BF00718782.
[81] A. C. Gracetto *et al.*, “Unusual 1,6-diphenyl-1,3,5-hexatriene (DPH) spectrophotometric behavior in water/ethanol and water/DMSO mixtures,” *Journal of the Brazilian Chemical Society*, vol. 21, no. 8, pp. 1497–1502, 2010, doi: 10.1590/S0103-50532010000800013.
[82] J. T. Vivian and P. R. Callis, “Mechanisms of tryptophan fluorescence shifts in proteins.,” *Biophys J*, vol. 80, no. 5, pp. 2093–2109, May 2001.
[83] “The tryptophan fluorescence lifetime puzzle. A study of decay times in aqueous solution as a function of pH and buffer composition - Canadian Journal of Chemistry.” https://www.nrcresearchpress.com/doi/10.1139/v81-154#.Xj_r_euIbUo (accessed Feb. 09, 2020).

[84] L. Brancaleon, G. Lin, and N. Kollias, “The In Vivo Fluorescence of Tryptophan Moieties in Human Skin Increases with UV Exposure and is a Marker for Epidermal Proliferation,” *Journal of Investigative Dermatology*, vol. 113, no. 6, pp. 977–982, Dec. 1999, doi: 10.1046/j.1523-1747.1999.00799.x.

[85] A. B. T. Ghisaidoobe and S. J. Chung, “Intrinsic tryptophan fluorescence in the detection and analysis of proteins: a focus on Förster resonance energy transfer techniques,” *Int J Mol Sci*, vol. 15, no. 12, pp. 22518–22538, Dec. 2014, doi: 10.3390/ijms151222518.

[86] S. Galdiero, A. Falanga, M. Cantisani, M. Vitiello, G. Morelli, and M. Galdiero, “Peptide-Lipid Interactions: Experiments and Applications,” *Int J Mol Sci*, vol. 14, no. 9, pp. 18758–18789, Sep. 2013, doi: 10.3390/ijms140918758.

[87] “ISS Chronos Spectrometer - Google Search.” https://www.google.com/search?q=ISS+Chronos+Spectrometer&rlz=1C1GGRV_enUS752US753&source=lnms&tbm=isch&sa=X&ved=2ahUKEwiG0v2qva3xAhVWtZ4KHVKRDZ4Q_AUoAXoECAEQAw&biw=1164&bih=778#imgrc=5o2cbeMfBuqeFM (accessed Jun. 23, 2021).

[88] Y. Gu, “The Effect of Docosahexaenoic Acid (DHA)-Containing Phosphatidylcholine (PC) on Liquid-Ordered and Liquid-Disordered Coexistence,” Jan. 2000. doi: 10.15760/etd.1949.

[89] R. F. Steiner, “Fluorescence Anisotropy: Theory and Applications,” in *Topics in Fluorescence Spectroscopy: Principles*, J. R. Lakowicz, Ed. Boston, MA: Springer US, 2002, pp. 1–52. doi: 10.1007/0-306-47058-6_1.

[90] “Principles of Fluorescence Spectroscopy | Joseph R. Lakowicz | Springer.” https://www.springer.com/gp/book/9780387312781 (accessed May 06, 2021).

[91] M. G. Badea and L. Brand, “Time-resolved fluorescence measurements,” *Methods Enzymol*, vol. 61, pp. 378–425, 1979, doi: 10.1016/0076-6879(79)61019-4.

[92] J. R. Lakowicz, E. Gratton, H. Cherek, B. P. Maliwal, and G. Laczko, “Determination of time-resolved fluorescence emission spectra and anisotropies of a fluorophore-protein complex using frequency-domain phase-modulation fluorometry.,” *Journal of Biological Chemistry*, vol. 259, no. 17, pp. 10967–10972, Sep. 1984, doi: 10.1016/S0021-9258(18)90607-1.

[93] J. R. Lakowicz and A. Balter, “Direct Recording of the Initially Excited and the Solvent Relaxed Fluorescence Emission Spectra of Tryptophan by Phase Sensitive Detection of Fluorescence,” *Photochemistry and Photobiology*, vol. 36, no. 2, pp. 125–132, 1982, doi: https://doi.org/10.1111/j.1751-1097.1982.tb04353.x.

[94] “Determination of time-resolved fluorescence emission spectra and anisotropies of a fluorophore-protein complex using frequency-domain phase-modulation fluorometry. | Elsevier Enhanced Reader.” (accessed May 14, 2021).

[95] G.-J. Kremers, E. B. van Munster, J. Goedhart, and T. W. J. Gadella, “Quantitative Lifetime Unmixing of Multiexponentially Decaying Fluorophores Using Single-Frequency Fluorescence Lifetime Imaging Microscopy,” *Biophysical Journal*, vol. 95, no. 1, pp. 378–389, Jul. 2008, doi: 10.1529/biophysj.107.125229.

[96] A. M. Weljie and H. J. Vogel, “Steady-State Fluorescence Spectroscopy,” in *Calcium-Binding Protein Protocols: Volume 2: Methods and Techniques*, H. J. Vogel, Ed. Totowa, NJ: Springer New York, 2002, pp. 75–87. doi: 10.1385/1-59259-184-1:075.
[97] “Principles of Fluorescence Spectroscopy | Joseph R. Lakowicz | Springer.” https://www.springer.com/us/book/9780387312781 (accessed Jun. 22, 2021).
[98] C. Albrecht, “Joseph R. Lakowicz: Principles of fluorescence spectroscopy, 3rd Edition,” *Anal Bioanal Chem*, vol. 390, no. 5, pp. 1223–1224, Mar. 2008, doi: 10.1007/s00216-007-1822-x.
[99] J. A. Ross and D. M. Jameson, “Time-resolved methods in biophysics. 8. Frequency domain fluorometry: applications to intrinsic protein fluorescence,” *Photochem Photobiol Sci*, vol. 7, no. 11, pp. 1301–1312, Nov. 2008, doi: 10.1039/b804450n.
[100] L. Liu, Q. Yang, M. Zhang, Z. Wu, and P. Xue, “Fluorescence lifetime imaging microscopy and its applications in skin cancer diagnosis,” *J. Innov. Opt. Health Sci.*, vol. 12, no. 05, p. 1930004, Sep. 2019, doi: 10.1142/S1793545819300040.
[101] R. F. M. de Almeida, A. Fedorov, and M. Prieto, “Sphingomyelin/Phosphatidylcholine/Cholesterol Phase Diagram: Boundaries and Composition of Lipid Rafts,” *Biophys J*, vol. 85, no. 4, pp. 2406–2416, Oct. 2003.
[102] M. Y. Berezin and S. Achilefu, “Fluorescence Lifetime Measurements and Biological Imaging,” *Chem. Rev.*, vol. 110, no. 5, pp. 2641–2684, May 2010, doi: 10.1021/cr900343z.
[103] D. C. Mitchell and B. J. Litman, “Effect of cholesterol on molecular order and dynamics in highly polyunsaturated phospholipid bilayers.,” *Biophys J*, vol. 75, no. 2, pp. 896–908, Aug. 1998.
[104] D. Shrestha, A. Jenei, P. Nagy, G. Vereb, and J. Szöllősi, “Understanding FRET as a research tool for cellular studies,” *Int J Mol Sci*, vol. 16, no. 4, pp. 6718–6756, Mar. 2015, doi: 10.3390/ijms16046718.
[105] J. A. Levitt *et al.*, “Multidimensional multiphoton fluorescence lifetime imaging of cells,” in *Multiphoton Microscopy in the Biomedical Sciences VIII*, Feb. 2008, vol. 6860, p. 68601G. doi: 10.1117/12.763468.
[106] A. Gijsbers, T. Nishigaki, and N. Sánchez-Puig, “Fluorescence Anisotropy as a Tool to Study Protein-protein Interactions,” *J Vis Exp*, no. 116, p. 54640, Oct. 2016, doi: 10.3791/54640.
[107] R. Favicchio, A. I. Dragan, G. G. Kneale, and C. M. Read, “Fluorescence spectroscopy and anisotropy in the analysis of DNA-protein interactions,” *Methods Mol Biol*, vol. 543, pp. 589–611, 2009, doi: 10.1007/978-1-60327-015-1_35.
[108] F. Jähnig, “Structural order of lipids and proteins in membranes: evaluation of fluorescence anisotropy data,” *Proc Natl Acad Sci U S A*, vol. 76, no. 12, pp. 6361–6365, Dec. 1979, doi: 10.1073/pnas.76.12.6361.
[109] K. Simons and E. Ikonen, “Functional rafts in cell membranes,” *Nature*, vol. 387, no. 6633, pp. 569–572, Jun. 1997, doi: 10.1038/42408.

[110] M. Ameloot, H. Hendrickx, W. Herreman, H. Pottel, F. Van Cauwelaert, and W. van der Meer, “Effect of orientational order on the decay of the fluorescence anisotropy in membrane suspensions. Experimental verification on unilamellar vesicles and lipid/alpha-lactalbumin complexes,” *Biophys J*, vol. 46, no. 4, pp. 525–539, Oct. 1984, doi: 10.1016/S0006-3495(84)84050-3.

[111] A. Szabo, “Theory of fluorescence depolarization in macromolecules and membranes,” *The Journal of Chemical Physics*, vol. 81, no. 1, pp. 150–167, Jul. 1984, doi: 10.1063/1.447378.

[112] J. Repáková, P. Čapková, J. M. Holopainen, and I. Vattulainen, “Distribution, Orientation, and Dynamics of DPH Probes in DPPC Bilayer,” *J. Phys. Chem. B*, vol. 108, no. 35, pp. 13438–13448, Sep. 2004, doi: 10.1021/jp048381g.

[113] J. Repáková, P. Čapková, J. M. Holopainen, and I. Vattulainen, “Distribution, Orientation, and Dynamics of DPH Probes in DPPC Bilayer,” *The Journal of Physical Chemistry B*, vol. 108, no. 35, pp. 13438–13448.

[114] B. Christiaens *et al.*, “Tryptophan fluorescence study of the interaction of penetratin peptides with model membranes,” *Eur J Biochem*, vol. 269, no. 12, pp. 2918–2926, Jun. 2002, doi: 10.1046/j.1432-1033.2002.02963.x.

[115] H. Raghuraman and A. Chattopadhyay, “Interaction of Melittin with Membrane Cholesterol: A Fluorescence Approach,” *Biophys J*, vol. 87, no. 4, pp. 2419–2432, Oct. 2004, doi: 10.1529/biophysj.104.043596.

[116] F. W. J. Teale and G. Weber, “Ultraviolet fluorescence of the aromatic amino acids,” *Biochem J*, vol. 65, no. 3, pp. 476–482, Mar. 1957.

[117] J. Dufourcq and J. F. Faucon, “Intrinsic fluorescence study of lipid-protein interactions in membrane models. Binding of melittin, an amphipathic peptide, to phospholipid vesicles,” *Biochim Biophys Acta*, vol. 467, no. 1, pp. 1–11, May 1977, doi: 10.1016/0005-2736(77)90236-x.

[118] T. Benachir, M. Monette, J. Grenier, and M. Lafleur, “Melittin-induced leakage from phosphatidylcholine vesicles is modulated by cholesterol: a property used for membrane targeting,” *European Biophysics Journal*, vol. 25, no. 3, pp. 201–210, Jan. 1997, doi: 10.1007/s002490050032.

[119] Z. Oren, J. Ramesh, D. Avrahami, N. Suryaprakash, Y. Shai, and R. Jelinek, “Structures and mode of membrane interaction of a short α helical lytic peptide and its diastereomer determined by NMR, FTIR, and fluorescence spectroscopy,” *European Journal of Biochemistry*, vol. 269, no. 16, pp. 3869–3880, 2002, doi: https://doi.org/10.1046/j.1432-1033.2002.03080.x.

[120] M. Ghose, S. Mandal, D. Roy, R. K. Mandal, and G. Basu, “Dielectric relaxation in a single tryptophan protein,” *FEBS Letters*, vol. 509, no. 2, pp. 337–340, Dec. 2001, doi: 10.1016/S0014-5793(01)03202-1.

[121] G. Gramse, A. Dols-Pérez, M. Edwards, L. Fumagalli, and G. Gomila, “Nanoscale measurement of the dielectric constant of supported lipid bilayers in aqueous solutions with electrostatic force microscopy.,” *Biophysical journal*, 2013, doi: 10.1016/j.bpj.2013.02.011.

[122] A. A. Abd El-Wahed *et al.*, “Bee Venom Composition: From Chemistry to Biological Activity,” in *Studies in Natural Products Chemistry*, vol. 60, Elsevier, 2019, pp. 459–484. doi: 10.1016/B978-0-444-64181-6.00013-9.
[123] J. Hong, Z. Oren, and Y. Shai, “Structure and Organization of Hemolytic and Nonhemolytic Diastereomers of Antimicrobial Peptides in Membranes,” *Biochemistry*, vol. 38, no. 51, pp. 16963–16973, Dec. 1999, doi: 10.1021/bi991850y.
[124] M. C. Chang, J. W. Petrich, D. B. McDonald, and G. R. Fleming, “Nonexponential fluorescence decay of tryptophan, tryptophylglycine, and glycyltryptophan,” *J. Am. Chem. Soc.*, vol. 105, no. 12, pp. 3819–3824, Jun. 1983, doi: 10.1021/ja00350a013.
[125] R. J. Robbins, G. R. Fleming, G. S. Beddard, G. W. Robinson, P. J. Thistlethwaite, and G. J. Woolfe, “Photophysics of aqueous tryptophan: pH and temperature effects,” *J. Am. Chem. Soc.*, vol. 102, no. 20, pp. 6271–6279, Sep. 1980, doi: 10.1021/ja00540a016.
[126] “Interaction of Melittin with Membrane Cholesterol: A Fluorescence Approach | Elsevier Enhanced Reader.” https://reader.elsevier.com/reader/sd/pii/S0006349504737157?token=1898F6AF62F5AA59B758E079CDB6C4BFF6D23F93EAD383685DC3BC3730A4E8755EBF1F0F7B0E88BFBB92007AA48B127D&originRegion=us-east-1&originCreation=20210605165450 (accessed Jun. 05, 2021).
[127] “Photophysics of aqueous tryptophan: pH and temperature effects | Journal of the American Chemical Society.” https://pubs.acs.org/doi/abs/10.1021/ja00540a016 (accessed May 29, 2021).
[128] A. B. T. Ghisaidoobe and S. J. Chung, “Intrinsic tryptophan fluorescence in the detection and analysis of proteins: a focus on Förster resonance energy transfer techniques,” *Int J Mol Sci*, vol. 15, no. 12, pp. 22518–22538, Dec. 2014, doi: 10.3390/ijms151222518.
[129] H. Hevekerl, J. Tornmalm, and J. Widengren, “Fluorescence-based characterization of non-fluorescent transient states of tryptophan - Prospects for protein conformation and interaction studies,” *Scientific Reports*, vol. 6, p. 35052, Oct. 2016, doi: 10.1038/srep35052.
[130] N. Matoga, T. Kubota, and W. B. Person, “Molecular Interactions and Electronic Spectra,” *PHYSICS TODAY*, p. 4, 1973.
[131] D. W. Pierce and S. G. Boxer, “Stark effect spectroscopy of tryptophan.,” *Biophys J*, vol. 68, no. 4, pp. 1583–1591, Apr. 1995.
[132] A. Mishra, S. Sahu, S. Tripathi, and G. Krishnamoorthy, “Photoinduced intramolecular charge transfer in trans-2-[4′-(N,N-dimethylamino)styryl]imidazo[4,5-b]pyridine: effect of introducing a CC double bond,” *Photochem. Photobiol. Sci.*, vol. 13, no. 10, pp. 1476–1486, Sep. 2014, doi: 10.1039/C4PP00237G.
[133] J. Zhou *et al.*, “Temperature dependent optical and dielectric properties of liquid water studied by terahertz time-domain spectroscopy,” *AIP Advances*, vol. 9, no. 3, p. 035346, Mar. 2019, doi: 10.1063/1.5082841.

[134] C. G. Malmberg and A. A. Maryott, “Dielectric constant of water from 0 to 100 C,” *J. RES. NATL. BUR. STAN.*, vol. 56, no. 1, p. 1, Jan. 1956, doi: 10.6028/jres.056.001.
[135] T. P. Dale and J. H. Gladstone, “On the Influence of Temperature on the Refraction of Light,” *Philosophical Transactions of the Royal Society of London*, vol. 148, pp. 887–894, 1858.
[136] E. P. Kirby and R. F. Steiner, “The Tryptophan Microenvironments in Apomyoglobin,” *Journal of Biological Chemistry*, vol. 245, no. 23, pp. 6300–6306, Dec. 1970, doi: 10.1016/S0021-9258(18)62609-2.
[137] R. Swaminathan, G. Krishnamoorthy, and N. Periasamy, “Similarity of fluorescence lifetime distributions for single tryptophan proteins in the random coil state,” *Biophysical Journal*, vol. 67, no. 5, pp. 2013–2023, Nov. 1994, doi: 10.1016/S0006-3495(94)80685-X.
[138] Y. Chen, R. D. Ludescher, and T. J. Montville, “Influence of Lipid Composition on Pediocin PA-1 Binding to Phospholipid Vesicles,” *Appl Environ Microbiol*, vol. 64, no. 9, pp. 3530–3532, Sep. 1998.
[139] M.-T. Lee, T.-L. Sun, W.-C. Hung, and H. W. Huang, “Process of inducing pores in membranes by melittin,” *PNAS*, vol. 110, no. 35, pp. 14243–14248, Aug. 2013, doi: 10.1073/pnas.1307010110.
[140] I. Konopásek, P. Kvasnicka, E. Amler, A. Kotyk, and G. Curatola, “The transmembrane gradient of the dielectric constant influences the DPH lifetime distribution,” *FEBS Lett*, vol. 374, no. 3, pp. 338–340, Nov. 1995, doi: 10.1016/0014-5793(95)01138-5.
[141] “Diphenylhexatriene membrane probes DPH and TMA-DPH: A comparative molecular dynamics simulation study | Elsevier Enhanced Reader.” https://reader.elsevier.com/reader/sd/pii/S0005273616302668?token=2BC8FAF229D672EE01D3989894A37181AA73B89E8400B74502123B56015238F170C9257901744893553F9EC943BCF95B&originRegion=us-east-1&originCreation=20210616114518 (accessed Jun. 16, 2021).
[142] J. Repáková, J. M. Holopainen, M. R. Morrow, M. C. McDonald, P. Čapková, and I. Vattulainen, “Influence of DPH on the Structure and Dynamics of a DPPC Bilayer,” *Biophysical Journal*, vol. 88, no. 5, pp. 3398–3410, May 2005, doi: 10.1529/biophysj.104.055533.
[143] C. R. Mateo, M. P. Lillo, J. González-Rodríguez, and A. U. Acuña, “Molecular order and fluidity of the plasma membrane of human platelets from time-resolved fluorescence depolarization,” *Eur Biophys J*, vol. 20, no. 1, pp. 41–52, 1991, doi: 10.1007/BF00183278.
[144] B. R. Lentz, “Use of fluorescent probes to monitor molecular order and motions within liposome bilayers,” *Chem Phys Lipids*, vol. 64, no. 1–3, pp. 99–116, Sep. 1993, doi: 10.1016/0009-3084(93)90060-g.
[145] S. Wang, J. M. Beechem, E. Gratton, and M. Glaser, “Orientational distribution of 1,6-diphenyl-1,3,5-hexatriene in phospholipid vesicles as determined by global analysis of frequency domain fluorimetry data,” *Biochemistry*, vol. 30, no. 22, pp. 5565–5572, Jun. 1991, doi: 10.1021/bi00236a032.

[146] S. J. Irudayam and M. L. Berkowitz, “Binding and reorientation of melittin in a POPC bilayer: Computer simulations,” *Biochimica et Biophysica Acta (BBA) - Biomembranes*, vol. 1818, no. 12, pp. 2975–2981, Dec. 2012, doi: 10.1016/j.bbamem.2012.07.026.
[147] D. Allende, S. A. Simon, and T. J. McIntosh, “Melittin-Induced Bilayer Leakage Depends on Lipid Material Properties: Evidence for Toroidal Pores,” *Biophys J*, vol. 88, no. 3, pp. 1828–1837, Mar. 2005, doi: 10.1529/biophysj.104.049817.
[148] C. K. Haluska *et al.*, “Combining Fluorescence Lifetime and Polarization Microscopy to Discriminate Phase Separated Domains in Giant Unilamellar Vesicles,” *Biophysical Journal*, vol. 95, no. 12, pp. 5737–5747, Dec. 2008, doi: 10.1529/biophysj.108.131490.
[149] M. Amaro, R. Šachl, P. Jurkiewicz, A. Coutinho, M. Prieto, and M. Hof, “Time-Resolved Fluorescence in Lipid Bilayers: Selected Applications and Advantages over Steady State,” *Biophys J*, vol. 107, no. 12, pp. 2751–2760, Dec. 2014, doi: 10.1016/j.bpj.2014.10.058.
[150] A. C. Gracetto, V. R. Batistela, W. G. Santos, C. C. Cavalheiro, and N. Hioka, “Unusual 1,6-diphenyl-1,3,5-hexatriene (DPH) spectrophotometric behavior in water/ethanol and water/DMSO mixtures,” 2010, doi: 10.1590/S0103-50532010000800013.
[151] V. Kilin, O. Glushonkov, L. Herdly, A. Klymchenko, L. Richert, and Y. Mely, “Fluorescence lifetime imaging of membrane lipid order with a ratiometric fluorescent probe,” *Biophys J*, vol. 108, no. 10, pp. 2521–2531, May 2015, doi: 10.1016/j.bpj.2015.04.003.
[152] K. Murzyn, T. Róg, and M. Pasenkiewicz-Gierula, “Phosphatidylethanolamine-Phosphatidylglycerol Bilayer as a Model of the Inner Bacterial Membrane,” *Biophysical Journal*, vol. 88, no. 2, pp. 1091–1103, Feb. 2005, doi: 10.1529/biophysj.104.048835.
[153] H. Saito, T. Minamida, I. Arimoto, T. Handa, and K. Miyajima, “Physical States of Surface and Core Lipids in Lipid Emulsions and Apolipoprotein Binding to the Emulsion Surface,” *The Journal of biological chemistry*, vol. 271, pp. 15515–20, Jul. 1996, doi: 10.1074/jbc.271.26.15515.
[154] D. J. Paterson, M. Tassieri, J. Reboud, R. Wilson, and J. M. Cooper, “Lipid topology and electrostatic interactions underpin lytic activity of linear cationic antimicrobial peptides in membranes,” *PNAS*, vol. 114, no. 40, pp. E8324–E8332, Oct. 2017, doi: 10.1073/pnas.1704489114.
[155] M. Dathe and T. Wieprecht, “Structural features of helical antimicrobial peptides: their potential to modulate activity on model membranes and biological cells,” *Biochimica et Biophysica Acta (BBA) - Biomembranes*, vol. 1462, no. 1, pp. 71–87, Dec. 1999, doi: 10.1016/S0005-2736(99)00201-1.
[156] B. Bechinger and K. Lohner, “Detergent-like actions of linear amphipathic cationic antimicrobial peptides,” *Biochim Biophys Acta*, vol. 1758, no. 9, pp. 1529–1539, Sep. 2006, doi: 10.1016/j.bbamem.2006.07.001.